THE ROLE OF INTERELECTRODE DISTANCE IN ELECTRICAL DISCHARGE MACHINING

by

HANS C. JUVKAM-WOLD

S.B., Massachusetts Institute of Technology  (1966)

S.M., Massachusetts Institute of Technology  (1967)

Submitted in partial fulfillment
of the requirements for the
degree of Doctor of Science

at the

MASSACHUSETTS INSTITUTE OF TECHNOLOGY

May, 1969

Signature of Author..................................................
                        Dept. of Mechanical Engineering, May 15, 1969

Certified by........................................................
                                                Thesis Supervisor

Accepted by........................................................
                Chairman, Departmental Committee on Graduate Students

THE ROLE OF INTERELECTRODE DISTANCE IN ELECTRICAL DISCHARGE MACHINING

by

Hans C. Juvkam-Wold

ABSTRACT

The interelectrode distance between tool and workpiece in
electrical discharge machining has been measured using a flow rate
technique. The magnitude of the electrode separation is found to be
approximately proportional to the one third power of the pulse energy.

The quantity of material eroded from a steel workpiece per
discharge in multiple discharge machining tests using a graphite tool
is proportional to the pulse energy, irrespective of the workpiece
polarity, for pulse durations from 20 to 500 microseconds and arc
currents from 40 to 300 amps.

Erosion products appear partly in the form of hollow spheres,
and measurements of the size distribution indicate that the mean size
increases with increasing pulse energy. The magnitude of the
interelectrode distance and the diameter of the largest spheres are
both of the same order, suggesting that the distance may be controlled
by the size of the spheres. An attempt was made to force the distance
to be large by introducing spheres into the EDM fluid, but the results
were unsatisfactory.

In reverse polarity the relative erosion of the graphite anode
is found to be greatly reduced at high pulse energies. A qualitative
erosion model which assumes (1) the power density at the anode surface
decreases as the interelectrode distance increases, and (2) material
transfer to the anode increases as the gap increases, is suggested and
examined in the light of the experimental data.

Thesis Supervisor: Robert E. Stickney

Title: Associate Professor of Mechanical Engineering

To Connie

## ACKNOWLEDGEMENTS

# TABLE OF CONTENTS

# LIST OF FIGURES

# 1. INTRODUCTION

As engineering applications place ever increasing demands on the strength and hardness of materials, it becomes correspondingly more difficult to shape and form these materials by conventional methods. It becomes even more difficult to make the tools with which these materials may be worked. Consequently, a number of new machining methods have developed in the last quarter century. One of the most promising of these appears to be electrical discharge machining.[1,2,3,4]

## 1.1 Description of EDM Process

Electrical discharge machining (EDM) is a process in which the erosive properties of electric sparks (or arcs) are used to erode the workpiece to any desired configuration by means of a large number of successive electrical discharges; a replica of the tool is formed on the workpiece. Hardness is no deterrent; any material which conducts electricity can be machined by EDM. A disadvantage of EDM is that the discharges which erode the workpiece also tend to erode the tool. The relative tool wear depends on the machining conditions, particularly on the energy per discharge.[5] It is the purpose of this thesis to try to understand why this is so.

A commercial EDM machine has a power supply which puts out a large number of successive pulses of electrical energy, usually between 200 and 500 000 pulses per second. Let us consider one of these pulses in detail (Fig. 1).
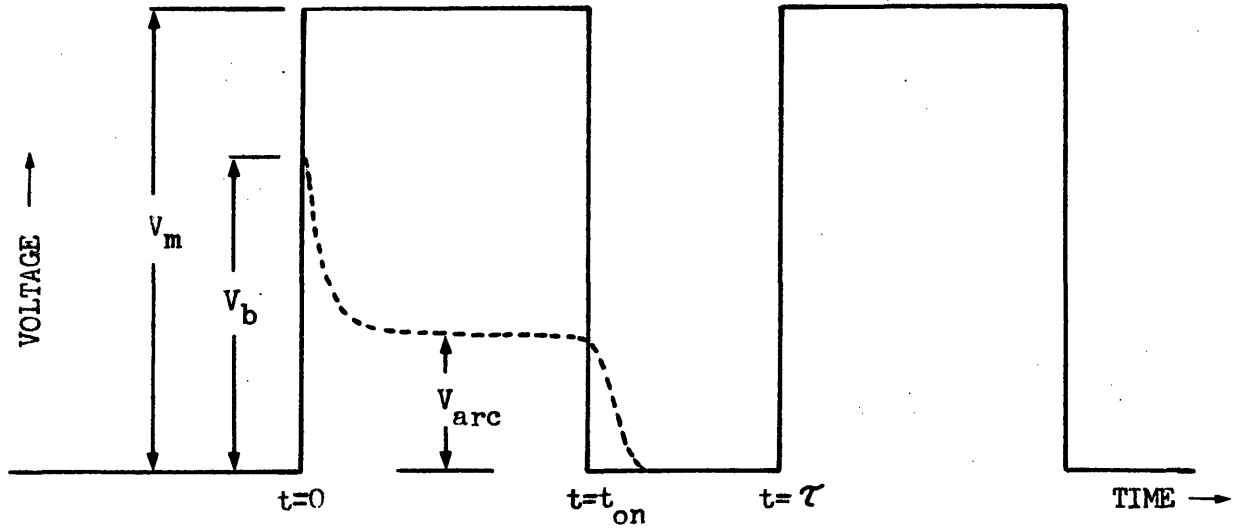
Fig. 1.    Schematic of voltage pulses from the power supply.

At time t = 0, a voltage, $V_m$, is applied across the electrode gap.
If the interelectrode spacing between the tool and the workpiece is too
large for the voltage $V_m$ to cause a breakdown* of the dielectric to
occur, a servomechanism connected to the tool will begin to decrease
the spacing until a discharge can occur. If no discharge occurs before
t = $t_{on}$, the voltage remains at $V_m$ until time $t_{on}$ when the power supply
shuts off the voltage to zero, until time $\tau$ when a voltage $V_m$ is again
applied. The servo will attempt to maintain a spacing such that breakdown
always occurs at some preset voltage, $V_b$ (Fig. 1). When breakdown does
occur, the voltage decreases rapidly for the first few microseconds.
After an initial transient, a steady - stage voltage, $V_{arc}$, may be
observed between the electrodes (Fig. 15).

---

*breakdown  is the process by which the EDM fluid is transformed from
          an insulator to a conductor.

-14-

During an arc discharge energy is transported to the two
electrodes from the arc.[6,39]  Let us here attempt to obtain a simplified
physical picture of how this occurs, and of what other phenomena
take place in the arc (the theory of arcs is treated in more depth
in Appendices A,B, and C).  For example, how does the flow of current
take place in the plasma?  Figure 2 illustrates the main carriers of
current in the different regions of the arc.  There is charge neutrality
in the two electrodes and in the plasma.  In the cathode fall region
there is considerable positive space charge (more ions[*] per unit
volume than electrons), and in the anode fall region there is usually

relative number of charge carriers per unit volume

relative importance of carriers

potential

$V_a$ = anode fall
          of
          potential

$V_c$ = cathode
          fall of
          potential

CATHODE    CATHODE          PLASMA          ANODE         ANODE
           FALL                             FALL
           REGION                           REGION
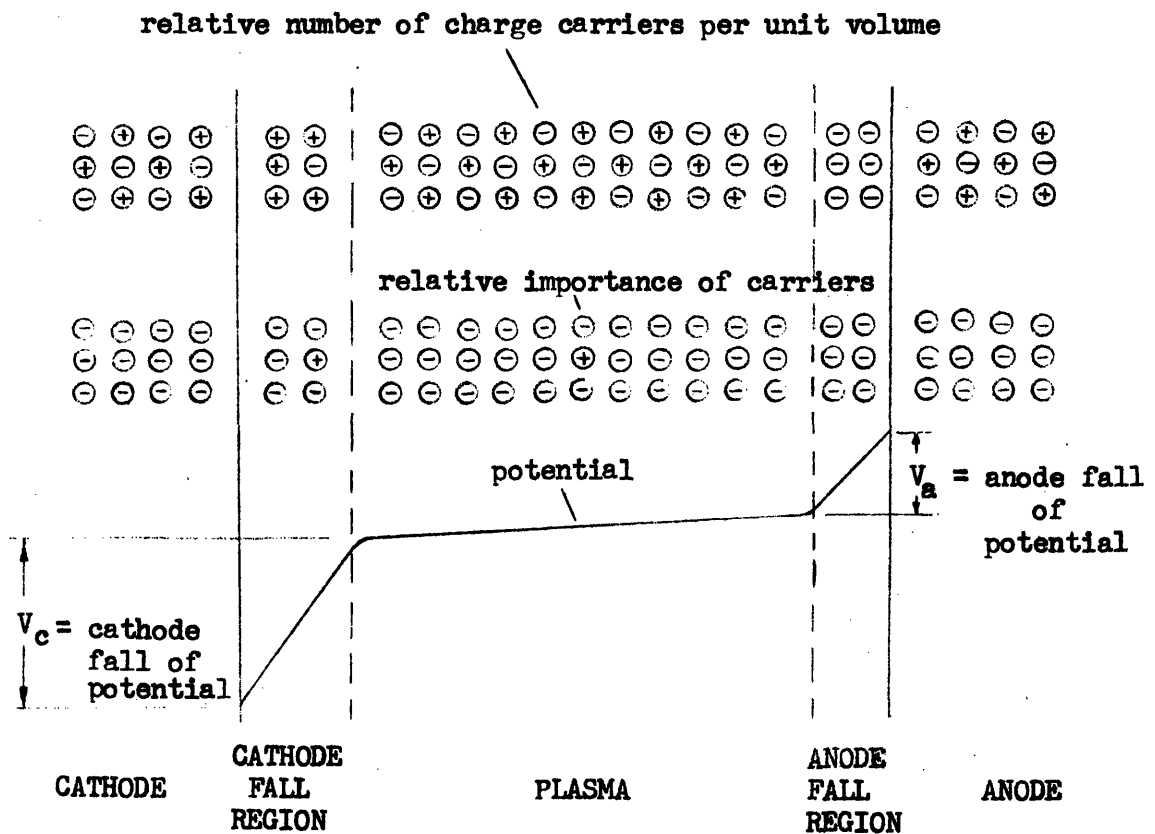
Fig. 2.   Schematic of the electric potential and of
          the current carriers in an electric arc.

* We here consider only singly ionized, positive ions.

-15-

considerable negative space charge. However, electrons are very much more mobile, and carry most of the current in all regions of the arc. In the two electrodes, and in the anode fall region, practically all the current is carried by electrons. In the plasma less than 1% of the current is carried by positive ions, and the rest by electrons. The only part with considerable ion transport is the cathode fall region, where perhaps 2 to 30% of the total current is carried by positive ions.

Energy is transferred from the arc to the cathode primarily by positive ions, and to the anode primarily by electrons. Figure 3 illustrates some of the phenomena occurring at the cathode. Electrons are emitted from the cathode. If the emission is thermionic (Appendix A) there is a cooling effect at the cathode of $e\phi_c$ per electron emitted. Here e is the charge per electron, and $\phi_c$ is the work function of the cathode material. The steps of how the energy is transferred to the surface are shown in detail in the figure. Some of this energy is used up for the emission of more electrons. Part of the energy is conducted into the solid, and part goes into melting and /or vaporization of the surface, i.e., erosion.

At the anode the phenomena are very much simpler (Fig. 4). A few positive ions may be produced in the anode fall region. These drift toward the plasma, and do not affect the energy transfer to the anode. The energy here goes mainly into conduction and erosion.

| CATHODE | CATHODE FALL REGION | PLASMA |
|---|---|---|

**TIME** ↓

Electron is emitted from cathode $(-e\phi_c)$

Electron is accelerated in cathode fall

Electron collides with neutral

Collision results in ionization

Ion is accelerated in cathode fall
Electrons drift through plasma toward anode

Ion is neutralized, giving up to the

cathode its ionization energy $(eV_i)$ and

the kinetic energy it gained in the

cathode fall region $(eV_c)$. It also

gains one electron.

Energy transferred to cathode per ion:   $E_c \simeq e(V_i + V_c - \phi_c)$

Fig. 3. Schematic of energy transport from
the arc to the cathode surface.

| PLASMA | ANODE FALL REGION | ANODE |
|---|---|---|

Electron drifts toward the anode

Electron is accelerated in anode fall

Electron reaches the anode surface, gives up

the kinetic energy gained in the anode fall $(eV_a)$,

and "falls down" the anode work function barrier $(\phi_a)$.

Energy transferred to anode per electron:   $E_a \simeq e(V_a + \phi_a)$
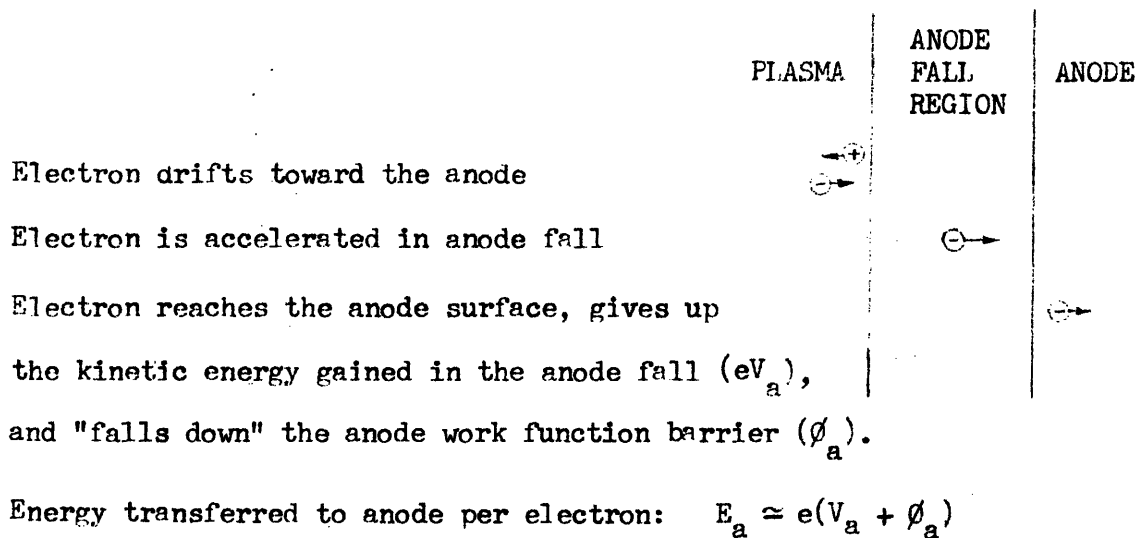
Fig. 4. Schematic of energy transport from the arc to the anode surface.

We hasten to stress the fact that the above treatment is highly

oversimplified, and its primary purpose is to give the reader who

is not very familiar with the subject a simple sketch of the main

processes in the arc.

A number of theories have been proposed to explain the mechanism

of erosion in EDM.  These are discussed in the next section.

## 1.2  Mechanism of Erosion

The <u>Electric Field Theory</u> is proposed by Williams and

coworkers.[7,8,9]  They suggest that erosion from the anode is primarily

a result of positive metal ions being ripped out of the material by

the intense electric fields caused by the extremely high current

densities at, about, and beneath a point on the surface of the material.

According to this theory the size of the detached fragment is limited

by the fact that the normal component of current density decreases

below the surface due to spreading of the current.  Using single

discharges they have shown experimentally,[7] for ON-times* ($t_{on}$) of

the order of $10^{-6}$ seconds and peak currents (I) below 23 amps, that

the volume of each crater, $\mathcal{V}$, is given by:

$$\mathcal{V} = K_1 \; t_{on} \; (I)^{3/2}$$

where $K_1$ is a material constant which is inversely proportional to the

tensile strength of the material.  In support of the theory the authors

give correlations between crater volume and tensile strength.

* ON-time refers to the pulse duration, i.e., $t_{on}$ in Fig. 1.

-18-

Probably the strongest objection to this theory is the fact that
it cannot possibly explain the very substantial erosion which often
occurs at the cathode, where the electric field would tend to force the
metallic ions into the electrode. Williams himself is fully aware of this,
as pointed out in one of his patents.[10] When discussing the erosion
mechanism at the cathode, he[8] shows that crater volume correlates with
material melting point, so here he is implicitly assuming the validity
of the Thermal Theory which is discussed later. Furthermore, it appears
to us that Williams' own data on anode erosion[7] correlate  just as well
with material melting point as they do with material tensile strength.

Mandel'shtam and Raiskii[11] are the proponents of the Vapor Jet or
Flare Theory. They state that the electrode metal vaporizes in the form
of luminescent jets or flares, which are ejected in a normal direction
with respect to the electrode surface  with a velocity that attains
several thousands of meters per second. The trajectory of these flares
need not coincide with that of the discharge channel. The properties of
the flares - high propagation velocity and elevated pressure - render them
similar to the explosion products of explosives. It follows from this, so
say the authors, that these flares must naturally be capable of destroying
obstacles encountered by them, and especially the opposite electrode.
Hence electro-erosion is not directly connected with the electric
discharge, but is a secondary process, caused by the mechanical action
of metal-vapor jets produced by the discharge. Flares from the cathode
are more powerful  than flares from the anode, and that is why the anode
usually erodes more. When they insert an object in the path of the vapor

jets, that object is eroded rather than the opposite electrode. This last, and some of their other data, is hard to explain by other theories, but the flare theory of erosion is nowadays given little consideration.

Maecker[12] also observed vapor jets from the electrodes, and explains their presence by the self magnetic field of the arc (the pinch effect), but he says nothing about any erosive action of these flares.

One strong objection to this theory is the fact that the tool material which has the greatest resistance to erosion by EDM also has the lowest mechanical strength (graphite).[1] Besides, as has been pointed out by Rudorff,[13] it is not easy to see why, if the cathode is the source of the flares, this electrode should show the least erosion.

The Thermal Theory proposed by B.R. and N.I. Lazarenko[14] has developed into what is today by far the most widely accepted theory of the erosion mechanism in EDM. We may interpret this theory as follows:

The energy from the arc is transported to the surface and causes the surface temperature to increase. As mentioned earlier, this transport of energy is carried out primarily by electrons to the anode, and by positive ions to the cathode.[6] After some time,[15] $t_m$, the surface reaches its melting point and begins to melt. If the ON-time of the pulse satisfies the condition $t_{on} < t_m$, then no melting occurs, and no erosion of the surface occurs by this mechanism. If $t_{on} > t_m$, some material may melt. A number of possibilities now present themselves:

1. The molten material is immediately removed; or

2. The molten material is removed after the power is shut off; or

3. The molten material is not removed, and resolidifies after the power is shut off; or

4. The molten metal is further heated until some or all of it is vaporized.

The true story appears to be a combination of these.*

Exactly how the molten metal is removed is still an open question. The Lazarenkos[16] suggest that the current flowing through the molten metal exceeds a definite critical magnitude and creates a selective displacement of the molten metal. By using highspeed photography, up to 500 000 frames per second, Zolotykh et al.[17] show that an expanding gaseous cavity forms between the electrodes. Continuous expansion of the gas cavity leads to an abrupt pressure drop (below atmospheric) within the cavity. And this, they claim, causes gas dissolved in the metal to be liberated, resulting in emission of vapor and ejection of drops of metal from the hole, some time after the current has ceased. Zingerman,[18] working with discharges of considerably longer duration, claims that the metal is removed during the discharge. However, these last two observations are not necessarily contradictory.[19]

The main strength of the thermal theory seems to lie mainly in the fact that nobody has been able to raise any valid objections to it, and it has been found by a very large number of independent

---

*Graphite is an important exception. Since this material cannot exist as a liquid at pressures below 100 atmospheres[15] it is more likely that graphite sublimes directly from the solid state. Observation of the erosion products suggests that some erosion of graphite may occur also in the form of flaking (Appendix J).

-21-

investigators[1] to explain the erosion observed at both cathode and anode. The shape of the erosion products (hollow spheres) also strongly supports the theory.

## 1.3 History of EDM.

As far back as 1762 Priestly[20] observed the erosion of material by spark discharges. In 1766 he discussed and illustrated erosion craters on metal knobs in a letter[21] to a friend. Since the beginning of this century, colloidal solutions have been produced by electric pulverization of electrodes in a liquid. Rudorff[13] has discussed this, and also some patents awarded in the U.S. and Great Britain during the thirties for sawing metal by means of continuous or interrupted DC arcs. Interruption was obtained through poor contact. In 1942 Burnett (U.S. patent 1947) proposed the utilization of interrupted arc discharges between a vibrating tool electrode and an immersed workpiece for the removal of broken taps and reamers.

However, up to that time the controlled erosion of a workpiece in such a way that it could truly be called machining had not yet been achieved. Also, the erosive effect of electric discharges was better known for the harmful part it plays in a number of practical applications of the discharge. It leads to intensive destruction of high-voltage switches, relay contacts, internal combustion engine spark plugs, and other discharge equipment.[11] It was, in fact, research work on electrical contacts that brought about the circumstances which led to the modern concept of electrical discharge machining as we know it today.

In a recent paper B.R. Lazarenko[22] recounts these circumstances. In 1942, he says, at the All-Union Electrotechnical Institute in Russia, N.I. Lazarenko conducted an experiment on electrical contacts with the goal of finding out the change of the electrical erosion of metals due to the current density on the contacting surfaces of the electrodes. On carrying out this experiment, the researcher found that the copper cathode always cuts deeply into the anode for a number of different anode materials. It was noticed that the cathode not only cuts into the anode, but in so doing very accurately copies into it the geometric form and size given to the cathode. Working together on this discovery, and sometimes in conjunction with others, B.R. and N.I. Lazarenko rapidly developed the art of EDM. Their work has since appeared in a long series of publications, starting in 1943.[23] One reason for the rapid development of this discovery is that Russia at that time was hampered by a lack of industrial diamonds[1] for production of war material.

EDM was first tried in Japan by S. Hoh[24] in 1948. A review article by H. Kurafuji (1964)[25] summarizes the considerable research carried out there since that time. During the fifties EDM also developed in Europe and the U.S. In the early sixties a comprehensive study of EDM, including numerous improvements, was carried out by the Cincinnati Milling Machine Company[1] for the U.S. Air Force. A concise description of the process and some of its problems has been given by Cook (1965).[4] The present state of EDM has been summarized in a series of papers[2] and in a book[3] by Mironoff.

At the present time electrical discharge machining has developed

-23-

to the stage where Russia[22] and Japan[26] claim erosion rates in steel of about 13 and 10 $cm^3$/min respectively. Twice the first rate has been claimed in this country,[27] and it has been predicted[28] that by 1970, 5 to 6 % of all machining will be carried out by EDM.

## 1.4  Present Applications

Any list of EDM applications would soon be obsolete, so the purpose of this section is not to present an exhaustive discussion, but rather to indicate the wide range of applications in use today. First let us point out that size presents no limitation. Applications range from the making of stamping or forging punches and dies used in the automotive industry and weighing several tons, down to the manufacture of tools for watchmaking[3] or for the cutting of single crystals.[29] Such delicate work is possible because the tool need never be in physical contact with the workpiece so no mechanical force is transmitted. Machining accuracy of 2 microns* and slots of 7 microns width can be cut. Surface roughness down to 0.2 microns is obtainable, and the depth of the affected layer need be no more than 1 micron[22]. EDM has also been applied to certain unique processes which are generally unattainable by other machining methods; number 2 in the list below is an example.

Here are some of the present day applications:[3,22,29,30]

1.  Drilling of holes down to a few hundredths of a mm diameter.

2.  Making holes with curvilinear axes, and a cross section of any complexity.

3.  Manufacture of single-piece metallic nets and meshes.

---

*micron = $10^{-6}$ meter $\simeq$ 0.04 mil (thousandths of an inch).

4.  Fine cutting with moving, thread-shaped electrode.

5.  Grinding, external and internal.

6.  Cutting of threads or helical profiles.

7.  Rough cutting of metal.

8.  Preparation of specimens with different crystallographic orientations from the same single crystal.

9.  Manufacture of all kinds of forging dies, drawing dies, slotting dies, molds, pressing forms and stamping instruments.

10. Cutting of complicated profiles.

11. Cutting of fine slots in discs for molecular beam studies.

12. These applications all refer to the machining of materials which are conductors of electricity, but recently it has been possible even to apply the process to the drilling of 1 micron diameter holes in glass.[31]

13. Yet another application is that of hardfacing.[32,33]

A list of illustrated applications is included in Mironoff's book.[3]


## 1.5 Purpose of Present Research Program

The main objective of this thesis is to advance the present knowledge and understanding of electrical discharge machining. This is an extremely broad and complex subject, covering a long list of independent and dependent variables.[34] We are considering only a small part of the whole problem. Some aspects of the problem have been considered by other members of our research group. These include the study of heat transfer in EDM,[15,34] characteristics of electric arcs,[35] and erosion by single discharges.[19] Erosion characteristics of different materials, and the

-25-

effect of material transfer between the electrodes have also been studied.[34] In the present thesis particular emphasis is placed on explaining the surprisingly low anode (tool) wear obtained in "NO WEAR" reverse polarity EDM. This effect is often referred to as the "polarity inversion," a term derived from the observation that with increasing pulse duration the larger removal shifts from the anode to the cathode (similar electrode materials).

A substantial body of EDM research from several different countries has accumulated over the past quarter century, but due to the large number of variables involved the data often appear contradictory. This is mainly because the conditions of the different experiments are seldom fully specified and probably not kept the same, so comparisons between them are hardly very meaningful. However, in spite of this the data are usually in much better agreement than the theories proposed for the purpose of explaining the data. An example is the polarity inversion referred to above which we shall now consider in some detail.

A number of investigators have observed the polarity inversion, and they have attempted to explain it in different ways. Mandel'shtam et al.[11] state that the anode erosion decreases with increasing interelectrode distance, and this is due to the decrease in the erosive efficiency of the cathode vapor jets which cause the erosion at the anode. Holm[36] has observed the same effect and explains it by saying that as the gap increases, the arc spreads so that the anode spot size becomes larger and more conduction cooling of the anode surface occurs, resulting in less anode erosion. Zingerman et al.[48] have a different explanation. They state that for a constant arc power, as the interelectrode distance increases, the voltage drop in the plasma becomes an increasing fraction of the arc voltage, so less power is left

for the anode. The Lazarenkos[37] state that there is an inversion boundary between spark and arc discharges, with anode erosion prevailing during the spark, and cathode erosion being most significant during the arc. They apparently refer to continuous arcing over a long time duration, a mode of operation which is highly undesirable in EDM. The most recent and perhaps most interesting theory of the polarity inversion is proposed in a paper by Pahlitzsch et al.[38] Their theory appears to be reconcilable with the Lazarenkos' observations. They do not introduce the concept of interelectrode distance, but suggest that anode erosion occurs primarily early in the discharge due to electron bombardment; ionization increases with time during the discharge, and therefore cathode erosion gradually increases due to increased positive ion bombardment. Figure 5 shows schematically their view of electron and ion current as a function of time, and the theory they present seems to explain their data quite well. However, we feel that several points in their discussion are contradictory to arc theory. According to Somerville,[6] Ecker,[39] Kesaev[40] and many others, in the anode fall region near the anode surface the whole current is carried by electrons. Near the cathode surface the
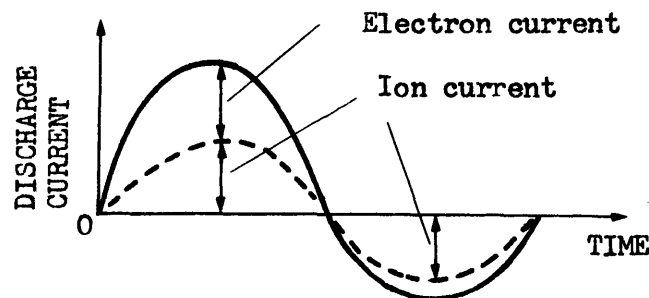


Fig. 5. Schematic of ion and electron current during pulse according to Pahlitzsch et al.[38]

major part of the current is carried by electrons, but a considerable fraction is carried by positive ions. These ions are essential from the very early stages of the discharge since they supply the necessary conditions for emission of electrons at a high current density from the cathode. The only way* that emission from the cathode is possible without heating (thermionic emission) is for an extremely strong electric field (field emission) to be present (Appendices A and C), and this field is supplied by the net positive space charge due to the incoming ions in the cathode fall region.[41] A very small change in this ion current can make a very large change in the electron current.[42] Furthermore, the authors[38] say that considerable cathode erosion occurs during the second half-pulse because by this time the ion current is quite high. But it is obvious that the plasma must be deionized after each discharge, otherwise continuous arcing will result, and this clearly cannot be permitted if controlled erosion is the object. It is not clear from their paper whether Paulitzsch et al. are discussing single discharges or continuous machining, and in the first case absence of rapid deionization would not be a problem, but for continuous machining it certainly would.

In view of these conflicting theories it is evident that more work is required in this area. We shall propose a model to explain "NO - WEAR" EDM based on the concept of interelectrode distance. Most of the work carried out in this thesis can be used for testing the model, and seems to support it. We do not suggest that our model is correct in every detail, but it is helpful for explaining the data, and we believe it to be based

---

*An exception is the very short arc, of the order of one mean free path, where electrons can strike the anode without undergoing any ionizing collisions with atoms. This plasmaless arc is not important in EDM where considerably longer arc distances are involved.

on a sound theoretical basis, and hope that it will serve to aid in the understanding of EDM.

## 1.6  Proposed Model

In this section we shall propose a qualitative model to explain the changes in wear ratio* that occur as a result of changing the machining conditions in EDM. The assumptions involved in the model are discussed in chapter 4. The predictions from the model are tested throughout the thesis, and the results are summarized in chapter 6.

Assumptions:

1.  The power density at the anode surface decreases as the interelectrode distance increases.

2.  Material transfer to the anode increases as the interelectrode distance increases.

3.  Larger interelectrode distances are brought about at higher pulse energies due to increased material removal per pulse.

The first assumption is a result of the arc spreading with distance from cathode to anode.[36,43,44] It results in a prediction of lower anode wear and therefore lower wear ratios in reverse polarity, where the tool is the positive electrode. The second assumption also predicts lower anode wear at larger interelectrode distances because a plated layer on the tool will tend to protect the tool against erosion.[34] The third assumption is illustrated in Fig. 6 below, and may be tested directly by experiment.

* wear ratio - the volume of material eroded from the tool per unit volume of material eroded from the workpiece.
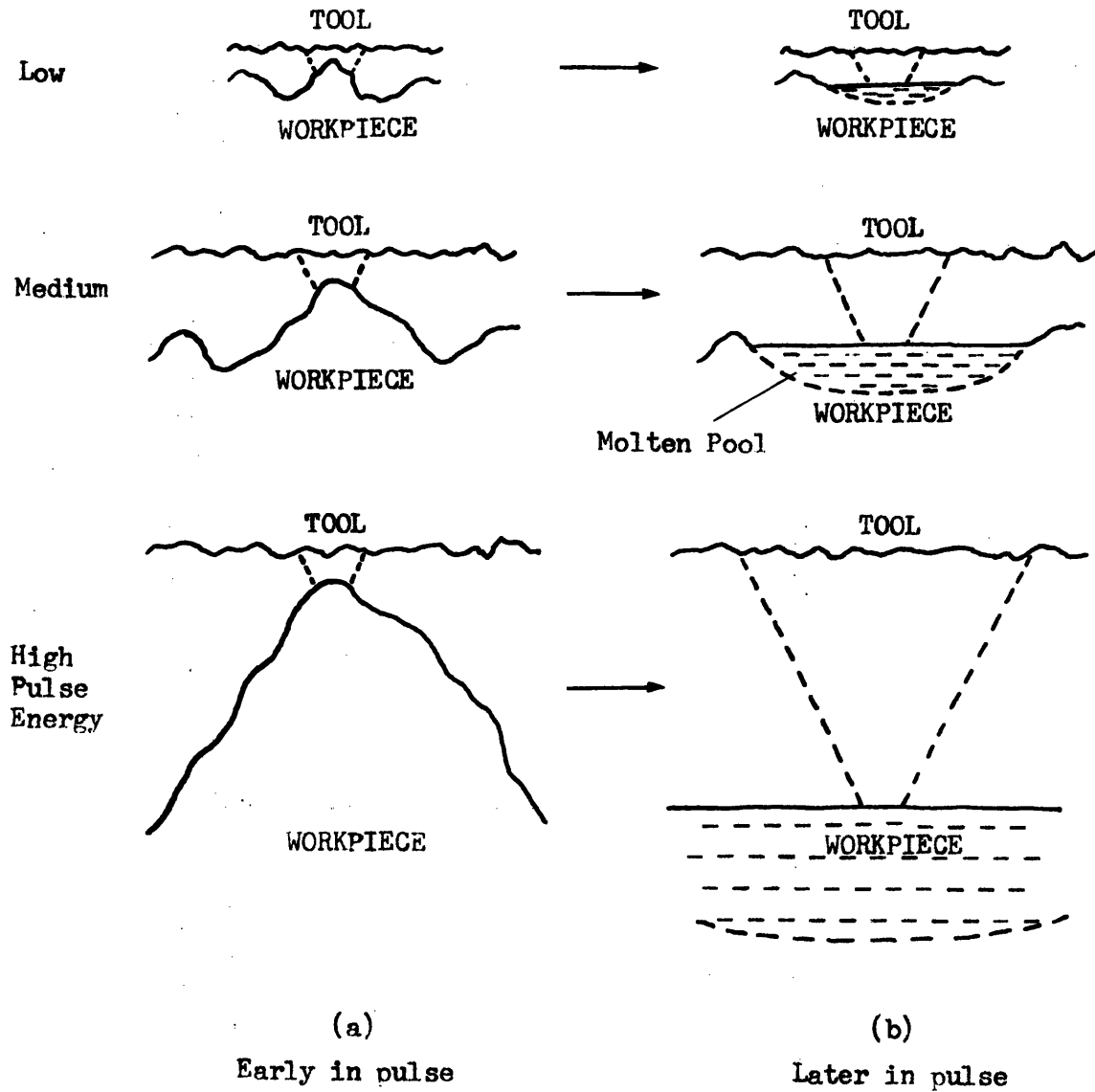
Fig. 6.  Schematic of how, for a given workpiece material, higher
         pulse energies result in increased arc lengths.


Figure 6 represents an effort at illustrating part of the model.
It indicates how the arc length may vary during a particular pulse, and
between pulses of different energies. It should be pointed out that the
above model is a considerable oversimplification of the actual process.
For example, it is implicitly assumed in the model that the discharge
will occur where the physical distance between the electrodes is the

shortest. This is not necessarily so because of inhomogeneities in the EDM fluid; in particular, particles may bridge the gap and cause discharges between points which are far apart. This is known to occur along the sides of the tool,[2] across the overcut, and may also occur in the spark gap when the gap is preset to be large, and large particles are injected (section 3.3), so it might also occur during normal machining conditions. Furthermore, it is clear that in any given region of the gap, the distance between the electrodes must be at least as large as the diameter of the largest particle in that region. But will such a particle force the gap to be larger than the particle, or will the position of the electrodes at that place force the particle to be smaller[*] than the gap? Also, the simple picture of the spreading arc is oversimplified (Fig. 6). First of all, there are time dependent factors involved in the plasma, and secondly, there may also be some contraction near the anode. These factors will be discussed in more detail later. The model assumes that the volume of material removed per pulse is the factor which determines the gap size. How is this in general accomplished? Clearly, it is the volume of material per pulse that determines the surface roughness and therefore the size of the protrusions, and it must also set an upper limit on the size that the eroded particles can obtain, but which of these two factors, if any, plays the most important role in controlling the gap size?

---

[*] It is difficult to imagine a particle growing to be larger than the gap at that particular point. And yet, if several particles in succession bridge the gap, the overall effect would probably be to force the tool to retract.

Being now aware of some of the simplifications involved in the model, let us return to the three assumptions stated above, and see what predictions can be made.

Predictions:

1. The average interelectrode distance should increase with increasing energy per pulse, i.e.,with:

    (a)  decreasing frequency,

    (b)  increasing duty cycle, and with

    (c)  increasing arc current.

2. In reverse polarity the wear ratio should decrease with increasing energy per pulse, i.e., with:

    (a)  decreasing frequency,

    (b)  increasing duty cycle, and with

    (c)  increasing arc current.

3. The volume of material eroded per pulse should be determined by the pulse energy.

4. If the size of the surface protrusions govern the gap size, then these should be of the same order as the gap.

5. If the size of the particles govern the gap size, then these two sizes should be of the same order.

6. If the illustrations in Fig. 6 are correct, then the initial breakdown gap should not change much with changes in the pulse energy.

7. If it is possible to artificially force the gap to be large, then a reduction in the anode/cathode wear ratio should result.

## 2. EXPERIMENTAL APPARATUS AND PROCEDURE

### 2.1  Basic EDM Equipment

The apparatus consists primarily of an EDM machine, a power supply,
and miscellaneous measuring devices, including a dual beam oscilloscope.
A schematic of the basic equipment is shown in Fig. 7.

Electrical Discharge Machine. The EDM machine used in these experiments
is an Elox HRP - 63 unit. This is a rigid and accurate machine capable of
close tolerances. The workpiece is located inside a workpan, under at
least two inches of EDM fluid (often called the "dielectric"). Eloxol # 13,
which is a commercial kerosine based fluid especially developed for EDM,
was used in all the experiments. The tool is attached to a ram whose vertical
motion is controlled by a servomechanism which in turn is controlled by the
distance between the electrodes (section 1.1). The machine also has a pump
and filter for providing a steady supply of clean EDM fluid to the electrode
gap. Another pump is provided for quick filling of the workpan.

Power Supply. At open circuit, square voltage pulses of about 65 volts
magnitude are supplied from an Elox SSD 400 NW experimental power supply.
This unit is capable of supplying pulses at frequencies from 0.34 kc to
130 kc, and arc currents up to about 400 amps. The duty cycle (% ON-time)
can be varied continuously from about 8% to 90%, except at very high
frequencies where the maximum duty cycle is lower. The power supply also
controls the feed rate of the servomechanism, so that a more or less
constant separation between the electrodes can be maintained. If a short
circuit is formed across the gap, the voltage drops and the servo
causes the tool to be retracted so that contact is broken. The voltage

-33-

EDM MACHINE

FEED SERVO

TOOL

WORK - PIECE

FILL PUMP

FILTER

PUMP

POWER SUPPLY

OSCILLOSCOPE

EDM FLUID STORAGE TANK
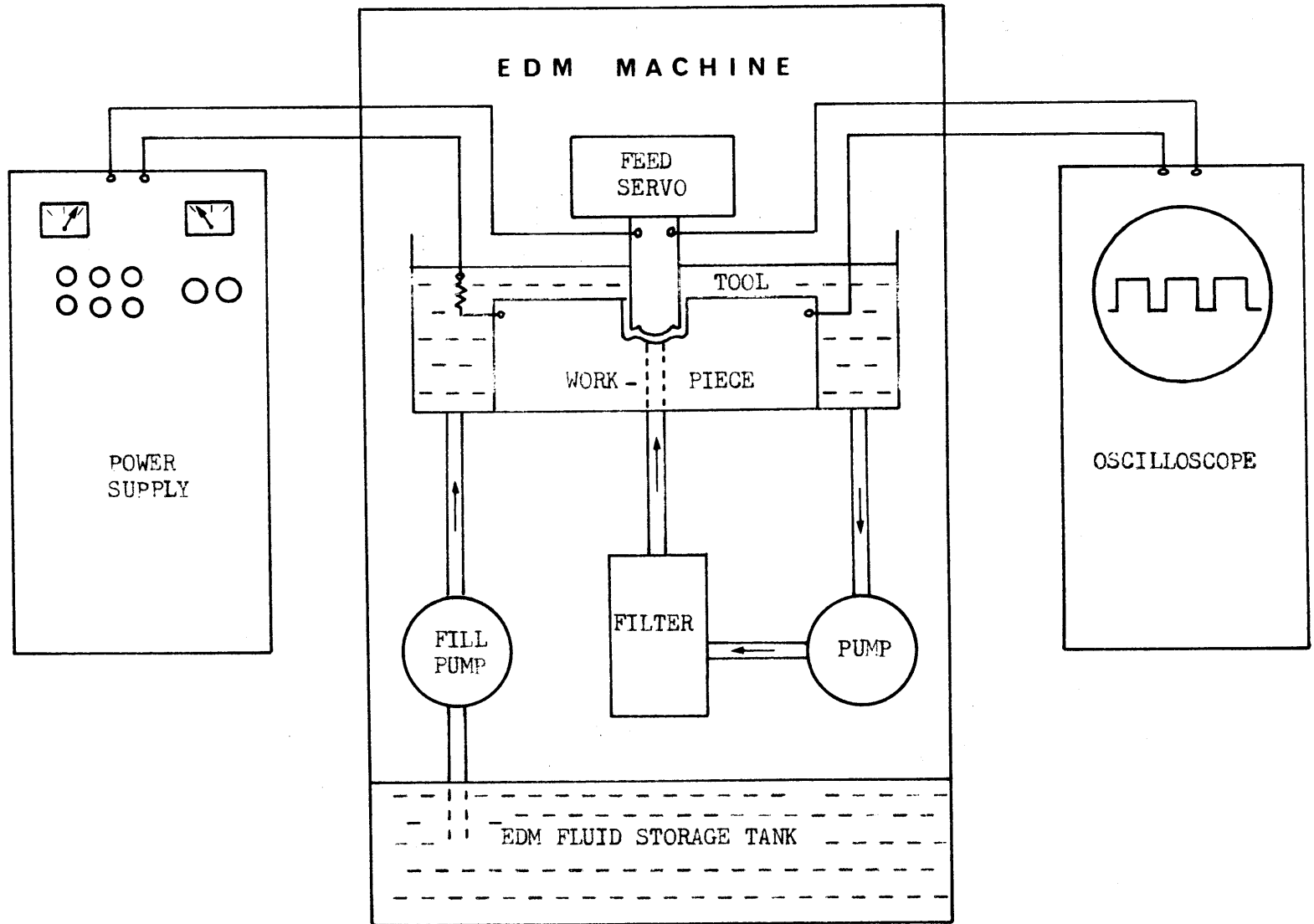
Fig. 7. Schematic view of basic EDM Equipment.

pulses remain square only at open circuit. When a discharge occurs the voltage rapidly drops to a value somewhere between 20 and 40 volts (Fig.15).

Tool and Workpiece Description. In the erosion rate and wear ratio test series, the geometry shown in Fig.8 was used. The tool is a cylindrical rod of 1.904 cm diameter. The workpiece is a block of square cross section, and has a 0.476 cm diameter hole drilled through the center to permit the flow of EDM fluid. This geometry permits good flushing. However, there is a pressure drop up along the sides of the tool and this makes it difficult to obtain accurate pressure measurements across the gap. Consequently a somewhat different geometry was chosen for the measurement of interelectrode distance, since a flow rate technique was used. In this geometry both tool and workpiece are cylindrical rods (Fig. 9) of 1.904 cm diameter. Both cylinders have 0.476 cm diameter axial holes.

The material of the workpiece is tool and die steel, H-13, produced by the Carpenter Steel Company under the number 883. Unhardened steel was used, but this has roughly the same erosion characteristics as hardened steel.[5] The tool material mostly used in these tests is Kost Kutter # 8, a commercial graphite electrode produced by the Speer Carbon Company. In a few tests, 99.9 % pure copper was used as tool material, since erosion craters show up much better on a copper surface.

2.2  Additional Equipment

Particle Injection. Large conducting particles of steel or tin were injected into the gap in an attempt to force the gap to be large. This requires some additional equipment (Fig.10). The particles are suspended in a rotating pyrex cylinder, 17 cm diameter by 43 cm long. The cylinder

-35-

WORKPIECE

3.8 x 3.8 x 1.3 cm

or 2.5 x 2.5 x 2.5 cm

TOOL

1.904 cm diam.

0.476 cm diam.

EDM Fluid Flow
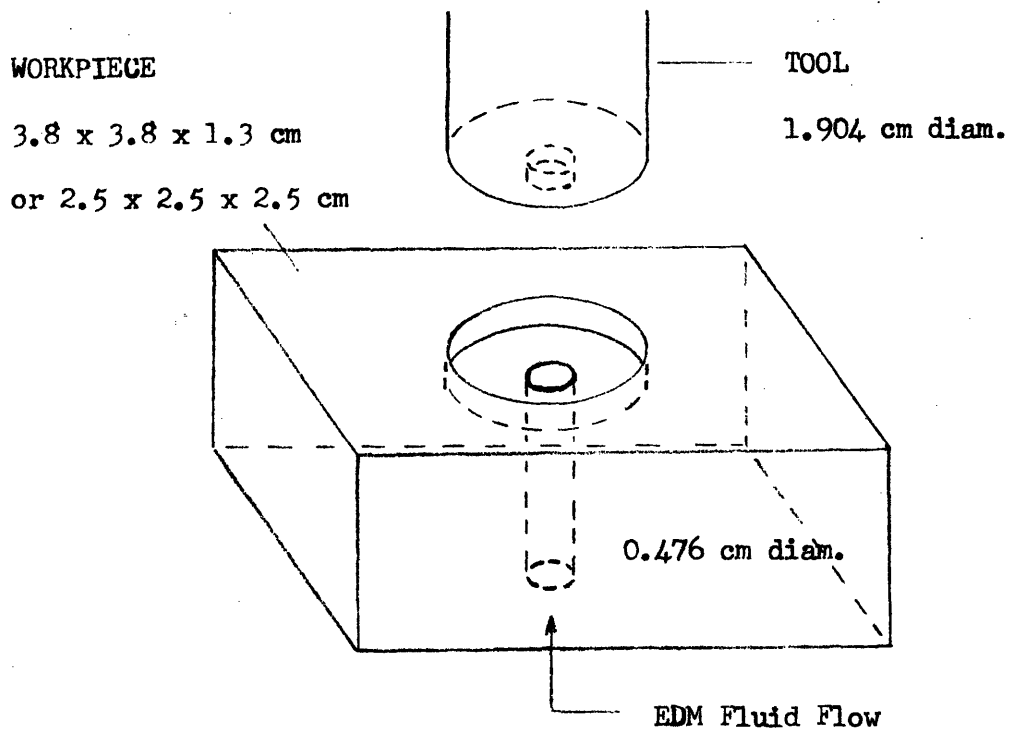
Fig. 8. Geometry of tool and workpiece used in erosion rate tests.

to mercury manometer

TOOL

1.904 cm diam.

WORKPIECE

1.904 cm diam.

EDM Fluid Flow
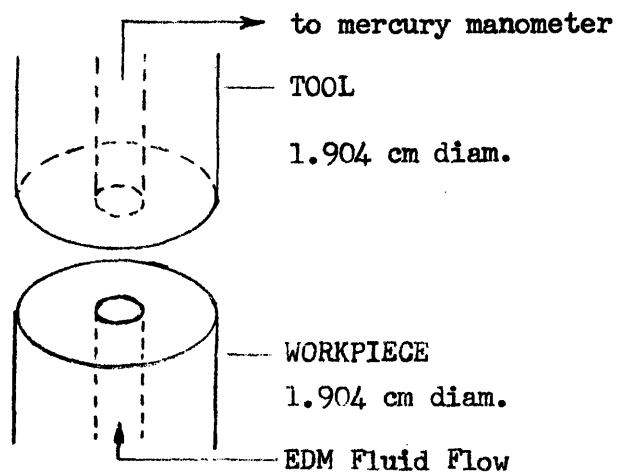
Fig. 9. Geometry of tool and workpiece used in the
measurement of interelectrode distance.

-36-
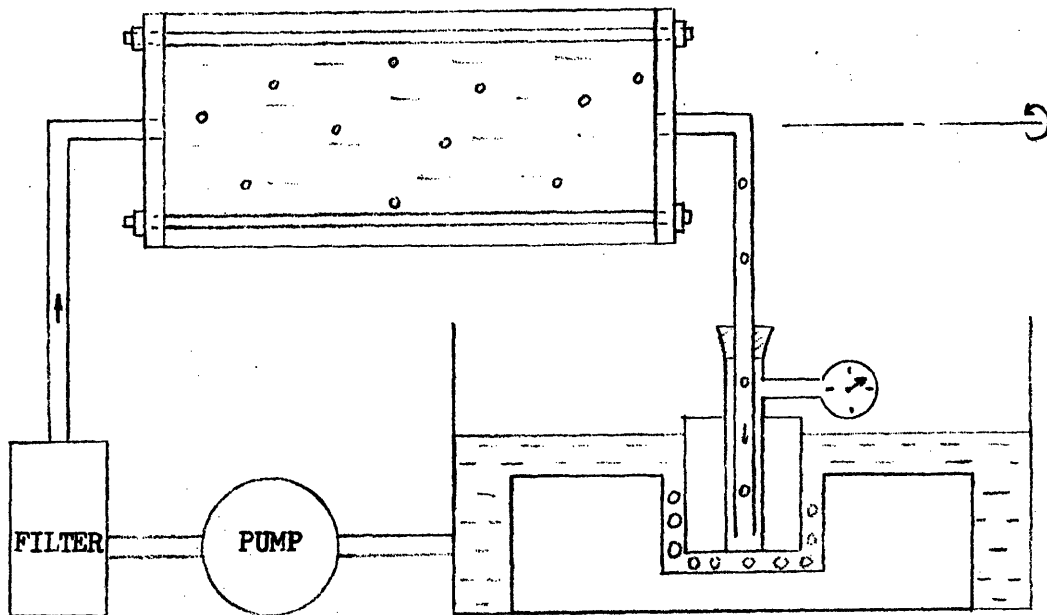
Fig. 10. Schematic view of particle injection equipment.

has plexiglass flanges at the ends and is held together by four threaded
aluminium rods. A 1/20 H.P. electric motor, geared down by two V-belts,
drives the cylinder at about 12 R.P.M., a speed of rotation at which
the particles remain well suspended in the fluid. Clean oil is supplied
to the cylinder through a pump and filter at any desired pressure. The
particles flow through a teflon tube, 0.15 cm diameter and 100 cm long,
through the tool and into the gap. This was found to be the best tube
size. Too thin a tube does not allow sufficient flow, and in a much wider
tube the particles settle out because the fluid does not move fast enough.
To further prevent particles from settling out, most of the tube is
positioned vertical, and with the 0.15 cm tube, good particle feeding
is achieved.

The particle concentration is measured by allowing the fluid with

particles to fill a graduated cylinder and allowing the particles to settle
out. If the particles appear to occupy, e.g. 0.1 % of the cylinder, then
that is taken to be the particle concentration. Since there is fluid in
between the particles, this is not a true concentration, and we shall
refer to it as the % concentration by apparent volume.

Particle Collection. The equipment shown in Fig.11 was used for particle
collection. In this case the EDM fluid is fed through a hole in the tool.
The workpiece is held in place by a clamp inside a 15 cm by 15 cm plexiglass
box, 7.5 cm high, from which fluid can escape only by overflow through
the channel shown on the left. The particles settle in the bottom of the
box, and are later removed by washing them out of the box and into a
container, or sieve. Some of the smaller particles remain suspended in
the fluid and get lost. At high pulse energies about 60 % of the material
eroded is collected. At very low pulse energies only about 5 % is collected.
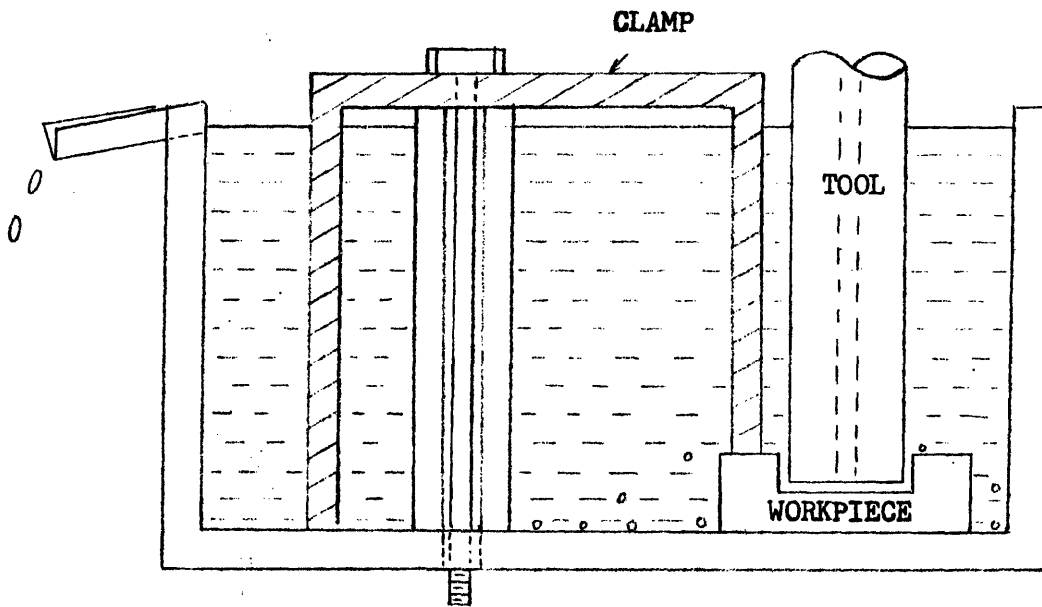


Fig. 11. Particle collection equipment.

Particle Size Distribution. Two different approaches were used: microscope, and sieves. Under the microscope the particles are placed on a sliding table. The motion of the table is controlled by cylindrical guides and a micrometer. A dial gauge is used to indicate the position of the table to the nearest 2.5 micron. The measurement of a particle diameter consists of lining up the cross-hairs in the microscope eyepiece in turn with the two extremities of a diameter of the particle, and noting the two dial gauge readings. This method is very accurate for obtaining the size of a given particle, but over 100 000 particles are formed in each run, and it is not easy to find a small but truly representative sample.

In order to make use of all the particles collected in each run, sieves of different sizes can be used. The particles are first transferred from the box in which they are collected onto the largest size sieve. By thorough washing with clean EDM fluid, the smaller particles pass through the mesh to the next largest sieve, and so on. Sieve sizes of 610, 330, 150, 74, and 44 microns were used. From each sieve the particles are then transferred to a filter paper in a Büchner funnel, and the fluid is removed by applying a vacuum under the funnel. Each filter paper is next weighed with and without the particles on an analytical balance, accurate to $10^{-3}$ gm. From these weights the particle size distribution is obtained.

## 2.3 Measurement of Interelectrode Distance.

The magnitude of the interelectrode distance (or gap) depends on how it is defined and on how it is measured. We shall distinguish between three different gaps: the electrical gap, the average flow rate gap or the geometrical average gap, and the arc gap. These are illustrated in Fig. 12.

TOOL
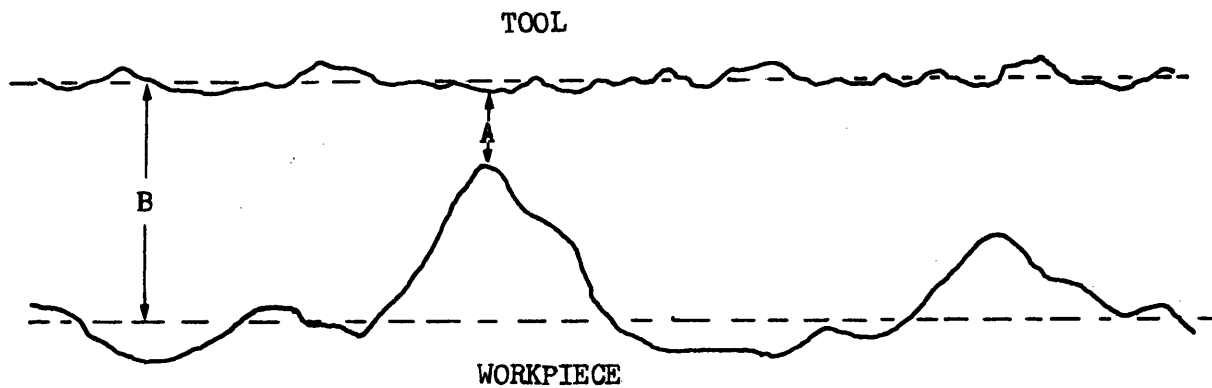


Fig. 12. Illustration of gap. A is the electrical gap and B the
average, or flow rate gap. The arc gap starts at a
value near A and ends up at about B.


The electrical gap, A, is usually of the order of $10^{-3}$ cm, and does

not vary much with machining conditions[*]. It represents the shortest physical

distance between the two electrodes, and indicates the point where the

next discharge is most likely to occur. It may be measured as follows:

Indicate the position of the tool at all times by means of a sensitive

dial gauge. While machining, suddenly turn the power supply off, and

note the reading on the dial gauge. Next, lower the tool manually until

electrical contact is made with the workpiece. The magnitude of the manual

advance of the tool corresponds to the electrical gap, and is obtained

from the dial gauge. Another method is to begin as above by turning the

power supply off, then back the tool off, turn the power supply on, lower

the tool again, and notice where machining resumes. The first method is

very sensitive to dirt in the gap, and may even indicate negative gaps, but

it usually yields readings from zero to about $3 \times 10^{-3}$ cm, with an average

value of about $1 \times 10^{-3}$ cm, independently of machining conditions

---

[*] As long as the applied voltage and the breakdown strength of the
fluid remain unchanged.

(Appendix I). The second method yields similar values, but is not very accurate since the applied voltage is now sufficient to cause breakdown in the fluid before contact is made.

The flow rate gap, indicated by B in Fig.12, is discussed in more detail in later sections. It may also be arrived at in different ways. Since surface roughness may influence the flow rate, we shall define the flow rate gap in the manner described below.

Consider the gap between two rough surfaces. Suppose that under a given set of conditions the flow rate of fluid through this gap is Q. This same flow rate could clearly also be obtained from a well defined gap between smooth electrode surfaces. For the size of the rough gap under consideration we shall report the size of the smooth gap that would give the same flow rate. We use this approach since the actual size of the rough gap could be defined in a number of ways. Hence, the term flow rate gap, as reported in this work, will refer to the size of the equivalent smooth gap. The gap thus reported is approximately equal to the gap that would be obtained if the whole surface were melted and the protrusions could fill up the crater holes (Appendix H). This gap would also be close to the gap obtained by geometrically averaging over the whole surface the physical distance between the two electrodes. Other ways of reporting the gap have been considered and discarded. We feel that this method is the simplest and best.

The arc gap is the actual physical length of the electric arc between the electrodes. This length starts at a value roughly equal to A, and as melting occurs it rapidly increases to a value of about B,

-41-

where it remains until the arc is extinguished. Appendix F shows that B is a much better value for the arc length than A, and is the value that is reported in this work. The importance of arc length is discussed in chapter 4, where the term "gap" or "interelectrode distance" refers to the arc length, and is taken to be equal to the flow rate gap. Alternate ways of measuring the gap are considered in Appendix M.

Theoretical Fluid Flow Rate. The radial flow rate of fluid, Q, for the geometry shown in Fig. 9 is calculated in Appendix H.

$$Q = \pi G^3 \Delta p / (6 \mu \ln(D/d)) \qquad (2-1)$$

where  G is the gap distance between the plane, parallel ends of the two electrodes.

$\Delta p$ is the pressure difference between the oil feed hole of the electrodes and a point just outside the gap (155 mm of Hg).

$\mu$ is the viscosity of the EDM fluid (9.3 centipoise at 30 $^\circ$C).

D is the diameter of the electrodes (1.904 cm).

d is the diameter of the oil feed hole (0.476 cm).

At constant pressure, viscosity, and geometry, Eq.(2-1) gives:

$$G \propto Q^{1/3} \qquad (2-2)$$

The straight line in Fig. 13 is obtained from Eq.(2-1). The other lines are obtained by the procedure discussed in the next section.

Experimental Flow Rate of EDM Fluid.  Machining here takes place inside a plexiglass box with an overflow channel (Fig. 14). While machining under some specified conditions, the power supply is

INTERELECTRODE DISTANCE, MICRON

$10^3$

$10^2$

$10$

REVERSE POLARITY

Tool: Graphite KK#8
Workpiece: Steel H-13

| | Freq. (kc) | Duty Cycle (%) | $I_{arc}$ (amp) |
|---|---|---|---|
| □ | 0.37 | 50 | 140 |
| O | 0.37 | 50 | 65 |
| △ | 9.0 | 50 | 80 |
| ● | 130 | 25 | 350 |

Theoretical
line from
Eq.(2-1)
(slope 1/3)

1.0          10          $10^2$          $10^3$

FLUID FLOW RATE, CC/MIN
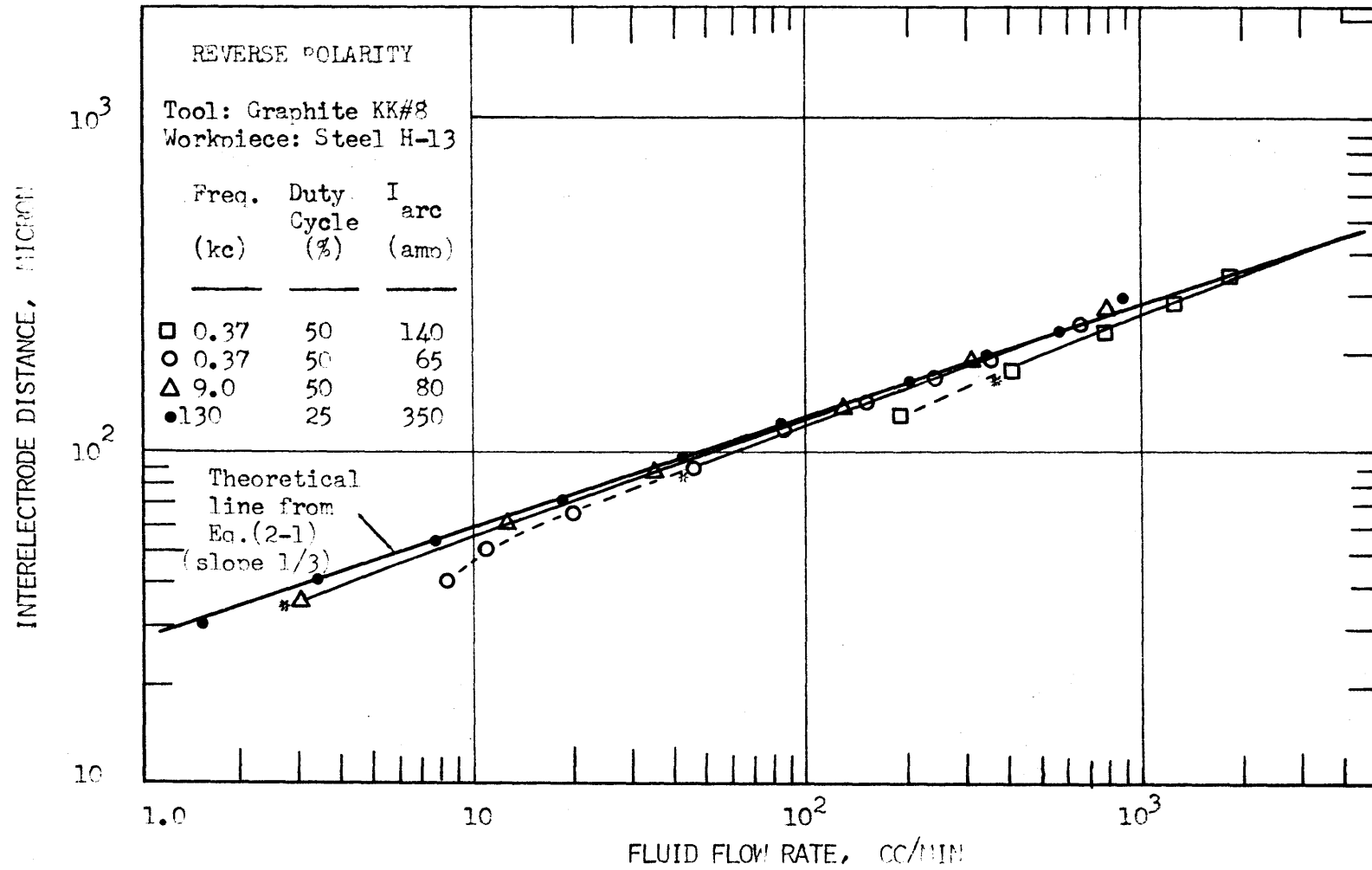
Fig. 13.   Experimental relationship between gap and fluid
flow rate, based on the results of Appendix H.
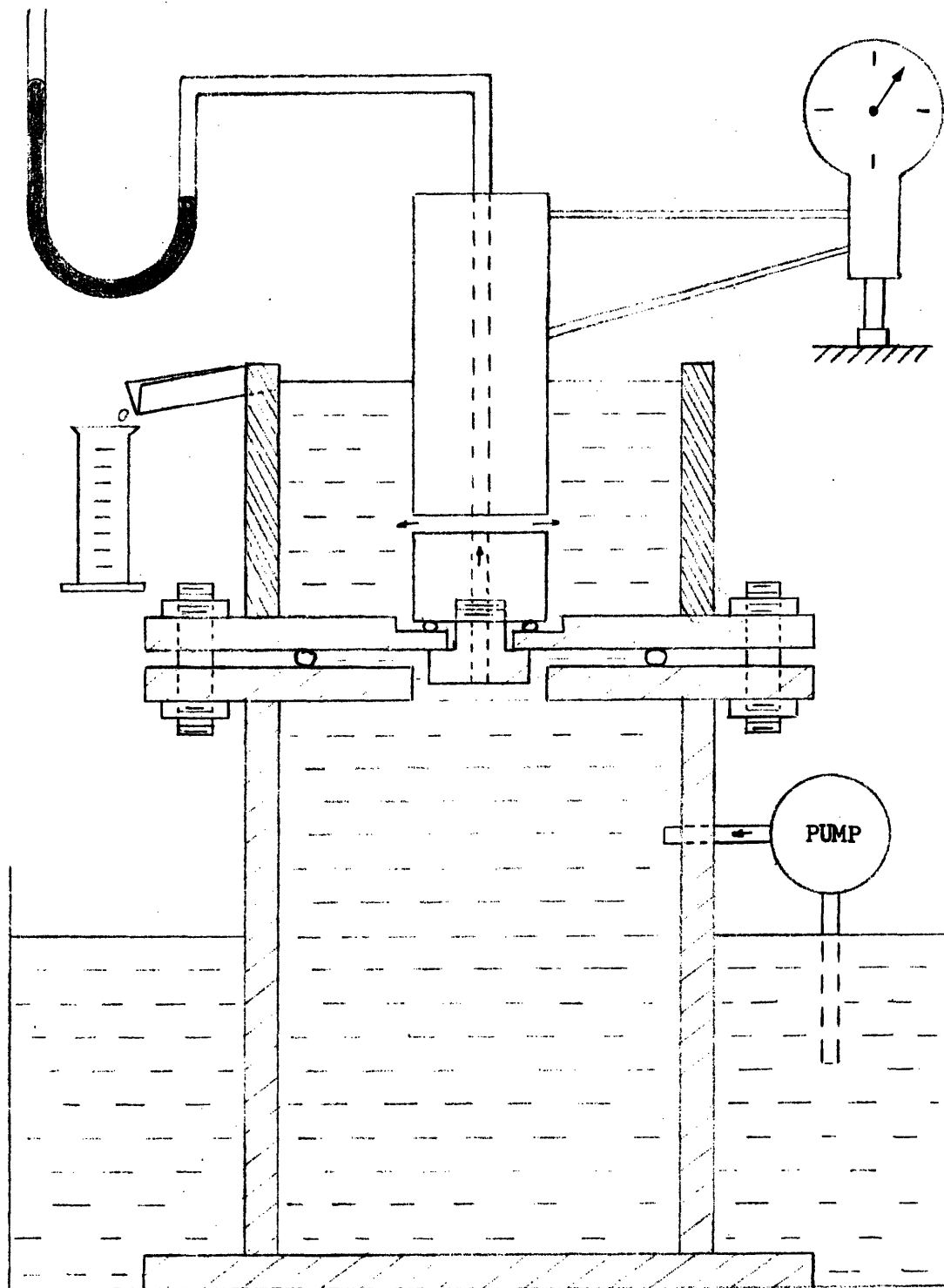
Fig. 14.  Schematic illustration of flow rate measurements.

suddenly shut off, and the position of the tool is noted on a dial gauge, accurate to 2.5 micron. The pump is then turned on and the tool is returned to the noted position. When conditions are steady, the flow rate is measured by allowing the overflow to come into a suitably sized graduated cylinder. The time required to fill the cylinder is noted. From this flow rate, $Q$, the size of the equivalent smooth flow rate gap may be obtained from the straight line in Fig. 13. For example, suppose the measured flow rate under a given set of conditions is 10 cc/min. We then go to Fig. 13 and obtain an equivalent smooth gap of 61.5 micron from the theoretical line. This value is then reported as the flow rate gap.

When the gap between two very rough surfaces is varied, calculations (Appendix H) indicate that for gaps which are small relative to the roughness, the relationship between gap and flow rate does not follow the pattern of Eq.(2-2), which, of course, was derived by assuming smooth surfaces. When the gap size is very large compared to the surface roughness, the relationship approaches Eq.(2-2) (Fig. H-2). On the basis of this information a guess of the absolute size of the rough gap may be made such that an experimental curve of gap vs. flow rate asymptotically approaches the theoretical line at very large gaps. The result of this approach is shown in Fig. 13. The star on each line corresponds to an actual set of machining conditions, and the rest of the line is obtained by manually varying the gap, taking position readings on a dial gauge, and measuring the flow rate. These curves show the deviation in flow rate between smooth and rough surfaces.

The temperature dependence of the viscosity of the EDM fluid is quite strong, and is considered in Appendix L.

Pressure of EDM Fluid. The pressure was measured by using a simple mercury manometer connected to the gap through a central hole in the tool (Fig. 9). This method gives an accurate measurement of the fluid pressure just where the fluid enters the gap. Where the fluid leaves the gap the pressure is very close to atmospheric. Almost all the tests were carried out with a pressure drop of 155 mm of Hg across the gap. The manometer was zeroed at zero flow rate with the plexiglass box full of fluid.

## 2.4 Additional measurements

Tool and Workpiece Erosion. For the electrode geometry shown in Fig. 8 the linear erosion on the tool and workpiece was measured at four different points about halfway between the inner and outer radii. An Ames No. 384 dial gauge, correct to $1 \times 10^{-3}$ cm, was used. Since very little rounding off of the edges of the electrodes occurred, the volume of material removed was obtained by multiplying the linear wear by the cross-sectional area. A few erosion tests were made with the geometry of Fig. 9 and in these cases the total length of the electrodes was measured before and after the test.

Frequency, Duty Cycle, and Arc Voltage. The variation of voltage (V) between the electrodes with time (t) was observed on a Tektronix Type 502A Dual Beam Cathode Ray Oscilloscope (Fig. 1). The frequency of the

pulses was obtained from the scope, and is simply the reciprocal of the total period of one pulse (Frequency $= 1/\tau$). The duty cycle, which is defined to be the percentage ON-time, may also be obtained from the oscilloscope (duty cycle $= t_{on}/\tau \times 100\%$). The oscilloscope sweep speed was calibrated using a Tektronix Type 181 Time – Mark Generator, accurate to 0.01%.

Current Measurements. Both time average current and arc current are measured. The average current is measured with a Weston D.C. ammeter connected across a 100 mV shunt in the line between the workpiece and the power supply. This ammeter was calibrated against a Hewlett Packard Model 412A DC Vacuum Tube Voltmeter. The arc current is obtained from the same shunt and is viewed on the second beam of the oscilloscope referred to above. Typical oscillographs of voltage and current are shown in Figs. 15 and 16 respectively. A storage scope was used for viewing individual current and voltage traces, whereas these pictures show traces from a number of superimposed discharges. The storage scope was also used to check that the Weston ammeter provides an accurate measurement of the time average current. The product of arc current, duty cycle and the fraction of the pulses put out by the power supply that result in effective discharges should equal the time average current. Under stable machining conditions the agreement is within 10%. For unstable conditions the ammeter reading varies considerably so an accurate comparison is no longer possible.
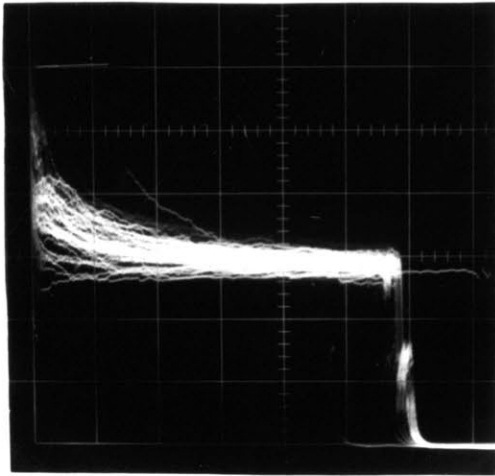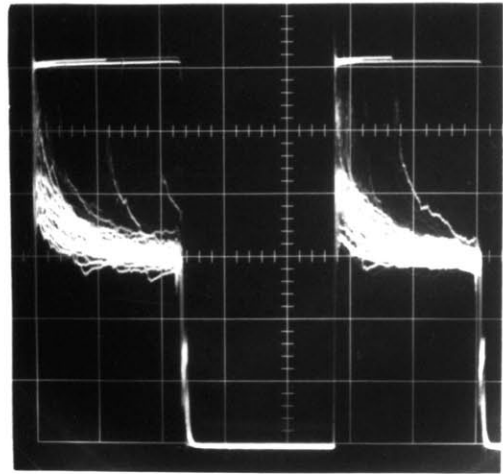
(a)                                        (b)

Fig.15.  Oscillographs of arc voltage:  Graphite cathode, steel anode.
         (a)  X-axis:  20 μsec/cm;   Y-axis:  10 volt/cm.
         (b)  X-axis:  50 μsec/cm;   Y-axis:  10 volt/cm.
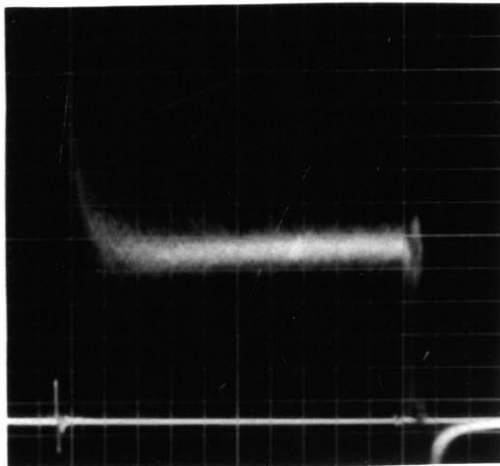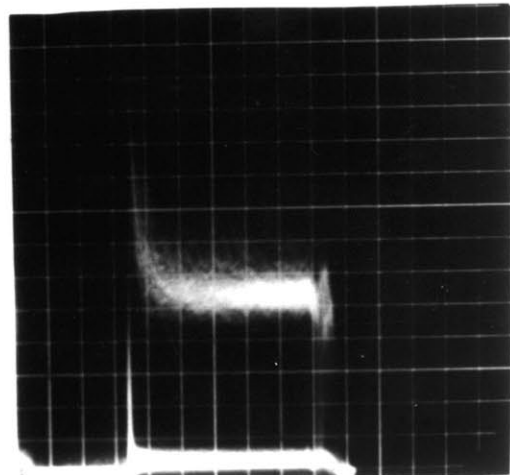


(a)                                        (b)

Fig.16.  Oscillographs of arc current:  Graphite cathode, steel anode.
         (a) and (b)  X-axis:  20 μsec/cm;   Y-axis:  20 amp/cm.

## 2.5 Production of Particles for Particle Injection Tests

In order to carry out the particle injection tests we had to obtain the necessary particles. One manufacturer quoted a price of $3.- per particle. Since several hundred thousand particles were required this price would unduly stretch our budget, so we decided to produce our own particles.

The particle collection equipment described in section 2.2 was used to collect a considerable amount of particles of steel and tin - separately. The sieves were then used for obtaining particles in the desired particle size ranges.

The steel particles were produced by machining with a positive graphite tool at a frequency of 0.36 kc, 50% duty cycle and 65 amps arc current. The tin particles were produced at a frequency of 9 kc, 50% duty cycle and 65 amps arc current; the other electrode was a graphite cathode.

# 3. EXPERIMENTAL RESULTS

This chapter briefly presents the data obtained under a wide variety of EDM machining conditions. The _independent variables_ tested are the polarity of the electrodes, the frequency of the electric pulses, the duty cycle, and the average current. Arc current is considered in the gap measurements. Two additional variables are used in section 3.3 on particle injection. These are particle size and particle concentration. Other independent variables are tool and workpiece materials, and type of EDM fluid. The first two have been studied by Viswanathan[34] and the last one by Kurafuji.[26] The materials used in the present work are graphite KK #8 as tool and steel H-13 as workpiece unless otherwise specified.

The _dependent variables_ discussed in this chapter are the erosion rates from the tool and the workpiece, the wear ratio, and the interelectrode distance (arc gap or fluid flow rate gap — see section 2.3). Other dependent variables are considered in chapters 4 and 5, where the data are discussed and interpreted.

## 3.1 Reverse Polarity Data

_Erosion Rate._ Figure 17 shows that the erosion rate from the workpiece at first increases with increasing _frequency_, goes through a maximum at about 10 kc, and decreases rapidly at higher frequencies. At the tool (anode) the erosion rate is very low at low frequencies (the "NO-WEAR" regime), but increases quite rapidly with frequency, and follows a pattern somewhat similar to the erosion rate at the workpiece. The peak in the tool erosion rate curve lies at about 30 kc, beyond which a gradual decrease takes place.
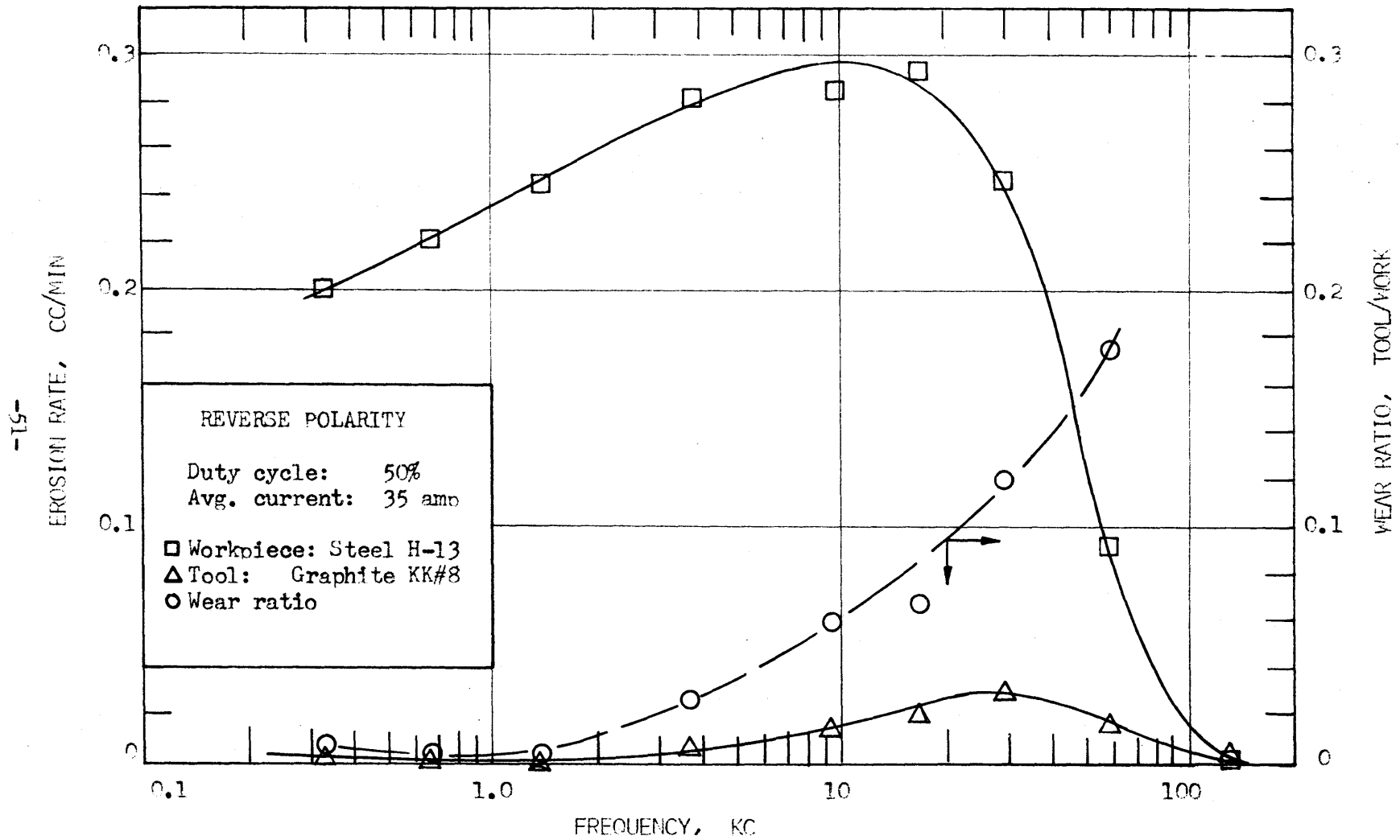
Fig. 17. Dependence of erosion rate and wear ratio on frequency: Reverse polarity.

The erosion rate from the workpiece remains approximately constant from 30 to 80% _duty cycle_, when the frequency and average current are kept constant (Fig. 18). The tool erosion rate decreases linearly with increasing duty cycle over the same range.

Figure 19 shows that the erosion rate at the workpiece increases with increasing _average current_* between 7 and 70 amps.

At workpiece: $\qquad$ (erosion rate) $\propto$ (average current)$^{0.85}$ $\qquad$ (3 - 1)

The tool erosion rate increases with current from 7 amps, goes through a maximum at about 30 amps, and then decreases again.

Wear Ratio. From the above section if follows that the wear ratio increases with increasing frequency* (Fig. 17). Above 3 kc this may be expressed approximately as:[5]

$$(\text{wear ratio}) \propto (\text{frequency})^{0.8} \qquad (3 - 2)$$

It can also be seen that the wear ratio decreases with increasing duty cycle (Fig. 18).

Figure 19 shows that the wear ratio decreases with increasing average current over the whole range tested. At low currents the decrease is rather gradual, but it becomes quite prounounced at average currents above 30 amps.

Interelectrode Distance. The separation between the electrodes was measured using the flow rate method described in section 2.3. It was found that the interelectrode distance decreases with increasing frequency

*Other independent variables are kept constant at values shown on graphs.

-52-
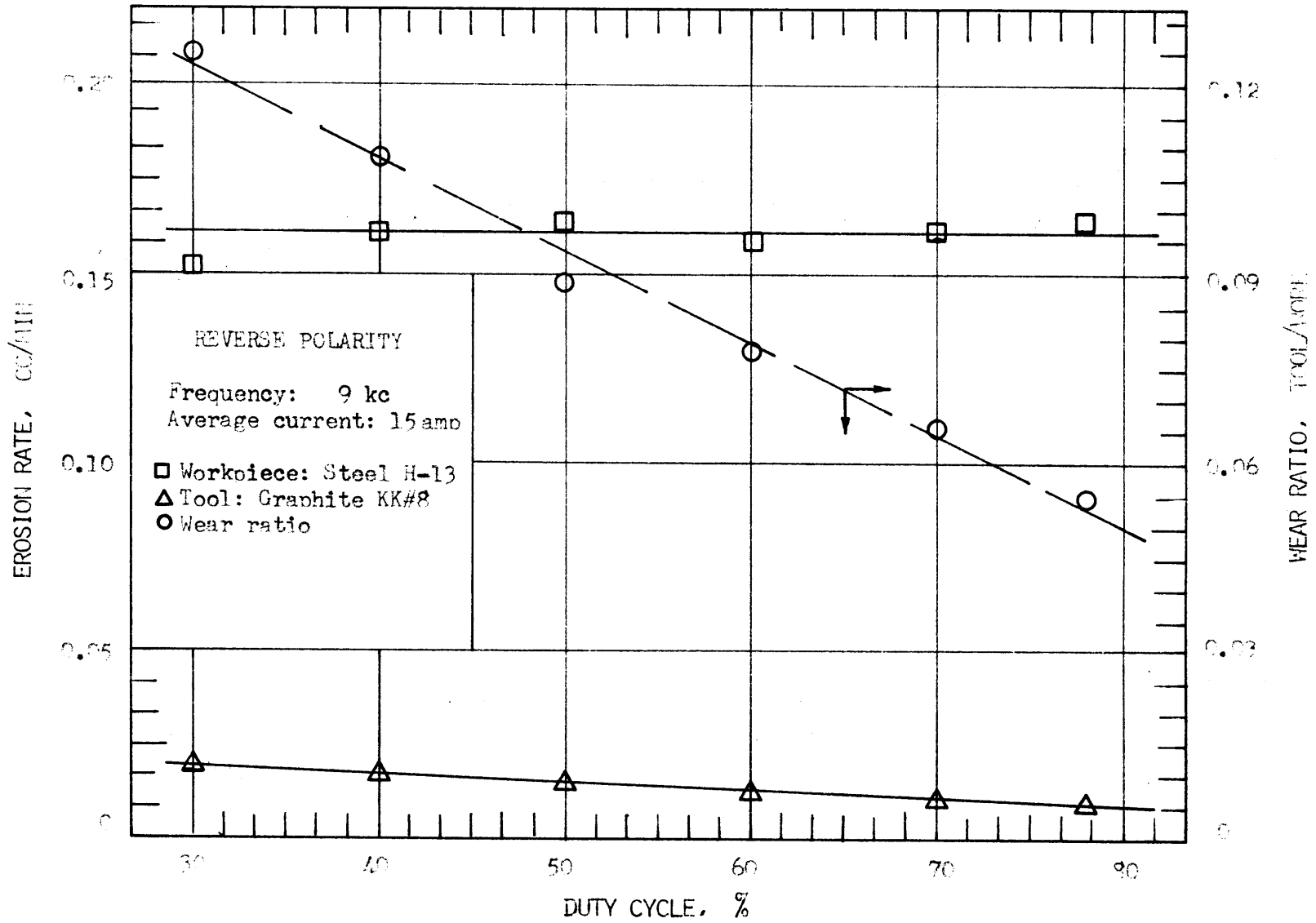
Fig. 18. Dependence of erosion rate and wear ratio on duty cycle: Reverse polarity.
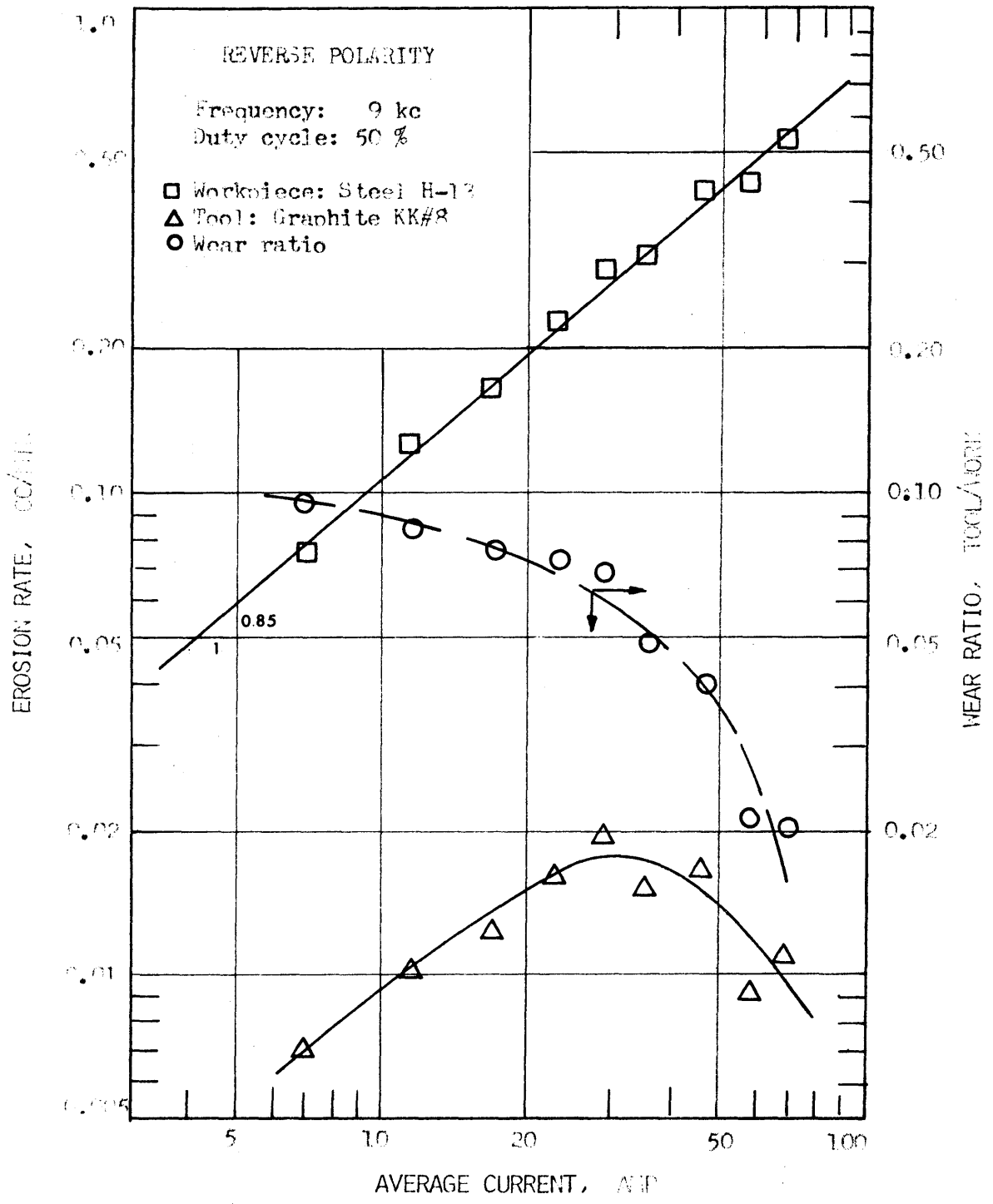
Fig.19. Dependence of erosion rate and wear ratio on
average current: Reverse polarity.

(Fig. 20). An increase of three orders of magnitude in the frequency causes the gap to decrease by approximately one order of magnitude. Actual values of the interelectrode distance varied from about 33 to 180 micron (i.e., 1.3 to 7.1 mils) over the frequency* range tested.

The gap increases with increasing duty cycle (Fig. 21). This is shown to hold at three different frequency settings, and at an arc current of 65 amps. The solid lines have a slope of 1/3; their significance is discussed in the next chapter.

An increase in the arc current brings about an increase in the interelectrode distance (Fig. 22). For arc currents* between 50 and 350 amps, the following relationship holds approximately:

$$(gap) \propto (arc\ current)^{0.25} \qquad (3-3)$$

## 3.2 Standard Polarity Data

Under standard polarity conditions the erosion rate from the steel workpiece (anode) follows a pattern very similar to that from the steel cathode under reverse polarity conditions. The erosion rate at the tool, and consequently the wear ratio, follow very different patterns in the two cases.

Erosion Rate.   At low frequencies the erosion rate from the workpiece at first increases with increasing frequency, then goes through a maximum at about 5 kc, and falls off again at higher frequencies (Fig. 23). The tool erosion rate follows a rather similar pattern.

*Other independent variables are kept constant at values shown on graphs.

-55-
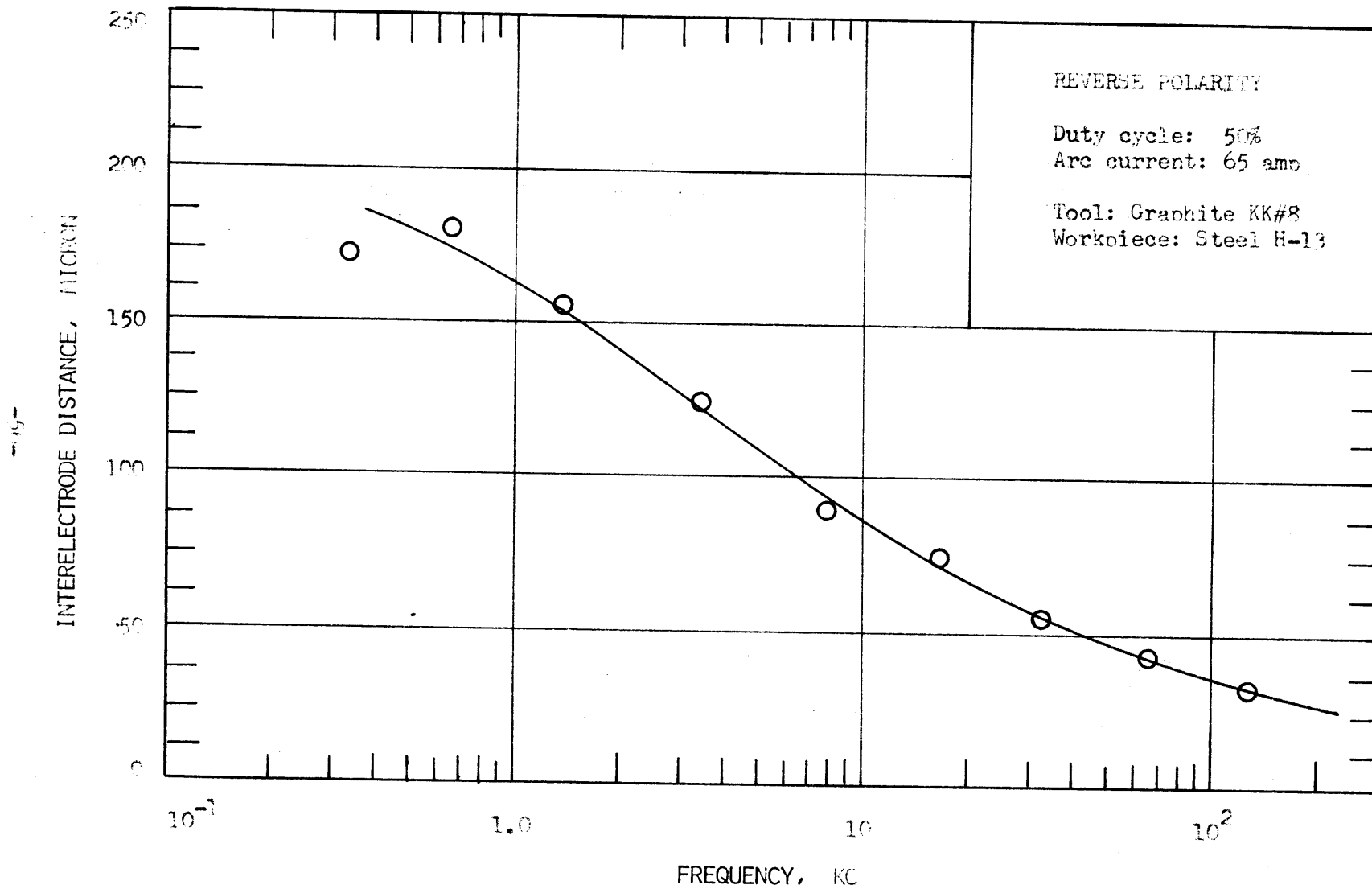
Fig. 20. Dependence of interelectrode distance on frequency: Reverse polarity.
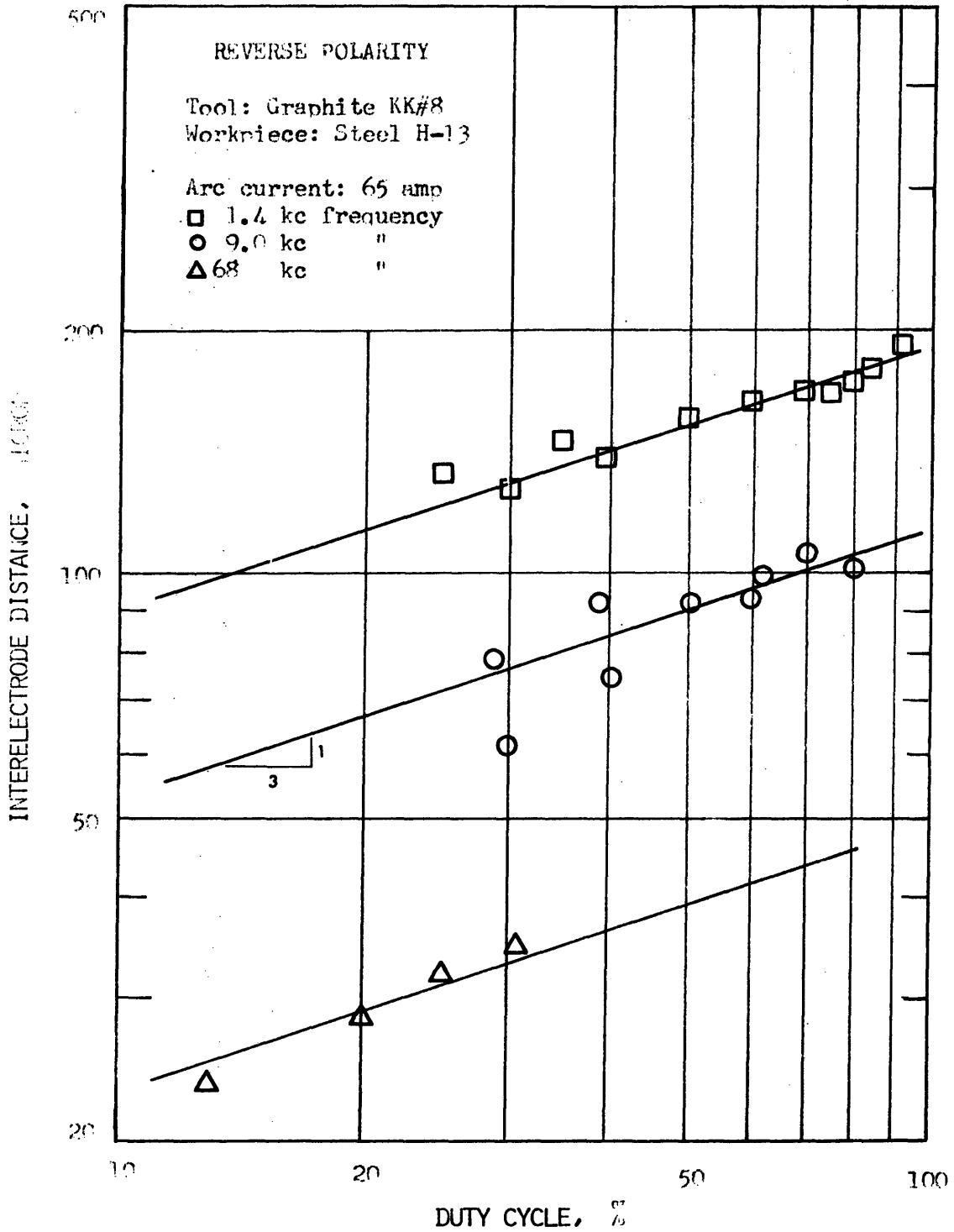
Fig. 21. Dependence of interelectrode distance
on duty cycle: Reverse polarity.

-57-
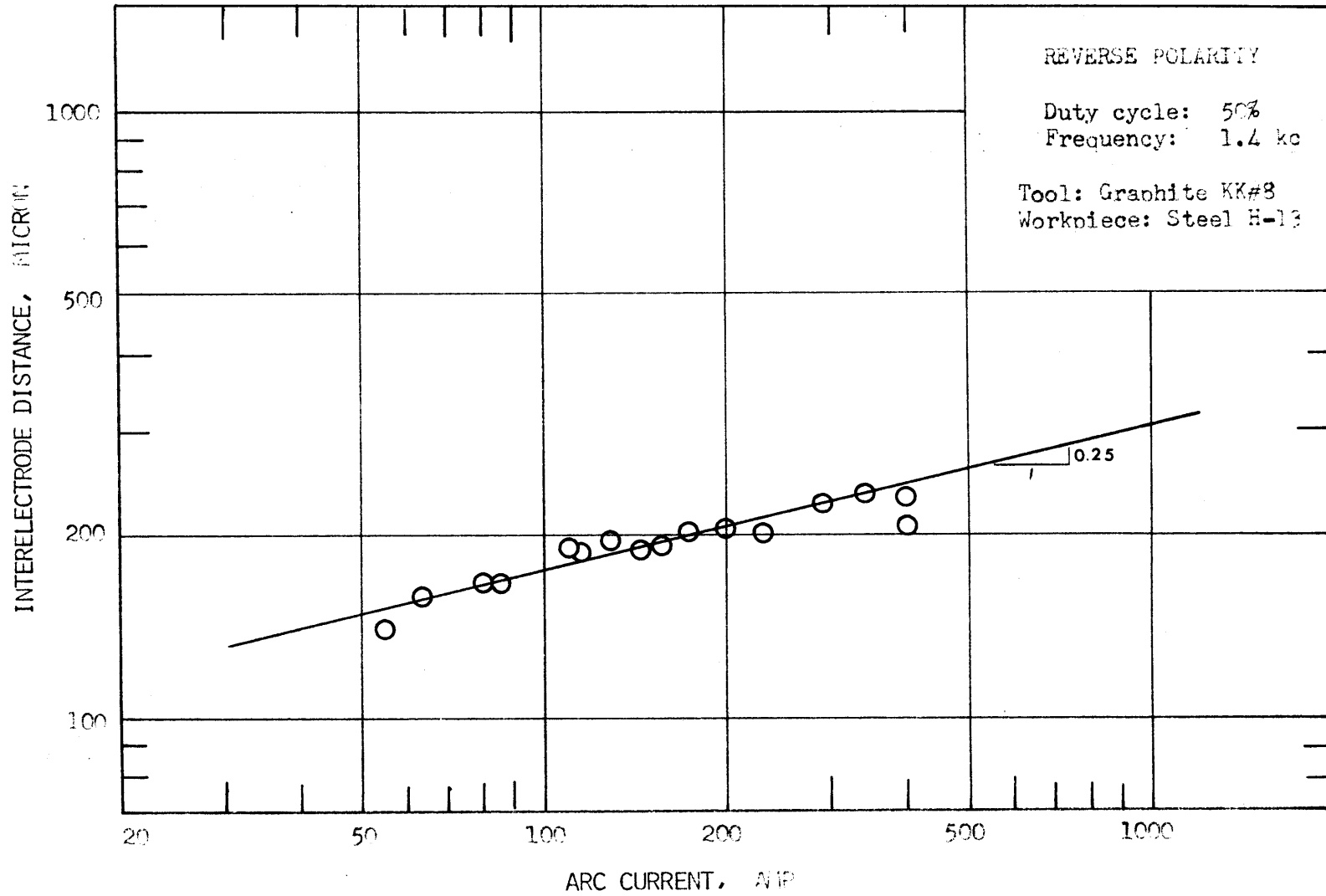
Fig. 22. Dependence of interelectrode distance on arc current: Reverse polarity.
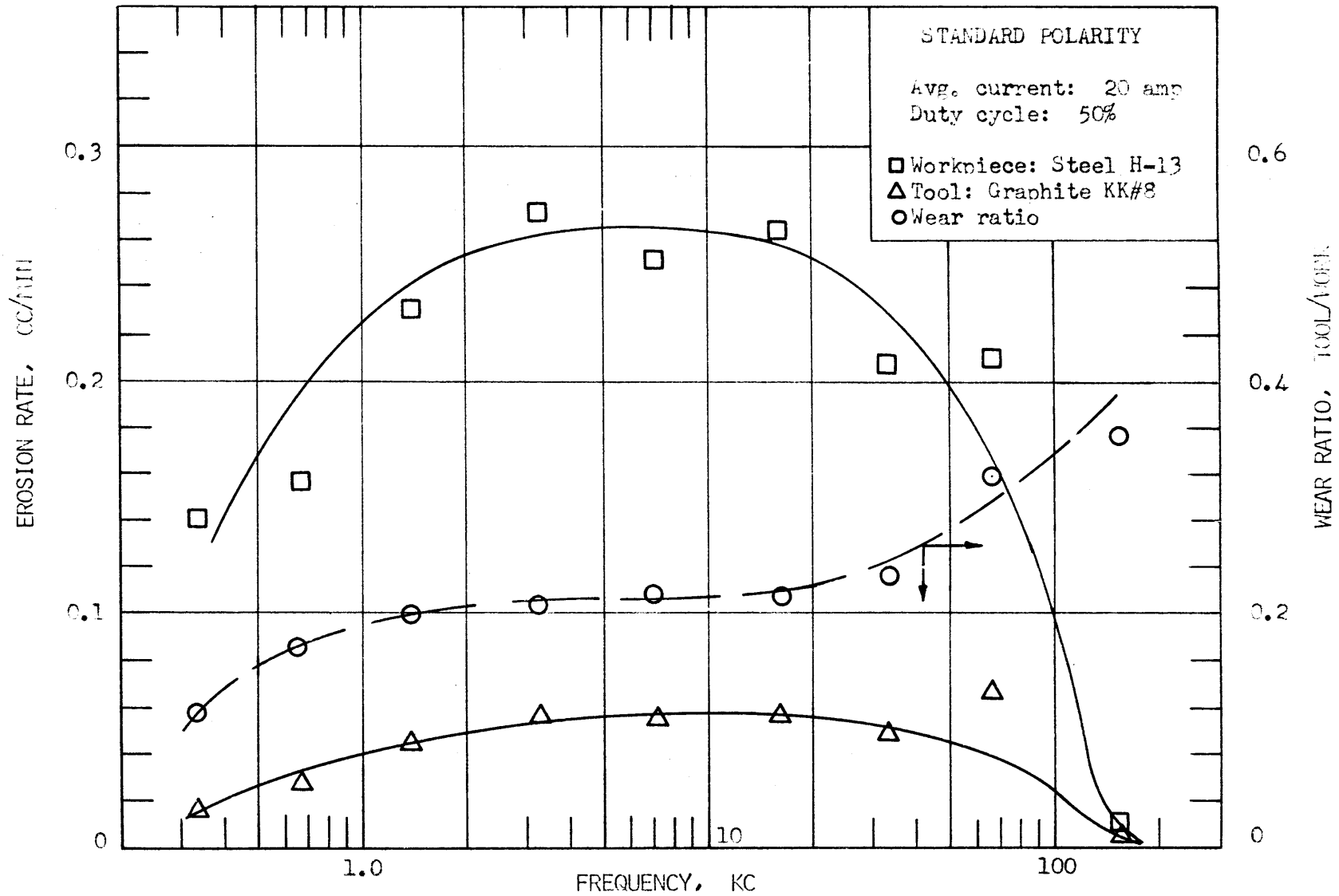
Fig. 23. Dependence of erosion rate and wear ratio on frequency: Standard polarity.

Figure 24 shows that the erosion rate at the workpiece is almost independent of duty cycle. The same holds for the tool erosion rate. In both cases there appears to be a very slight decrease in erosion rate with increasing duty cycle.

An increase in the average current brings about an increase in the erosion rate at either electrode (Fig. 25). These data hold for average current values from 6 to 40 amp, at constant frequency and duty cycle.

At workpiece:     (erosion rate) $\propto$ (average current)$^{0.91}$     (3 - 4)

At tool:     (erosion rate) $\propto$ (average current)$^{0.89}$     (3 - 5)

Wear Ratio.    Figure 23 shows little change in wear ratio between frequencies of 1.4 and 20 kc. Below 1.4 kc the wear ratio falls off, and above 20 kc it increases significantly.

Under the standard polarity conditions studied in this work it is found that the wear ratio is practically independent of duty cycle (Fig. 24) and of average current (Fig. 25), at constant frequency.

Interelectrode Distance.    The distance between the electrodes follows very similar patterns in standard and in reverse polarities. At standard polarity also, the interelectrode distance decreases with increasing frequency (Fig. 26), at constant duty cycle and arc current.

Figure 27 shows an increase in interelectrode distance with increasing duty cycle. This is shown to hold for three different frequencies, at constant arc current. The solid lines have a slope of 1/3.

-60-

EROSION RATE, CC/MIN

WEAR RATIO, TOOL/WORK

STANDARD POLARITY

Frequency: 2 kc
Avg. current: 20 amp

□ Workpiece: Steel H-13
△ Tool: Graphite KK#8
○ Wear ratio
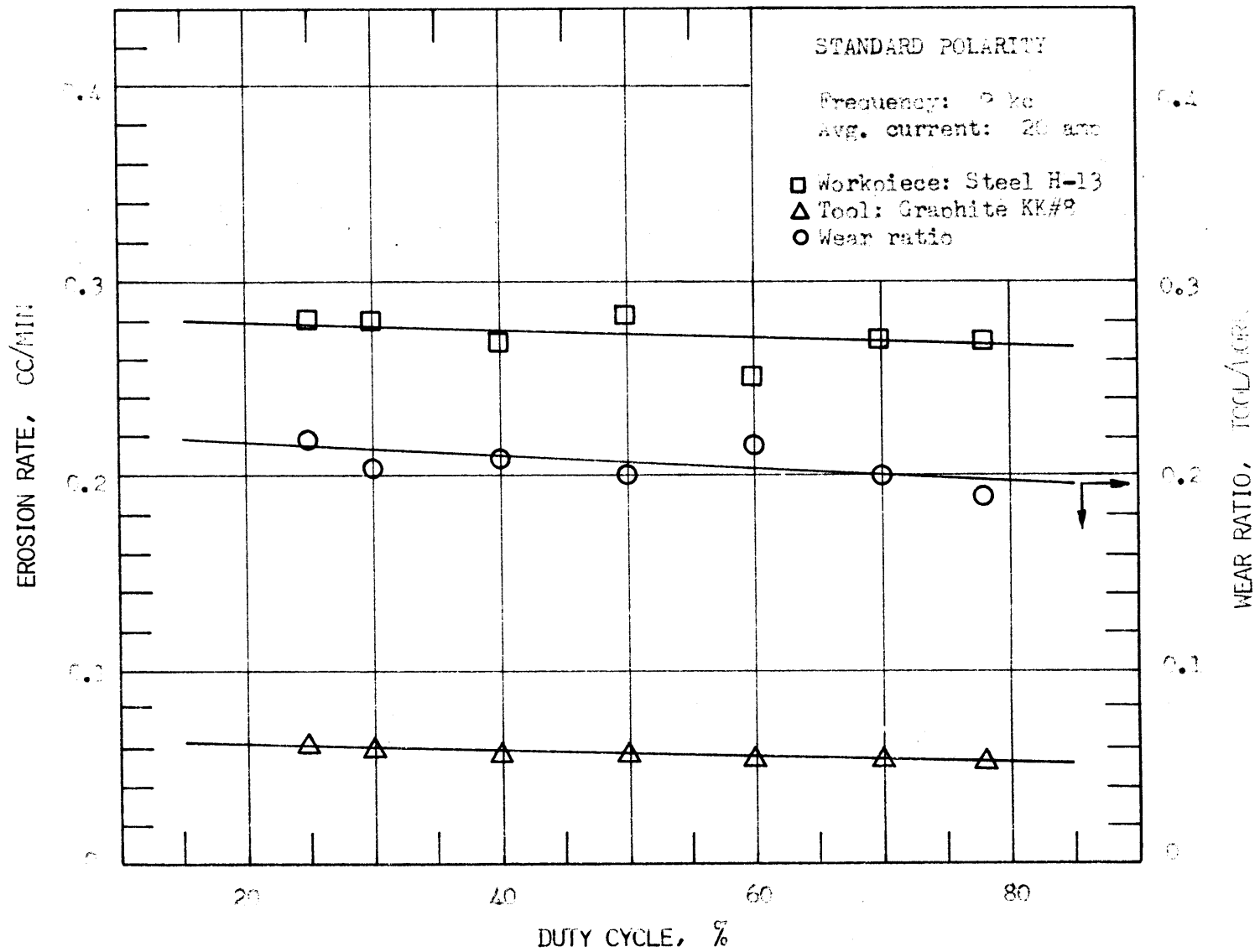
DUTY CYCLE, %

Fig. 24. Dependence of erosion rate and wear ratio on duty cycle: Standard polarity.
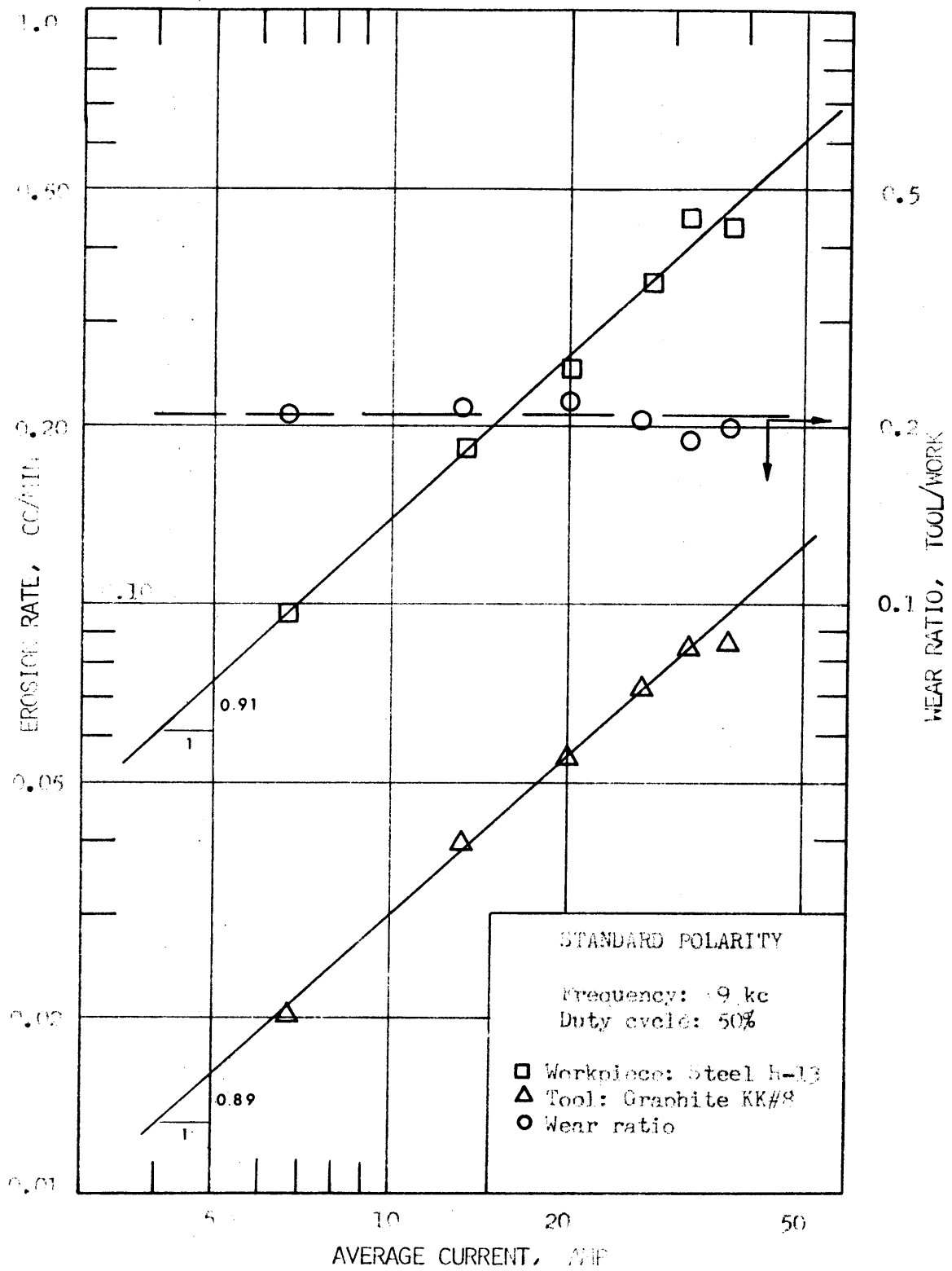
Fig. 25. Dependence of erosion rate and wear ratio on average current: Standard polarity.

STANDARD POLARITY

Duty cycle: 50%
Arc current: 50 amp

Tool: Graphite KK#8
Workpiece: Steel H-13

250

200

150

INTERELECTRODE DISTANCE, MICRON

100

50

0

$10^{-1}$          1.0          10          FREQUENCY, KC          $10^2$
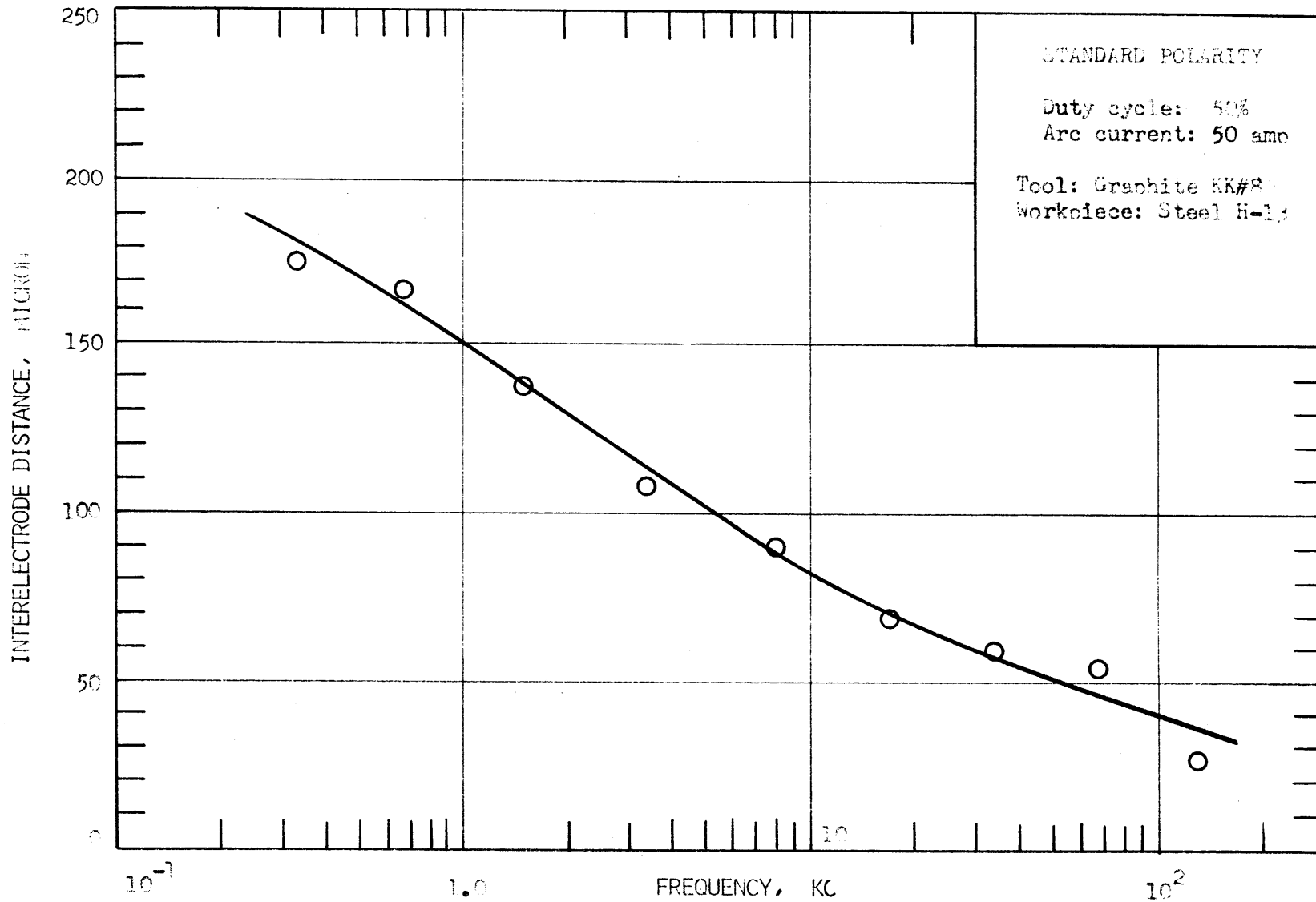
Fig. 26. Dependence of interelectrode distance on frequency:  Standard polarity.

STANDARD POLARITY

Tool: Graphite KK#8
Workpiece: Steel H-13

□ 1.4 kc  frequency
○ 9.0 kc     "
△ 68  kc     "

Arc current: 50 amp

INTERELECTRODE DISTANCE, MICRO...

500

200

100

50

20

1
3

10          20              50           100
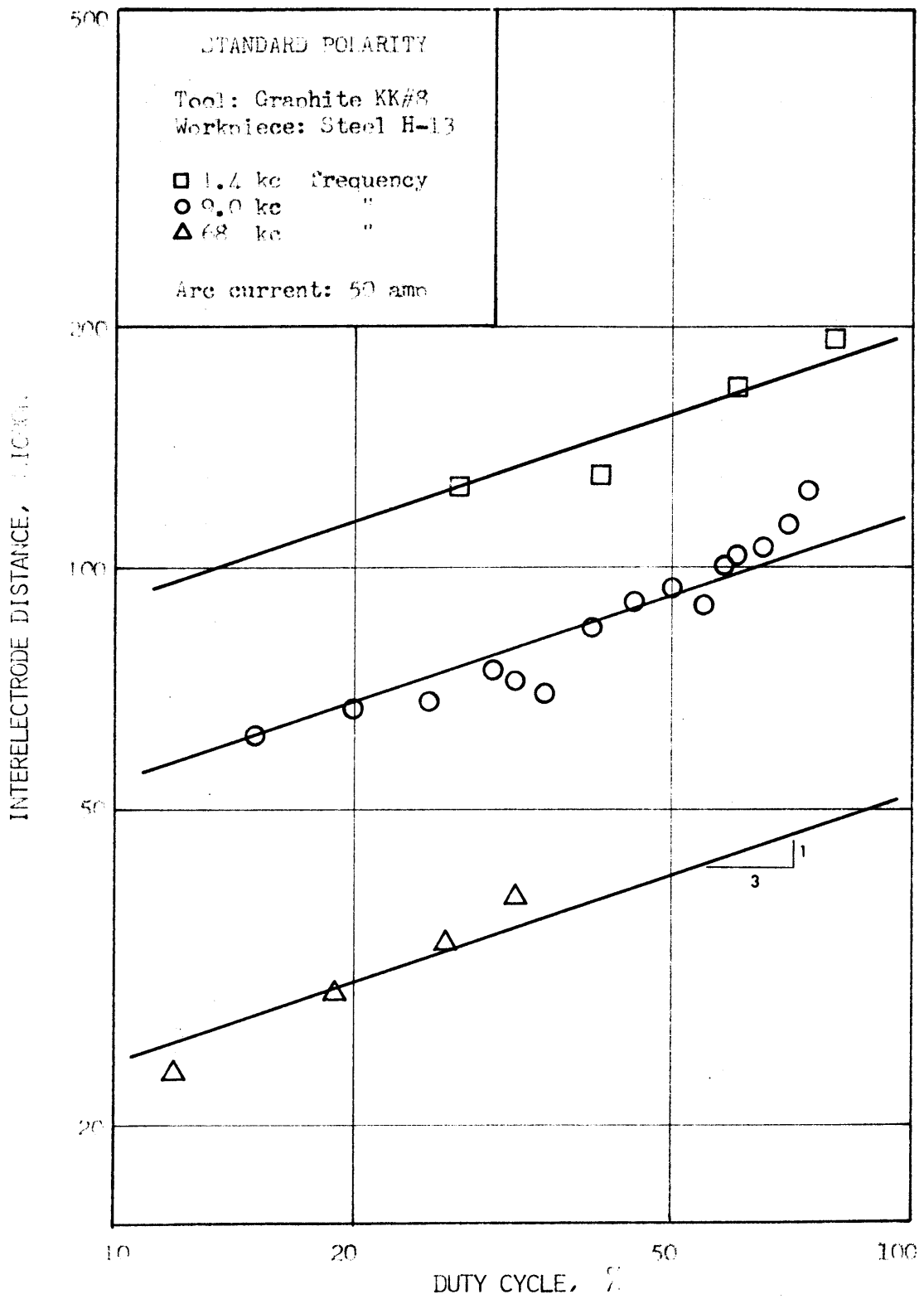
DUTY CYCLE, %

Fig. 27.  Dependence of interelectrode distance on duty
cycle:  Standard polarity.

According to Fig. 28, the gap size increases with increasing arc current between 40 and 350 amps, at constant frequency and duty cycle. The relationship may be approximated as follows:

$$(\text{gap}) \propto (\text{arc current})^{0.26} \qquad\qquad (3 - 6)$$

## 3.3 Particle Injection  -  Reverse Polarity

From section 3.1 it appears that the very same conditions which cause the wear ratio to decrease also cause the interelectrode distance to increase. In an attempt to find out if a large gap is in itself sufficient to obtain a low wear ratio, particles were injected into the gap to try to force the latter to be large under machining conditions which normally yield a small gap and therefore a high wear ratio. Such attempts were not successful. Both steel and tin particles were injected, at varying particle concentration and particle size.

Steel Particles. Machining was carried out at 8 kc, 50% duty cycle, and 65 amps arc current. Two particle size ranges were used: 74 to 150 microns diameter, and 150 to 330 microns diameter. Both copper and graphite electrodes were used as tools in these tests. When a copper tool is used there is no observable change in the wear ratio. In the case of a graphite tool a very slight increase in the wear ratio is observed at high particle concentrations. This is probably due to mechanical erosion by the moving particles. No decrease in the wear ratio due to larger gaps was observed.

The most noticable change was in the erosion rate from the workpiece. The injected particles cause the machining to become very

-65-
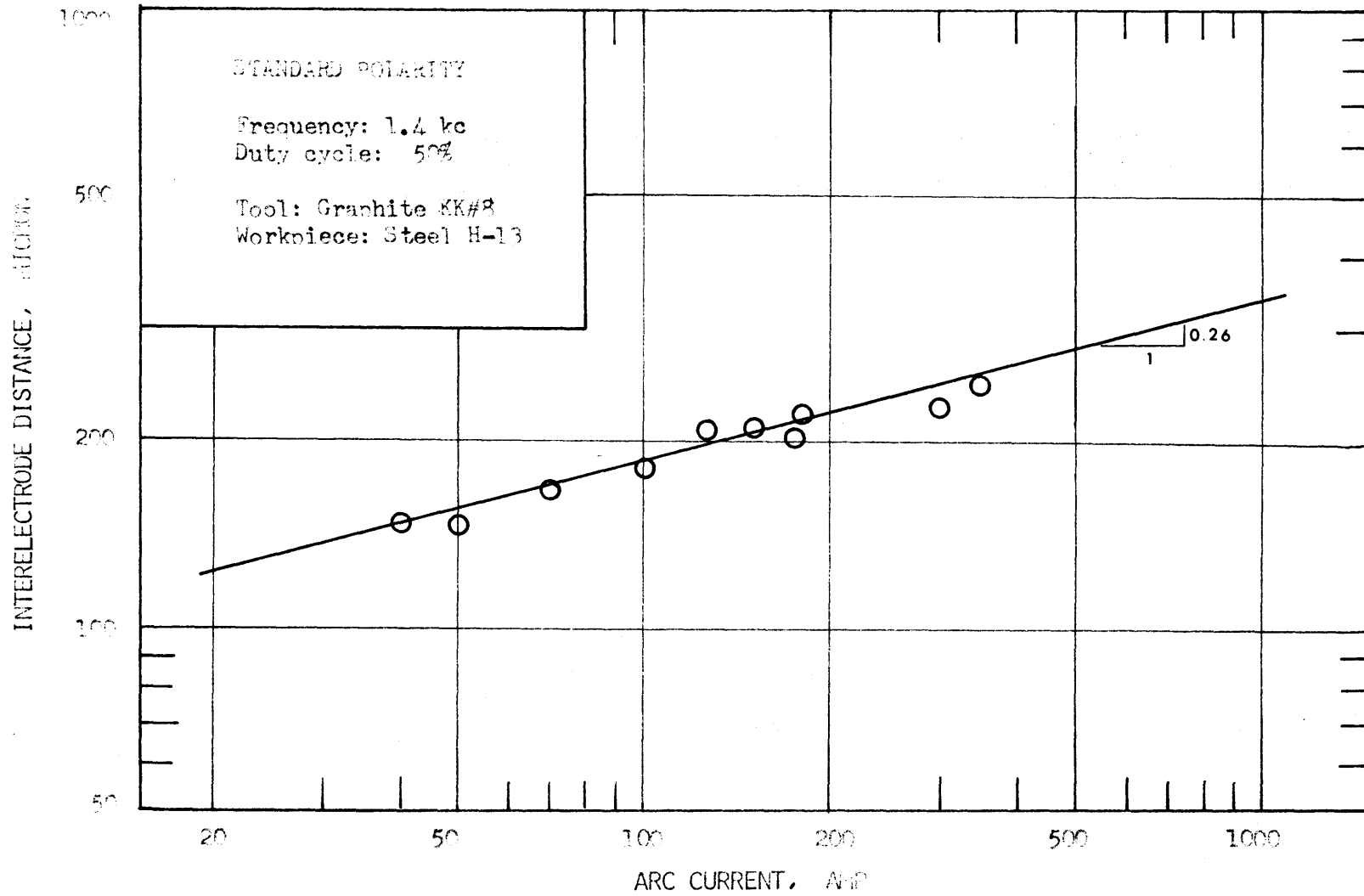
Fig. 28. Dependence of interelectrode distance on arc current: Standard polarity.

unstable, so the erosion rate invariably decreases with increasing

particle concentration. Figure 29 shows that with a copper tool and a

particle concentration of 0.1% by apparent volume of 150 to 330 micron

particles the erosion rate is only 15% of what it is at zero particle

concentration. With smaller particles the erosion rate falls off less,

and with a graphite tool it falls off less than it does with a copper

tool. These results are summarized in Table 3.1 below.

TABLE 3.1:  Workpiece erosion rate at 0.1% particle
            concentration as a percentage of the erosion
            rate at zero particle concentration.

| Particle diameter | Copper tool | Graphite tool |
|---|---|---|
| 74 to 150 microns | 40% | 75% |
| 150 to 330 microns | 15% | 40% |

Tin Particles. It appeared that one reason for the lack of success

with steel particles was that there was insufficient energy to melt

the particles. This is what brought about the instability and the

resulting reduced erosion rates. To overcome this problem, tin

particles, which have a very much lower melting point, were injected.

The results were rather surprising. There was no change in the

wear ratio, no instability, and no reduction in the erosion rate. In

fact, machining took place as if though there had been no injection of

particles, and this in spite of the fact that some of the particles

were very much larger than the gap. The gap was also measured, and it
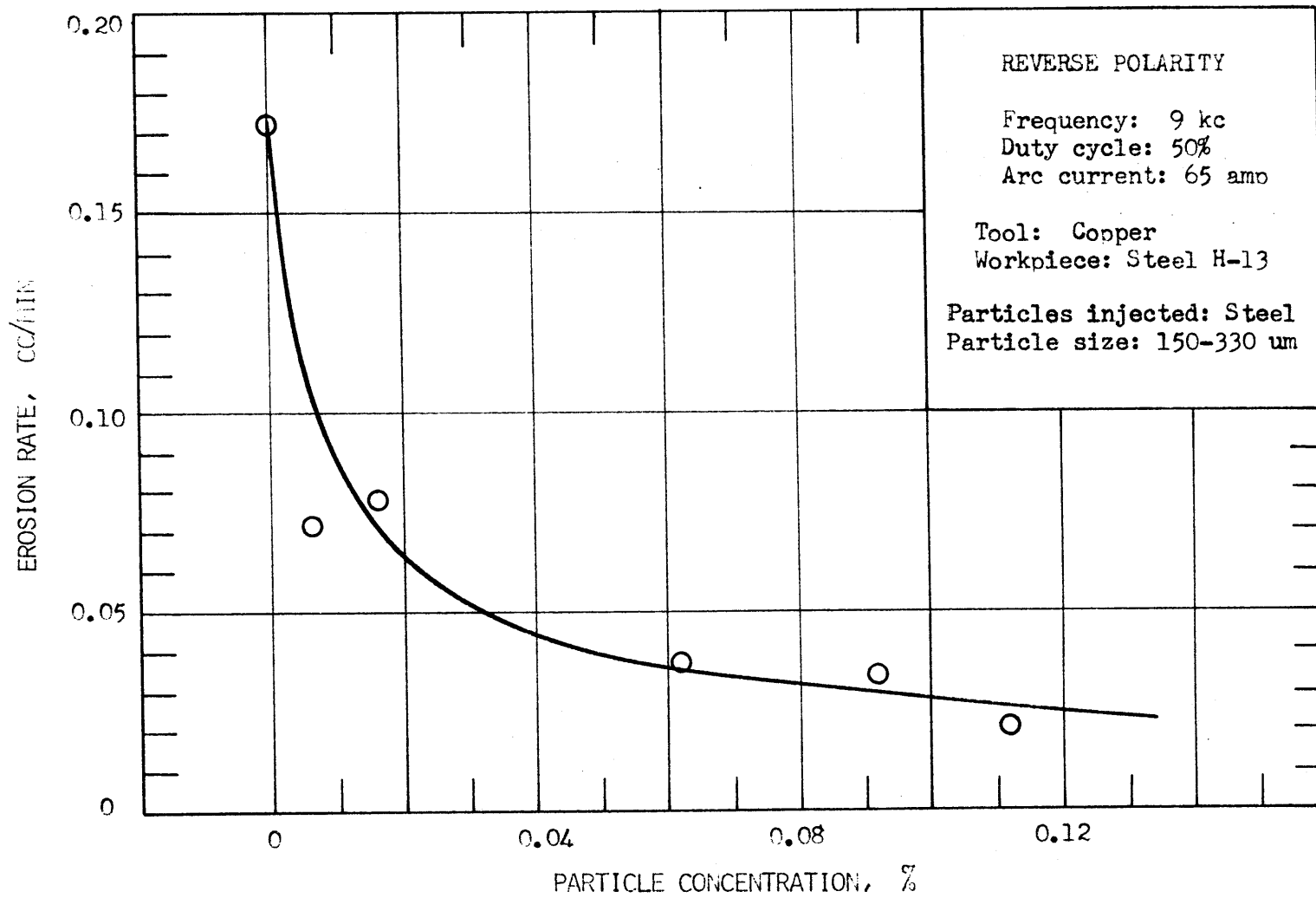
Fig. 29. Workpiece erosion rate as a function of concentration of injected particles.

had not changed. These results were found to hold both for graphite and for copper tool electrodes while using the same particle sizes and concentrations as were used with steel particles.

How do we know that the tin particles did reach the gap? First of all, the particles could be seen approaching the gap up to the point where they entered the axial hole in the tool, and there was no accumulation of particles in this hole, and secondly, tin particles were found among the erosion products after the machining was finished. These particles were all very much smaller than the injected tin particles. This is discussed further in section 4.3.

## 3.4  Size Distribution of Eroded Particles - Reverse Polarity

The material eroded by the EDM process usually appears in the form of spheres.[45,46] The spheres come in all sizes, and are usually hollow.[4,5] We find that spheres may be obtained from both electrodes. For example, when copper is used to machine steel, both copper and steel spheres are found among the erosion products. We have obtained spheres from low melting point material (see below) as well as from refractory materials (Appendix J). The only exception is graphite, whose erosion products are never spherical, but rather flaky or irregular in shape. Some graphite appears as an extremely fine powder, but this may be carbon from the EDM fluid, rather than from the graphite electrode.

The erosion products were collected as described in section 2.2. Sieve sizes of 44, 74, 150, 330 and 610 micron were used to find the particle size distribution. Figure 30 shows the size distribution of
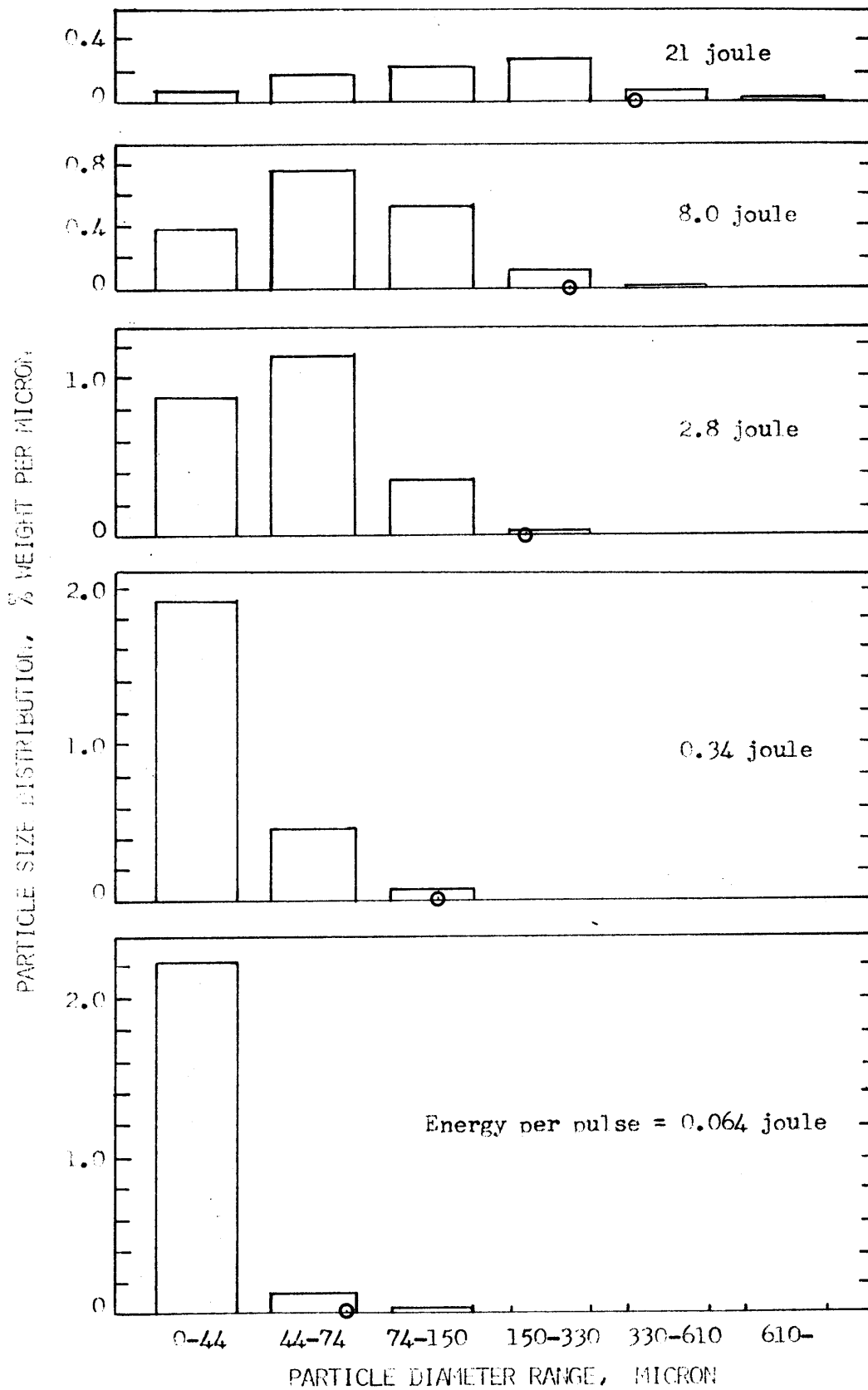
Fig. 30. Particle size distribution at different pulse energies.

particles from a steel cathode at pulse energies of 0.064, 0.34, 2.8, 8.0 and 21 joule. The actual machining conditions are summarized in Table 3.2. Each block on the graph gives the fraction of the total

TABLE 3.2. Machining conditions used for obtaining particle size distributions.

| Duty cycle (%) | $I_{arc}$ (amp) | $V_{arc}$ (volt) | $t_{on}$ (sec) | pulse energy (joule) $= I_{arc} V_{arc} t_{on}$ |
|---|---|---|---|---|
| 80 | 390 | 27 | $2.0 \times 10^{-3}$ | 21 |
| 50 | 220 | 26 | $1.4 \times 10^{-3}$ | 8.0 |
| 50 | 78 | 26 | $1.4 \times 10^{-3}$ | 2.8 |
| 50 | 78 | 28 | $1.6 \times 10^{-4}$ | 0.34 |
| 50 | 130 | 31 | $1.6 \times 10^{-5}$ | 0.064 |

weight of particles collected (expressed as a percentage) which lies within the specified particle diameter range, divided by the size of that range. For example, if 20% of the particles obtained at a given pulse energy have diameters between 74 and 150 microns, then the height of this particular block would be $20/(150 - 74) = 0.26$.

It is clear from the graph that higher pulse energies result

in larger particles, but some small particles are always present. The results seem to indicate that the energy per pulse puts an upper limit on the size of the particles. The material eroded in a given pulse may split up into any number of particles, but there appears to be a finite probability that only 1 or 2 particles may be formed in a particular discharge (Appendix G). The small circle on each graph indicates approximately the magnitude of the corresponding interelectrode distance, so it is clear that the gap is about the same size as the diameter of the largest particles collected.

A few of the particles are larger than the measured gap. How can these particles get out of the gap? There are two answers to this question. First of all, the tool sometimes backs off sufficiently to allow larger particles to escape, and secondly, these larger particles may have been formed near or at the outer edge of the gap and would therefore not have to pass through the gap.

Does the size distribution of the eroded particles correctly represent the size distribution at the time when the particles are formed, or are some of the particles remelted and split up on their way out of the gap? To throw some light on this question, a test was made to compare the results with the two geometries shown in Fig. 31. In (a) the standard geometry of Fig. 8 was used. Here the particles have to move out of the gap and up along the sides of the tool before they are free. There

(a)                                    (b)
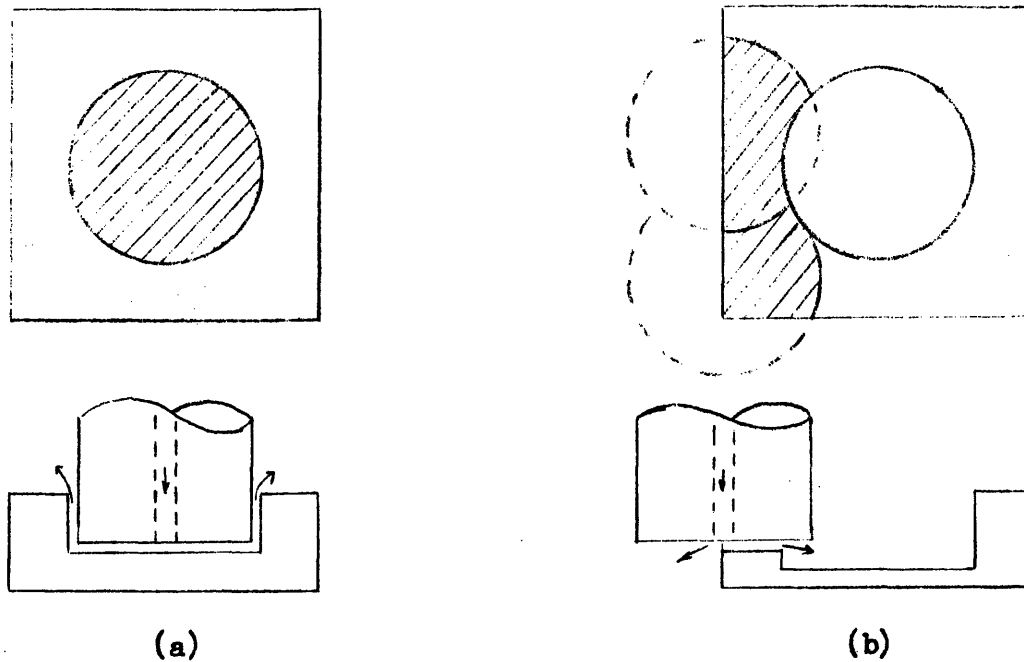
Fig. 31. Machining geometry used to show that more large particles
         are collected under some conditions (b) than under others (a).

is considerable opportunity for remelting. In (b) the shaded area was
machined in two separate steps, and here the particles can easily escape
shortly after being formed. Of course there are also more edge effects in
(b). The results are summarized in the table given below.

TABLE 3.3. % Weight Distribution of Particles.

| Size range (microns) | 610- | 330-610 | 150-330 | 74-150 | 44-74 | 0-44 |
|---|---|---|---|---|---|---|
| Fig. 31 (a)  (%) | 0.07 | 0.77 | 20.1 | 39.9 | 22.5 | 16.66 |
| Fig. 31 (b)  (%) | 0.80 | 1.90 | 27.1 | 41.5 | 18.9 | 9.80 |

On the whole the size distributions are quite similar, as might be expected since the pulse energies were the same, but there are some differences worth noting. In the group of particles of size 610 microns and larger (less than 1% of the total weight), there is more than ten times as much weight in (b) as in (a). To make up for this difference there are more small particles in (a).

From the above table it is possible to obtain the % weight distribution per micron which is what was done to obtain Fig. 30. By adding a considerable amount of our own interpretation, we may make a continuous plot of the results from table 3.3 and make the size distribution go to zero at zero particle size. This is done in Fig. 32 (a), and the results from Fig. 30 are replotted in a similar way in Fig. 32 (b). The size distributions incidentally strongly resemble those obtained for aerosol particles.[47] By assuming the particles to be 50% hollow (Appendix G), it is possible to convert the curves in Fig. 32 into probability distributions, giving the probability that a particle picked at random will lie in a certain size range. This conversion would result in a similar graph but blown up more on the left side and somewhat reduced on the right side. None of the earlier conclusions would be affected.

At high pulse energies about 60% of the total material eroded from the workpiece was collected. At the lowest energy about 5% was collected. The material which was lost consisted mostly of very small particles which were carried away suspended in the fluid. If 100% were collected, the graphs in Figs. 30 and 32 would be further blown up on the left side. In this case the change would, however, be considerably
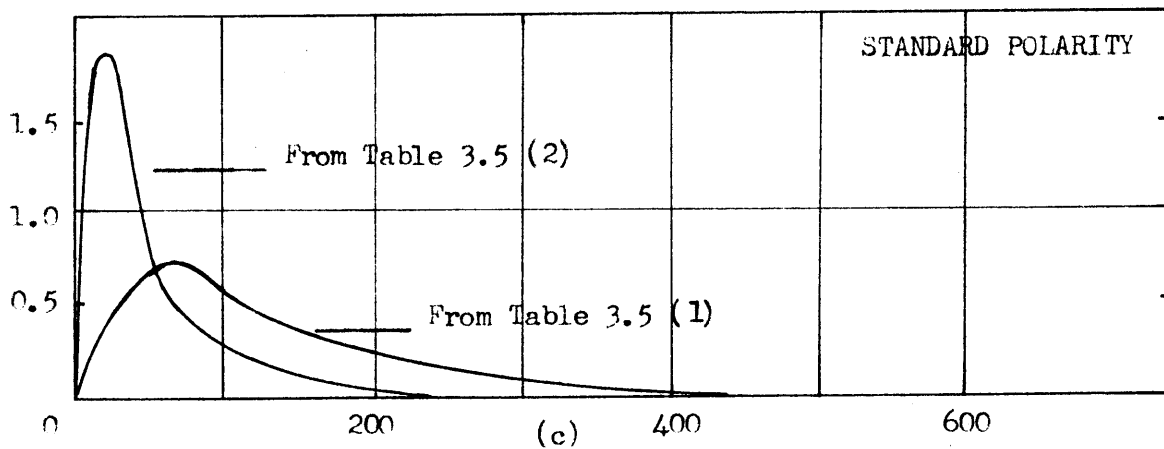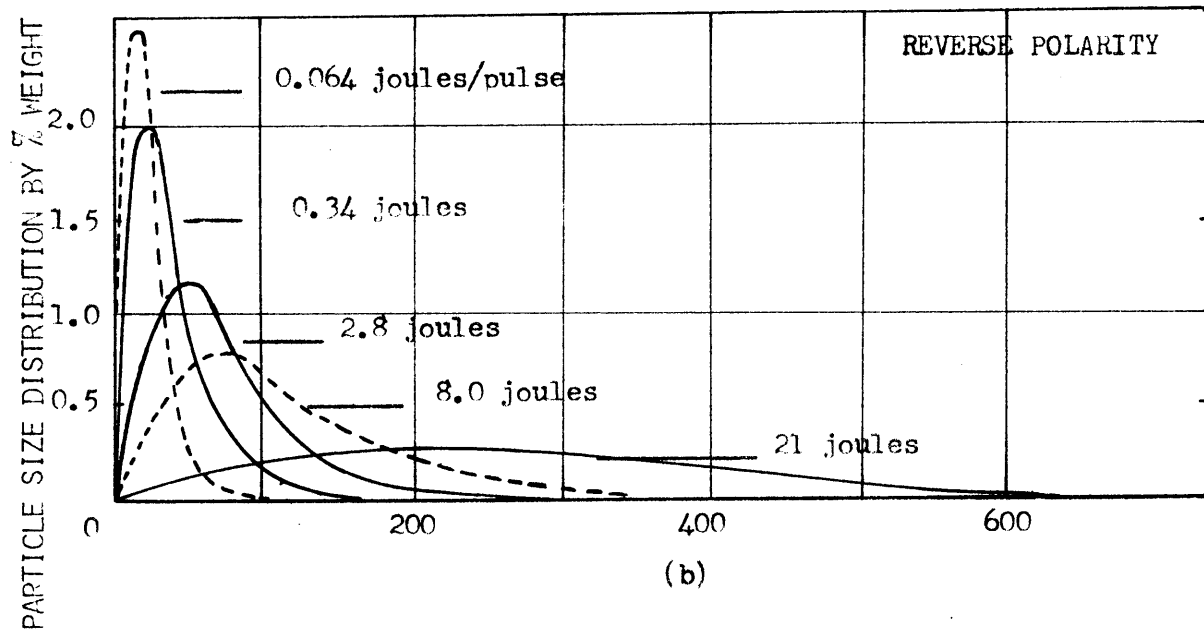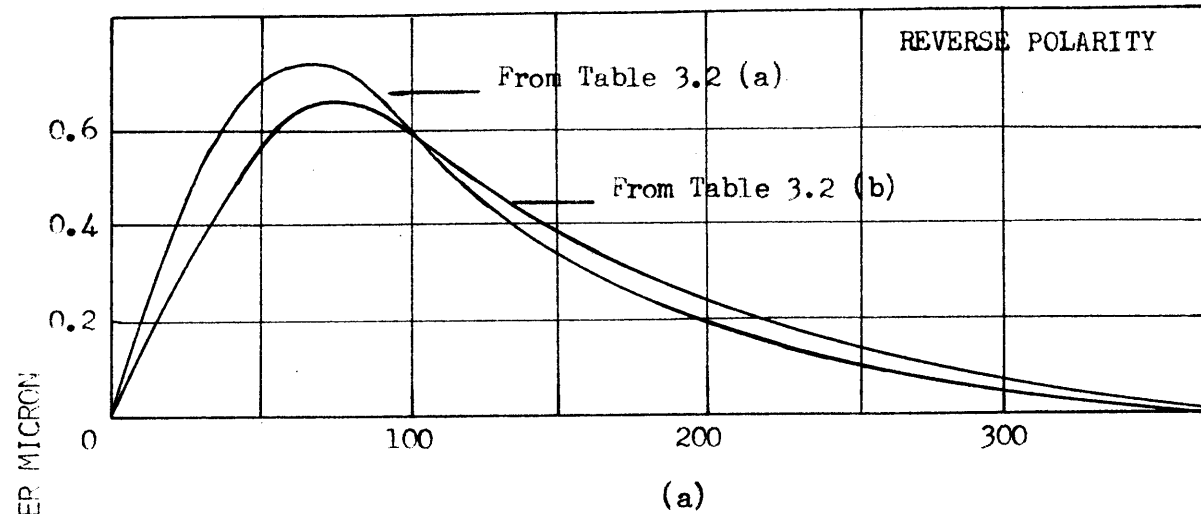
Fig. 32. Particle size distribution curves.

smaller than in the case discussed above.

In order to make an estimate of the actual number of particles collected in each size range we use the following procedure. Consider an average particle size for each size range, e.g., in the 74 - 150 micron range assume the average particle to have a diameter halfway between the two extremes, i.e., 74 + (150 - 74)/2 = 112 microns. Calculate the volume of this particle, and obtain its approximate weight by assuming it to be 50% hollow. Finally, divide the measured weight of particles in the size range by this calculated particle weight to obtain the number of particles in this particular range. The data from Fig. 30 are processed in this way and the results are summarized in the table below.

TABLE 3.4. Approximate number of particles in each size range.

| Particle size range (micron) | 610-1270 | 330-610 | 150-330 | 74-150 | 44-74 | 0-44 |
|---|---|---|---|---|---|---|
| Avg. particle diameter (cm) | $9.15 \times 10^{-2}$ | $4.70 \times 10^{-2}$ | $2.40 \times 10^{-2}$ | $1.12 \times 10^{-2}$ | $5.90 \times 10^{-3}$ | $2.20 \times 10^{-3}$ |
| Avg. particle weight (gm) | $1.25 \times 10^{-2}$ | $1.70 \times 10^{-3}$ | $2.26 \times 10^{-4}$ | $2.29 \times 10^{-5}$ | $3.35 \times 10^{-6}$ | $1.73 \times 10^{-7}$ |
| Number of particles: | | | | | | |
| 21 joule exper. | $1.06 \times 10^2$ | $1.45 \times 10^3$ | $2.60 \times 10^4$ | $1.02 \times 10^5$ | $1.98 \times 10^5$ | $2.07 \times 10^6$ |
| 8.0 " " | 8 | 68 | $1.35 \times 10^4$ | $2.64 \times 10^5$ | $1.02 \times 10^6$ | $1.45 \times 10^7$ |
| 2.8 " " | 0 | 3 | $1.18 \times 10^3$ | $1.47 \times 10^5$ | $1.28 \times 10^6$ | $2.74 \times 10^7$ |
| 0.34 " " | 0 | 3 | 31 | $1.03 \times 10^4$ | $1.77 \times 10^5$ | $2.02 \times 10^7$ |
| 0.064 " " | 0 | 0 | 35 | $3.49 \times 10^2$ | $8.65 \times 10^3$ | $4.43 \times 10^6$ |

It is interesting to note that according to the above table, in the 2.8 joule experiment, a total of about 30 million particles were collected, whereas the actual number of pulses put out by the power supply during the test was only about 0.6 million, so apparently there is considerable breakup, either at the time of particle formation, or while the particles are on their way out of the gap.

We mentioned earlier that particles may be obtained from either electrode. Let us compare (1) the 2.8 joule and (2) the 0.064 joule experiments above with results obtained by machining at standard polarity under identical machine settings.

TABLE 3.5.  % weight distribution in standard polarity tests.

| Size range (microns) | 610+ | 330-610 | 150-330 | 74-150 | 44-74 | 0-44 |
|---|---|---|---|---|---|---|
| (1)  (%) | 0.21 | 2.12 | 26.8 | 42.47 | 19.4 | 9.00 |
| (2)  (%) | 0 | 0 | 6.9 | 14.5 | 12.4 | 66.2 |

The results are plotted in Fig.32 (c) using the same plotting technique as that utilized in Fig. 32 (a) and (b). A comparison between the standard and reverse polarity ((c) and (b) respectively) particle size distributions shows that more large particles are obtained in standard polarity. Part of the reason is that more material is removed in each pulse in standard polarity (in 4 tests at identical machine settings of 9 kc, 50% duty cycle and varying average current using a graphite tool the erosion rate from the steel was on average 33% higher in standard polarity), but this does not appear to fully explain the difference.

## 3.5  Conclusions

The data presented in this chapter show that when steel is machined with a graphite tool the <u>interelectrode distance</u>:

    (a)  decreases with increasing frequency

    (b)  increases with increasing duty cycle

    (c)  increases with increasing current.

This holds true both in standard and reverse polarities.

In <u>reverse</u> polarity, the wear ratio:

    (a)  increases with increasing frequency

    (b)  decreases with increasing duty cycle

    (c)  decreases with increasing average current.

In <u>standard</u> polarity, there is little change in wear ratio with variations in duty cycle or average current.  At very low frequencies the wear ratio decreases and at very high frequencies it increases quite substantially.

Under normal machining conditions the gap distance is of the same order as the largest particles collected.  Attempts to force the gap to be larger, by means of particle injection, were unsuccessful.

## 4. DISCUSSION OF REVERSE POLARITY RESULTS

In chapter 3 we saw that, for reverse polarity machining, the wear ratio increases with increasing frequency, decreases with increasing duty cycle, and decreases with increasing average current. In other words, whenever the energy per pulse is increased, the wear ratio decreases. Under standard polarity conditions, very different results are obtained. In order to explain these results it is necessary to understand what factors determine the amount of erosion at the electrodes. Emission mechanisms in arcs, energy balance at the electrodes, and the electric field at the cathode are discussed in Appendices A, B, and C respectively. Here we shall attempt to get a physical picture of what happens as a result of an arc discharge.

### 4.1 Theoretical background

The most important factors in determing the amount of erosion at the electrodes are:

1. The energy per pulse,
2. The power density at the surface,
3. Material transfer between the electrodes,
4. The thermal characteristics of the material to be eroded,[15,34]
5. The type of EDM fluid used.[26]

Here we shall take a close look at the first two, and keep the last two constant. The importance of the third factor has been studied in detail by Viswanathan,[36] and we shall draw on his results when necessary.

Energy per Pulse. This is probably the most important quantity in EDM, and may be expressed as follows:[3]

$$E = \int_0^{\tau} I(t) \ V(t) \ dt \qquad (4-1)$$

where  E is the energy per pulse   (joules)

I(t) is the instantaneous current   (amps)

V(t) is the instantaneous voltage   (volts)

$\tau$  is the total period of one pulse   (sec)

After an initial transient (spark), both I(t) and V(t) settle down to fairly constant values, $I_{arc}$ and $V_{arc}$ (Figs. 15 and 16). For pulses of relatively long ON-times, these quantities may be substituted for I(t) and V(t) to a good approximation. For the relatively short (distance) arcs which occur in EDM there is little voltage drop in the plasma, so $V_{arc}$ is essentially fixed by the electrode materials, and therefore cannot be changed.[*]  Hence Eq. (4-1) becomes

$$E \simeq V_{arc} \int_0^{\tau} I(t) \ dt \qquad (4-2)$$

During the OFF-time of the pulse no current flows, so I(t) = 0. Hence,

$$E \simeq I_{arc} \ V_{arc} \ t_{on} \qquad (4-3)$$

The arc plasma places no internal restriction on $I_{arc}$ or on $t_{on}$, so there are still two independent ways of changing the pulse energy. Either the arc power may be changed by varying $I_{arc}$ , or the ON-time may be varied. $t_{on}$ can be changed through varying either the frequency or the duty cycle.

According to the thermal theory of erosion, the eroded material is either melted, or vaporized, or both. If, for example, all the energy

---

[*]When calculating pulse energies for very short ON-times, reasonable average values for I(t) and V(t) may be obtained from the oscilloscope. These values are usually higher than $I_{arc}$ and $V_{arc}$.

going to the surface is used for melting the electrode material, then

an increase by a factor of two in E should, as a first approximation,

double the quantity of material removed in each discharge. The same

statement holds if a constant fraction of the incident power goes into

melting the surface. What we are saying is that under these assumptions,

the volume of material eroded per pulse, $\mathcal{V}$, should be proportional to

the energy per pulse:

$$\mathcal{V} \propto E$$

i.e., using Eq.(4-3),

$$\mathcal{V} \propto I_{arc} \, V_{arc} \, t_{on} \qquad (4 - 4)$$

Let us <u>assume</u> a power law of the form $\mathcal{V} \propto I_{arc}^{a} \, V_{arc}^{b} \, t_{on}^{c}$, and

see to what extent this equation is verified by experiment.

In Fig. 33 the volume eroded per pulse is plotted against $t_{on}$ for

machining at 35 amps average current and 50% duty cycle, but at different

frequencies. To make this plot we had to assume that each pulse put out

by the power supply results in an effective discharge. This assumption

breaks down at very high and at very low ON-times, because of unstable

machining at these conditions.* Figure 33 shows that at the steel

workpiece:

$$\mathcal{V} \propto t_{on} \qquad (20\mu sec < t_{on} < 500\mu sec) \quad (4 - 5)$$

so that Eq. (4-4) is verified for ON-times between $2 \times 10^{-5}$ and $5 \times 10^{-4}$

seconds.

Next let us see what happens when the arc current is varied. From

Eq. (3.- 1), the workpiece erosion rate is proportional to the

---

*Unstable machining usually means that a considerable fraction of the
pulses put out by the power supply fail to result in effective
discharges. Under such conditions the feed rate of the tool is
erratic, and much 'hunting' is noticed.
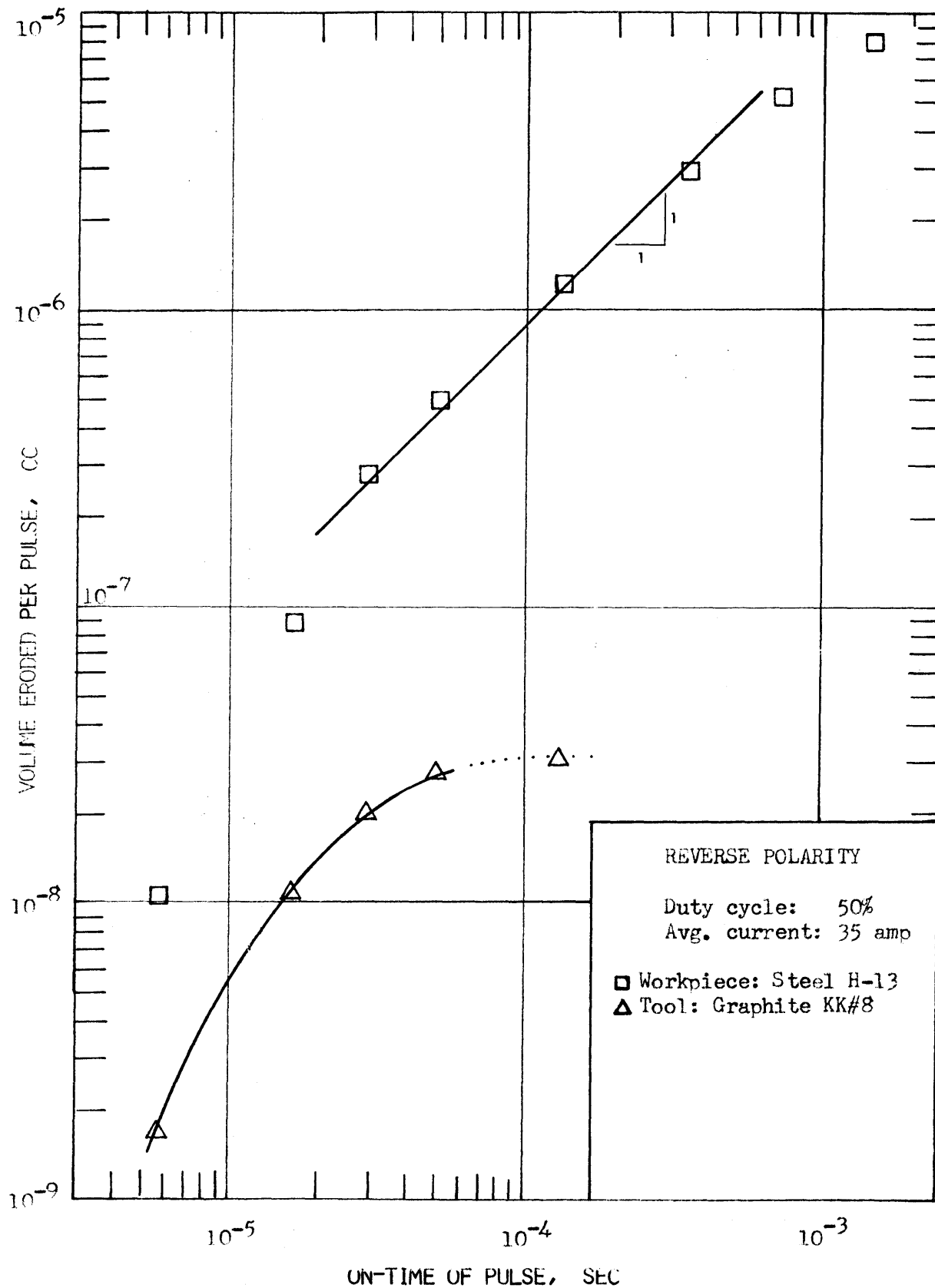
Fig. 33. Dependence of volume of material eroded per pulse
on pulse duration: Reverse polarity.

-82-

(average current)$^{0.85}$. If we now assume that the average current is proportional to the arc current (in general a fair assumption, except at very high currents, where machining is again very unstable), we get that the volume, $\mathcal{V}$, eroded per pulse is given by:

$$\mathcal{V} \propto (I_{arc})^{0.85} \qquad (4-6)$$

This equation holds for a negative steel workpiece being machined at an average current between 7 and 70 amps. It follows that Eq. (4-4) needs to be changed into the more accurate form:

$$\mathcal{V} \propto (I_{arc})^{0.85} V_{arc} t_{on} \qquad (4-7)$$

At this point it is worth noting that when a copper tool is used in place of graphite, Eq. (4-4) is verified over a large range of conditions.[5]

From the above discussion it is clear that over the range of ON-times and currents considered, the energy per pulse is the main factor in determining the relative amounts of erosion at the workpiece. However, the energy per pulse is not by itself sufficient for explaining the erosion at the graphite tool, nor can it explain the greatly reduced erosion at the workpiece when the ON-time is less than 20 $\mu$sec.

Power Density. Another factor of considerable importance in determining the quantitative erosion is the power density at the electrode surface. This is particularly important in the early stages of the discharge, or for very short ON-times, and may here be the main determining factor. The reason for this is that, due to conduction of heat into the solid, it takes a finite time, $t_m$, to bring the surface temperature of the electrode

up to the melting point of the material. This may be approximated as:[15]

$$t_m = \frac{k \, \rho \, c_p \, \pi \, (\Delta T)^2}{4H^2}$$

(4 - 8)

where  k = thermal conductivity

$\rho$ = density

$c_p$ = specific heat

$\Delta T = T_m - T_o$ = (melting temp.) - (room temp.)

H = incident power density

In order to obtain a better understanding of the importance of power density, let us consider a very simple thermal model. The assumptions involved are all questionable, but as a first step it aids in gaining insight into the EDM process, and particularly into the importance of power density.

Assumptions:

1.  The power density is constant during the ON-time of the pulse, and zero otherwise.

2.  When $t < t_m$ all the energy reaching the surface goes into heating the solid (i.e., is conducted into the solid).

3.  At time $t = t_m$ melting begins, and when $t > t_m$ all the energy reaching the surface goes into melting the metal, i.e., there are negligible conduction losses.

4.  All the molten metal, or a constant fraction of it, is removed.

5.  If $t_{on} < t_m$ no erosion occurs.

6.  Removal of metal by vaporization is negligible.

7.  Each pulse has to heat up the surface from room temperature.

-84-

By using this simple model we see that the fraction, F, of the

incident energy which is available for eroding the surface is simply:

$$F = (t_{on} - t_m)/t_{on} \qquad\qquad (4 - 9)$$

This quantity is plotted as a function of frequency, for different

values of the power density, in Fig. 34. Note that if the energy per

pulse were the only factor of importance, then we should expect no variation

of erosion rate with frequency, since at higher frequencies, even though

there is less erosion per pulse, there are many more pulses. Fig. 34

shows what happens when power density $\underline{is}$ taken into consideration. The

graph predicts that for a power density below $10^6$ watts/cm$^2$, there should

be no erosion whatsoever at frequencies above 200 kc. Also, at a power

density of $10^5$ watts/cm$^2$, there should be no erosion at frequencies

above 2 kc.

These numbers clearly show the importance of power density, and

through this concept we hope to explain the low wear ratios obtained

at high energies per pulse.

In spite of all the assumptions involved in the above model, Fig. 34

may be used to obtain an order of magnitude estimate of the power density

in an actual situation, by superimposing an actual erosion rate vs. frequency

curve on top of Fig. 34. Also note that this graph is for steel only,

and changes from one material to the next, since for a given power density,

different materials have different values for $t_m$.

Theoretical Support for proposed Model.    The data presented in chapter 3

shows that when a steel workpiece is machined with a graphite tool under
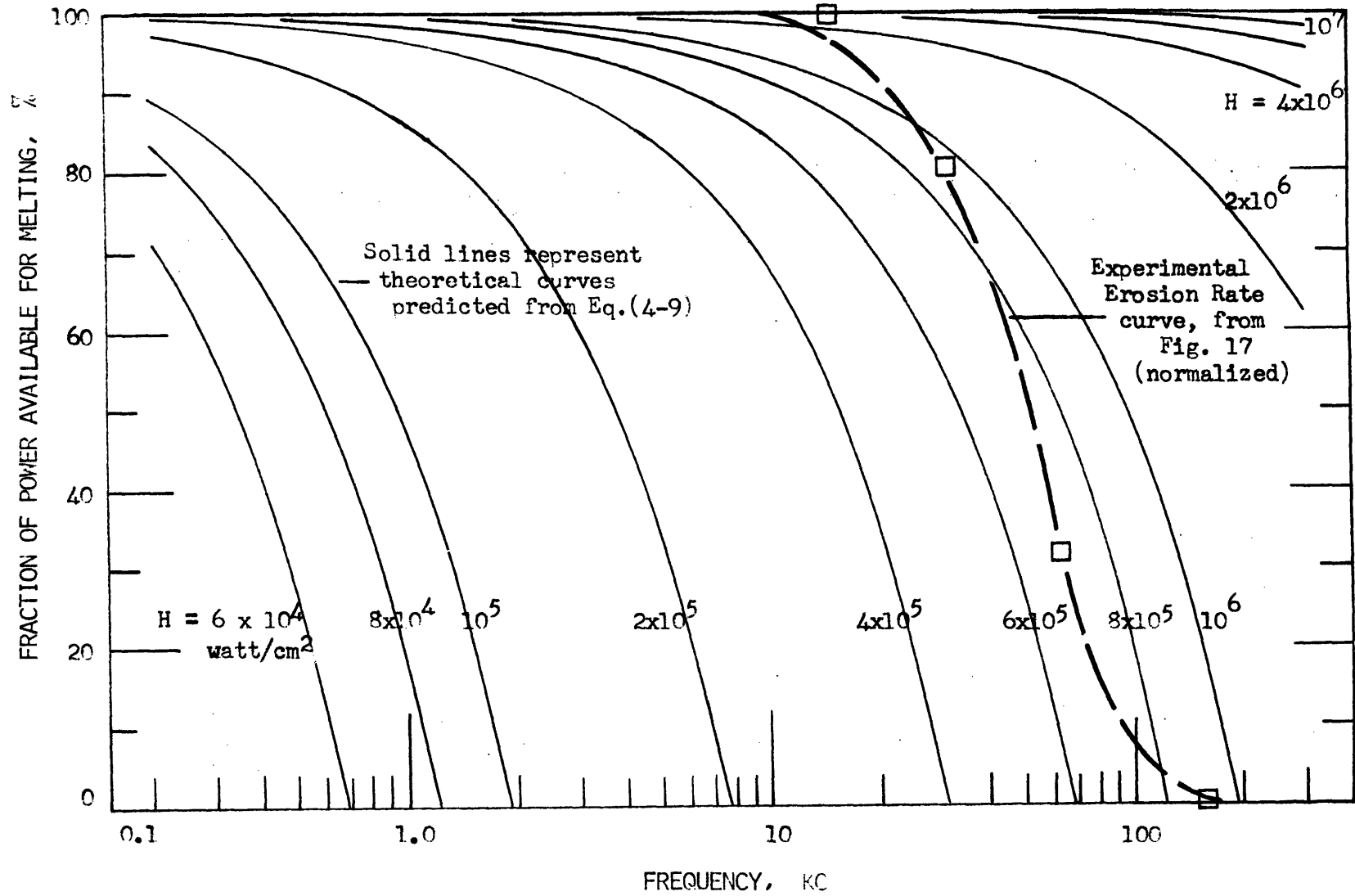
Fig. 34.  Fraction of ON-time available for melting iron surface, as a function of frequency and power density (H) at a duty cycle of 50%.

reverse polarity conditions, the wear ratio decreases with increasing

energy per pulse. This means that the relative anode erosion is lower

at high pulse energies, since the erosion per pulse from the workpiece

is close to being proportional to the energy per pulse. The data further

show that the magnitude of the interelectrode distance increases with

increasing energy per pulse. Hence reduced anode erosion occurs at larger

gap distances.

But why should anode erosion be lower (compared to cathode erosion)

at larger interelectrode distances? Below are four possible explanations.

1. Holm[36] is a strong supporter of the thermal theory. In his

   work on electrical contacts he has found that anode erosion

   is less at larger interelectrode distances. He explains this

   by saying that the discharge channel expands from the cathode

   to the anode so that at larger spacings the anode spot is larger.

   The anode power density is therefore lower. But if the power

   density is lower it takes longer to heat the surface up to

   its melting point, so less melting and hence less erosion

   takes place.

2. Mandel'shtam and Raiskii[11] suggest that anode erosion is

   caused by the mechanical impact of "vapor flares" from the

   cathode moving at thousands of meters per second in the gap and

   colliding with the anode surface. They say that the erosive

   action of these flares or jets becomes less effective at larger

   gap spacings, and in their experiments they did observe less

   erosion at the anode when the interelectrode distance was larger.

3. During an earlier study by the author[5] it was noticed that whenever low tool wear is obtained, the tool surface is covered with material from the cathode. In that study it was suggested that this plated layer of cathode material (steel) forms a protective layer against erosion of the tool (copper or graphite), since tool wear can only result after the protective layer is eroded away. Calculations carried out by Weetman[35] based on Maecker's jets[12] (a result of the pinch effect) suggest that material can be carried across the gap by these jets, which, according to the calculations, become more effective at larger gaps.

4. Zingerman and Kaplan[48] observe an increase in arc voltage with increasing electrode separation. They attribute this to an increase in the voltage drop in the plasma, and state that as a result, less energy reaches the anode. At a gap of 500 microns the energy transferred to a copper anode is reduced by a factor of 4.3, they claim.

These theories all agree that large gap spacings are conducive to low tool wear in reverse polarity EDM. In view of our present knowledge, let us see which is most likely to be correct. First of all, the theory of Zingerman et al. does not appear to be applicable in our case, since no increase in arc voltage is observed when the gap increases. Calculations by Spiridon[49]* yield a value of 0.012 ohm-cm for the resistivity of the plasma, so if this value is correct the total voltage drop in the plasma of an EDM arc should be only a fraction of one volt, except, perhaps, during

---

*based on electron conductivity only, in a 1 cm long arc at atmospheric pressure. Due to the relatively low mobilities of ions,[69] well over 99% of the current is carried by the electrons.[49]

the very early part of the discharge.

The theory of Mandel'shtam et al. was discussed in section 1.2,
where several objections to the theory were presented. We may further
note that the high velocities of the vapor jets, which have also been
reported by other authors,[50] are now believed to be considerably lower,
at least one order of magnitude,[12,51] which would undoubtedly reduce the
possible erosion from such jets quite substantially. This throws strong
doubt on two of the suggested explanations, and leaves plating and arc
spreading, both of which we believe to be of considerable importance.

In the study referred to earlier[5] more plating was observed on
graphite and copper electrodes when the wear ratio was low, i.e., when the
gap was large. We conclude from this that either the plating mechanism is
more effective at larger gaps, or the erosion mechanism is less effective,
or both. Viswanathan[34] has recently shown that plating does indeed reduce
erosion of the plated electrode, but cannot by itself at all times
completely eliminate erosion, since for some material combinations both
plating and erosion in substantial quantities are observed simultaneously.
From these latter results[34] it appears that the reduced plating which
was observed when machining at small gaps[5] was due to less effective
plating rather than to more effective erosion. It therefore seems reasonable
to assume that increased plating occurs at larger gaps.

Steel plating on a copper tool may offer good protection, since
the copper has a high conductivity which causes the steel layer to be cooled
effectively.[15] Also, melting of the copper without melting the steel layer
may occur since the melting point of steel is considerably higher than

that of copper. This effect presents a very efficient heat sink, since

the copper under such conditions would probably resolidify after the pulse

is over. De Nigris[15] has explained why steel plating may also offer

good protection to a graphite tool. Since steel vaporizes at temperatures

where graphite is still solid, the layer of steel would have to be completely

vaporized before any erosion of the graphite could occur. According to

his calculations it would take 210 $\mu$sec to remove a 25 micron layer of

steel from a graphite surface if the power density is $10^6$ watts/cm$^2$.

And now let us consider Holm's theory of the spreading arc. Let us

see if we can, at least qualitatively, justify the assumption that the

arc spreads as it moves from the cathode towards the anode (Fig. 35).
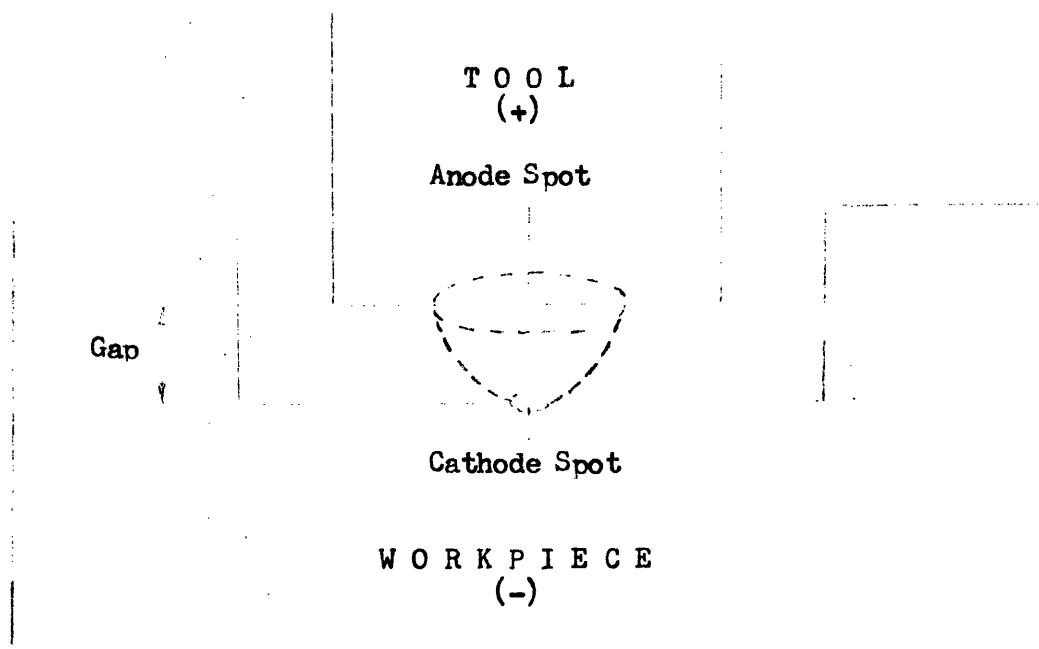


Fig. 35.  The anode spot size increases with gap distance.

The idea of a spreading arc is in no way unique with Holm. The same assumption has also been made by a number of other authors. There are two types of arc spreading which we shall consider here:

(1) Spreading with distance from the cathode.

(2) Outward spreading with time.

Both Holm[36] and Webb[43] have explained reduced anode erosion at larger gaps by assuming that the arc diameter increases with distance from the cathode; Holm arrived at this conclusion through his electrical contacts work, and Webb drew the same conclusion from his experience with EDM arcs. Ecker[39] has discussed the division of the cathode fall region into several zones (Fig. 36). He states that most of the voltage drop in the cathode fall occurs in the space charge region which extends about one mean free path ($\sim 0.1$ micron) out from the cathode. Further out there is a much larger section which he calls the contraction region, where most of the change in arc diameter occurs. Maecker[12] has also reported a spreading of the arc in the cathode fall region. He argues that because of this spreading the current density decreases with increasing distance from the cathode surface. The magnetic pressure, which is

Space charge region

Cathode        Contraction        Plasma
                   region
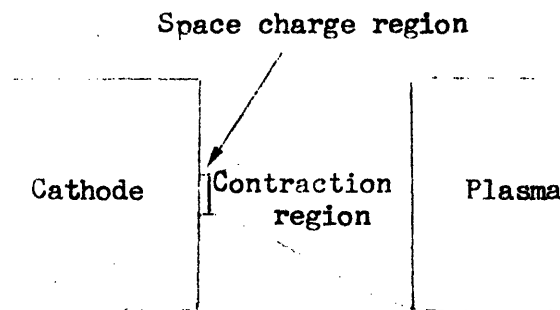
Fig. 36.  Zones in electric arc, according to Ecker.[39]

-91-

proportional to the current density, is therefore higher near the surface. Hence there must be a pressure gradient away from the surface, and Maecker has observed flows, or plasma streams, which he attributes to this effect.

In the initial stages after breakdown has occurred the current passes through a very thin conducting channel in the plasma. As time goes on and energy is dissipated this conducting channel spreads outward, at first very rapidly and then gradually slowing down. [54,55] It is known that the size of the mark left on the anode increases with pulse duration,[56] but this is not necessarily caused by a spreading arc. It has been suggested[6] that the anode current density does not change with time, and that the larger mark may be due to outward conduction and melting. Sowerville[6] states that the current density in the plasma decreases with time, indicating outward spreading, probably by ambipolar diffusion of ions and electrons. Ullman[44] has reported on EDM discharges and states that during the spark the current density is high at both electrodes, but in the arc (later in the discharge) there is spreading from cathode to anode (Fig. 37).



Spark                    Arc
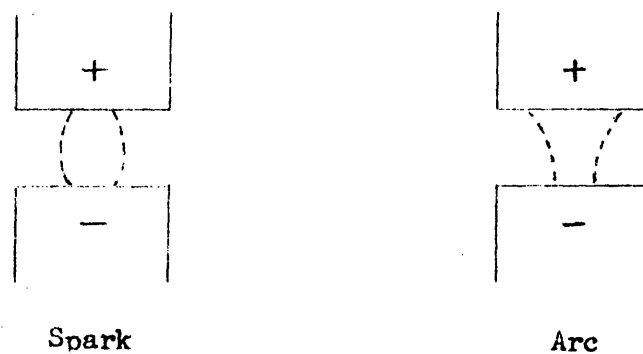
Fig. 37.  Illustration of channels in EDM discharges,
          according to Ullman.[44]

-92-

In spite of some uncertainties, there appears to be considerable evidence of the arc spreading with distance from the cathode, and there may also be spreading with time, so the assumption of reduced current densities seems justified even if not proven. Both types of spreading lend support to our model.

Let us now see how much the diameter of the anode spot would have to increase in order to make a significant change in the time required to bring the anode surface up to its melting point. To fix ideas let us consider a concrete example. In the case of a copper anode with a power density of $10^6$ watts/cm$^2$, Eq.(4-8)leads to the prediction that $\sim 13 \mu$sec are required to bring the surface up to its melting point. Let us now assume that the anode is moved sufficiently far away that the diameter of the anode spot doubles. This would mean an increase in the area of the spot by a factor of 4. According to Eq.(4-8), this would increase the time to bring the surface up to the melting point by a factor of 16. Hence $t_m$ would now be 208 usec instead of 13, and a pulse of 208 usec duration would now cause no erosion of the tool. Similarly, a 20% increase in the anode spot diameter would increase $t_m$ by 107%.

It is clear from the above that only a slight increase in the spot size will make a very significant change in $t_m$. Since this would cause the power density to become smaller at larger gaps we should expect the anode wear, and therefore the wear ratio, to decrease with increasing interelectrode distance, as indeed it does (Fig. 38).

REVERSE POLARITY

Duty cycle: 50%
Arc current: 65 amp
(varying frequency)

Tool: Graphite KK#8
Workpiece: Steel H-13
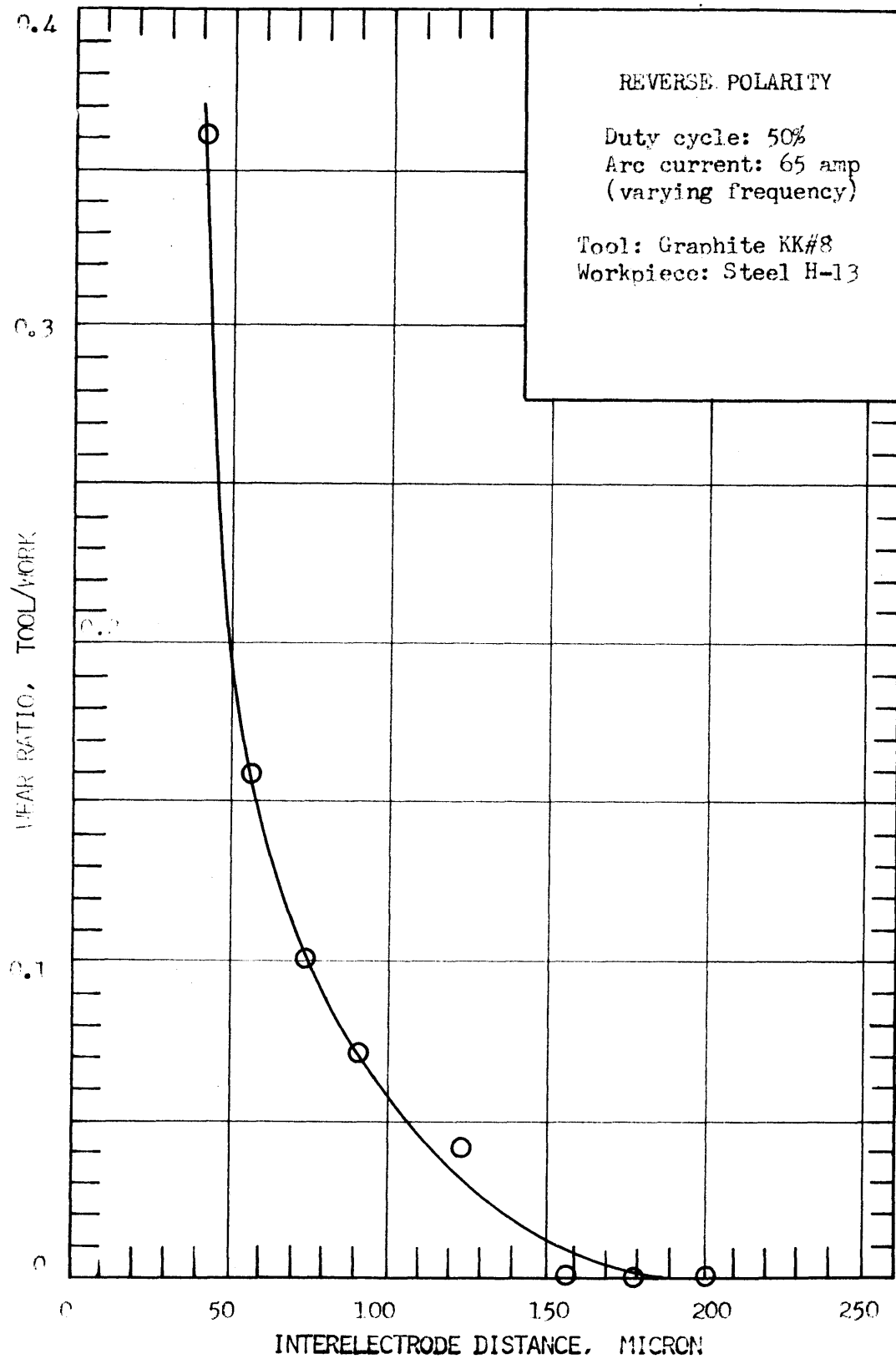
Fig. 39. Dependence of wear ratio on interelectrode
distance: Reverse polarity.

-94-

## 4.2  Interelectrode Distance and Energy per pulse

In chapter 3 we saw that increased energy per pulse correlates with increased size of the gap.  What brings about this increase in gap size, and how can it be predicted?  Is a high energy per pulse in itself sufficient to guarantee a large gap?  The answer to this last question is definitely: No.  We find (Appendix J) that when machining with refractory materials at both electrodes, the gap can be as much as four times smaller than the corresponding gap at the same energy per pulse when steel is one of the electrodes.  Regarding the earlier question, the model suggests that the volume of material removed per pulse is the determining factor.  Either the particle size or the resulting rough surface with large protrusions (or both) are thought to be the controlling factors, and analysis of the data will indicate to what extent the model appears to be correct.

Predicted relationship. Even if the particle size is not the controlling factor in determining the gap size, it seems reasonable to assume that at any given time the gap has to be at least as large as the diameter of the largest particle  in the gap at that time.  Let us then see how the diameter of the largest particle compares with the measured size of the gap.  But how large is the largest particle?

A high energy per pulse causes large amounts of material to be eroded from the workpiece in each pulse.  We know from section 3.4 that both large and small particles are collected, and that the energy per pulse both strongly influences the particle size distribution (Fig. 30), and seemingly sets an upper limit on the particle sizes.  The material eroded in each discharge may be removed as one single particle, or as a large number of

-95-

particles. So the largest particle would clearly be formed when all the

material eroded in a given pulse comes out as one single particle. But

from our experimental work (Eq. 4-7), we know that under reverse polarity

conditions, when a graphite tool is used to machine a steel workpiece,

the volume, $\mathscr{V}$, of material eroded per pulse is given by:

$$\mathscr{V} \propto (I_{arc})^{0.85} \, V_{arc} \, t_{on} \qquad\qquad (4-7)$$

This holds approximately for $50 < I_{arc} < 200$ amp and $20 < t_{on} < 500 \,\mu sec.$
But the volume of a spherical particle is proportional to the cube of its

diameter, so

$$\text{(max. particle diameter)} \propto \mathscr{V}^{1/3} \qquad\qquad (4-10)$$

i.e. $\qquad\qquad$ (max. particle diameter) $\propto (I_{arc})^{0.28} \, V_{arc}^{1/3} \, t_{on}^{1/3} \qquad (4-11)$

But if there is _any_ relationship between the gap size and the

maximum particle diameter, we would, as a first approximation, expect

a direct proportionality.

$$\text{(gap)} \propto \text{(max. particle diameter)} \qquad (?) \qquad (4-12)$$

so that: $\qquad$ (gap) $\propto (I_{arc})^{0.28} \, V_{arc}^{1/3} \, t_{on}^{1/3} \qquad\qquad (?) \qquad (4-13)$

Let us now assume a power law of the form (gap) $\propto I_{arc}^{a} \, V_{arc}^{b} \, t_{on}^{c}$,

and see how this agrees with experiment.

New Look at Experimental Results.  In Figs. 20 and 21 the interelectrode

distance was plotted vs. frequency and duty cycle respectively. In view

of our new information, we can now combine these two sets of results into

a plot of gap vs. ON-time. This is done in Fig. 39, where it is clear

that for ON-times between 10 and 800 µsec,
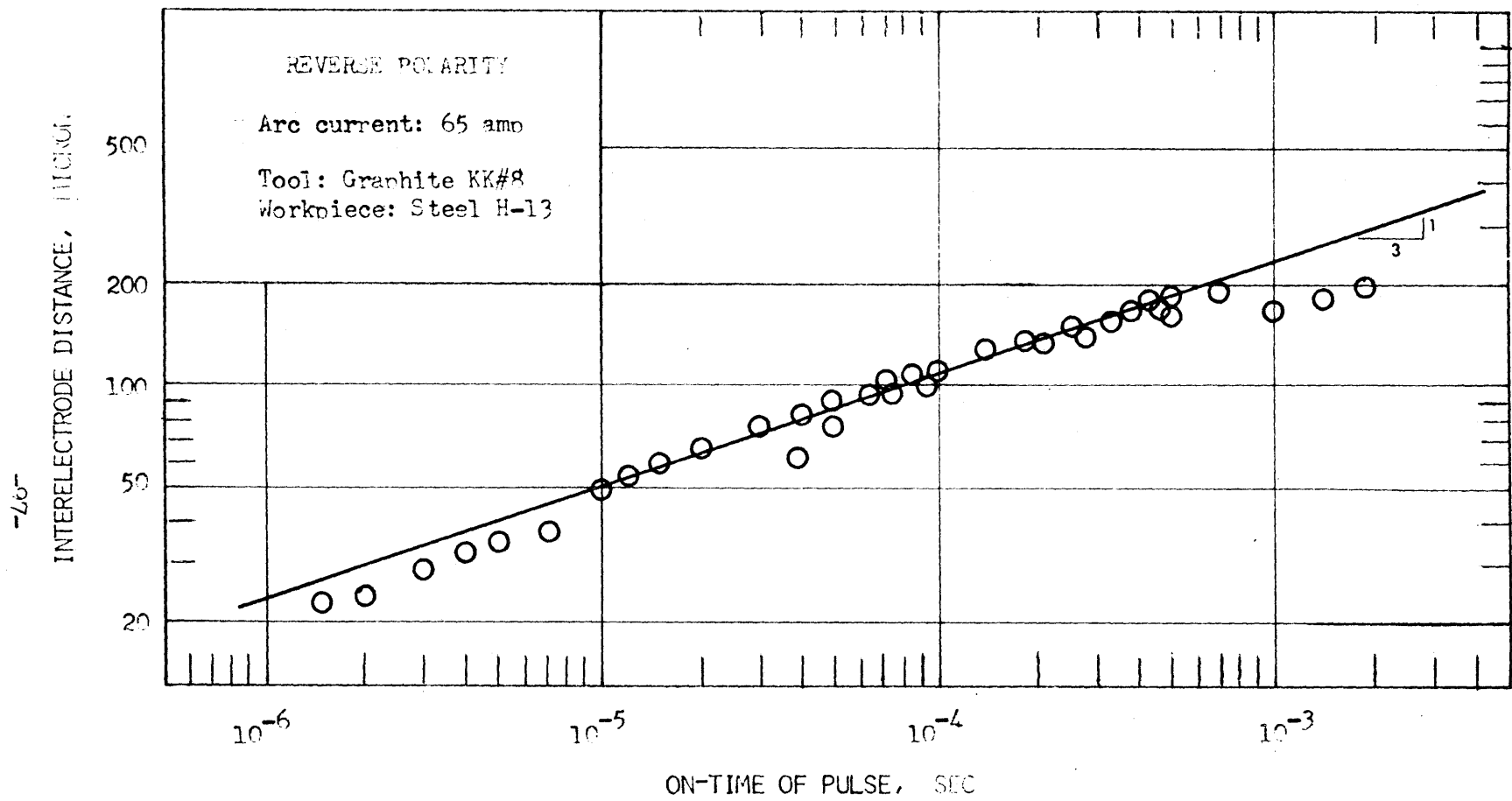
Fig. 39. Dependence of interelectrode distance on pulse duration:   Reverse polarity.

$$(\text{gap}) \propto (\text{ON-time})^{1/3} \qquad\qquad (4 - 14)$$

Combining this result with Eq.(3-3), i.e.,

$$(\text{gap}) \propto (\text{arc current})^{0.25} \qquad\qquad (3 - 3)$$

we get the following experimental result:

$$(\text{gap}) \propto I_{arc}^{0.25} \, t_{on}^{1/3} \qquad\qquad (4 - 15)$$

The agreement with the model (Eq. 4-13) could hardly be much better.

Comparison of Gap Size with "Theoretical" Particle Diameter.    So far we have shown that the interelectrode distance and the maximum particle size are both proportional to the same quantities, so they are proportional to each other. However, we have not yet determined the value of the constant of proportionality, which, from the model, should be of the order of unity.

To calculate the diameter of the largest particle we consider the total volume eroded from the workpiece in a given time, and divide this quantity by the number of pulses put out by the power supply in the same time. We shall also allow for the fact that the particles are hollow.

Assumptions:

1. Each pulse put out by the power supply results in an effective discharge.

2. The particles are 50% hollow by volume.

The first assumption is fairly good under stable machining conditions, otherwise it is poor. The second assumption is somewhat questionable, but

appears to be fairly good in the case of steel particles. The calculations are summarized in Appendix G, where the second assumption is also discussed in more detail, and the results are plotted in Fig. 40. The relative importance of the second assumption is also indicated in the figure. In view of the assumptions involved, the agreement between gap size and maximum particle diameter is much better than expected.

## 4.3  Particle Injection.

Steel particles.   We suggested earlier that the attempt at machining with injection of large particles failed, at least in part, because there was insufficient energy in each discharge to melt the large particles. This was suggested by the unstable machining, and was further substantiated by a simple experiment. The distance between a smooth copper tool and steel workpiece was preset at 250 microns, and a few large particles were injected to bridge the gap and cause discharges. After several discharges the electrodes were removed and inspected. When low pulse energies were used (Fig. 41 (a)), the particle was, in about half of the cases, fused

COPPER TOOL  (+)                COPPER TOOL  (+)

Scorchmark

STEEL
WORKPIECE
(-)

(a)                                    (b)
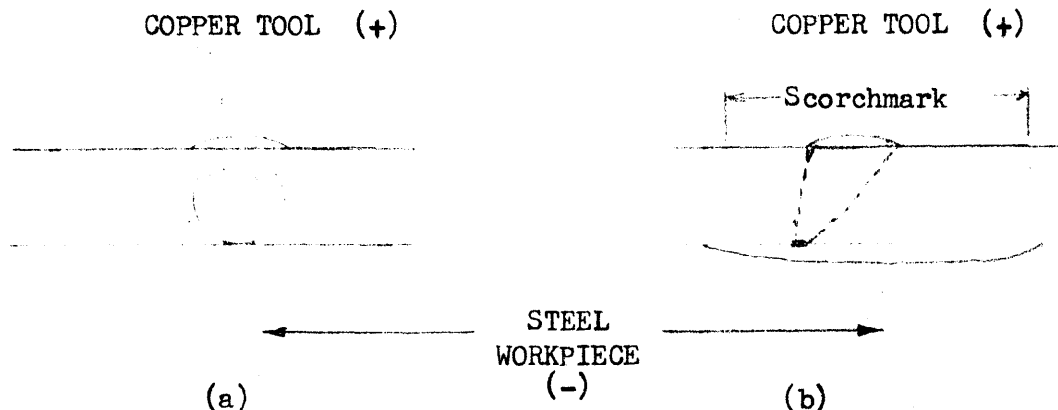
Fig. 41.  Particle injection at large preset gap.

INTERELECTRODE DISTANCE AND PARTICLE DIAMETER, MICRON

1000

100

10

50% hollow

75% hollow

25% hollow

Solid

REVERSE POLARITY

Arc current:    65 amp
Duty cycle:     50 %

O   Measured interelectrode distance
—   'Theoretical' particle size

1
3

10⁻¹

1.0

10

10²

FREQUENCY,  KC
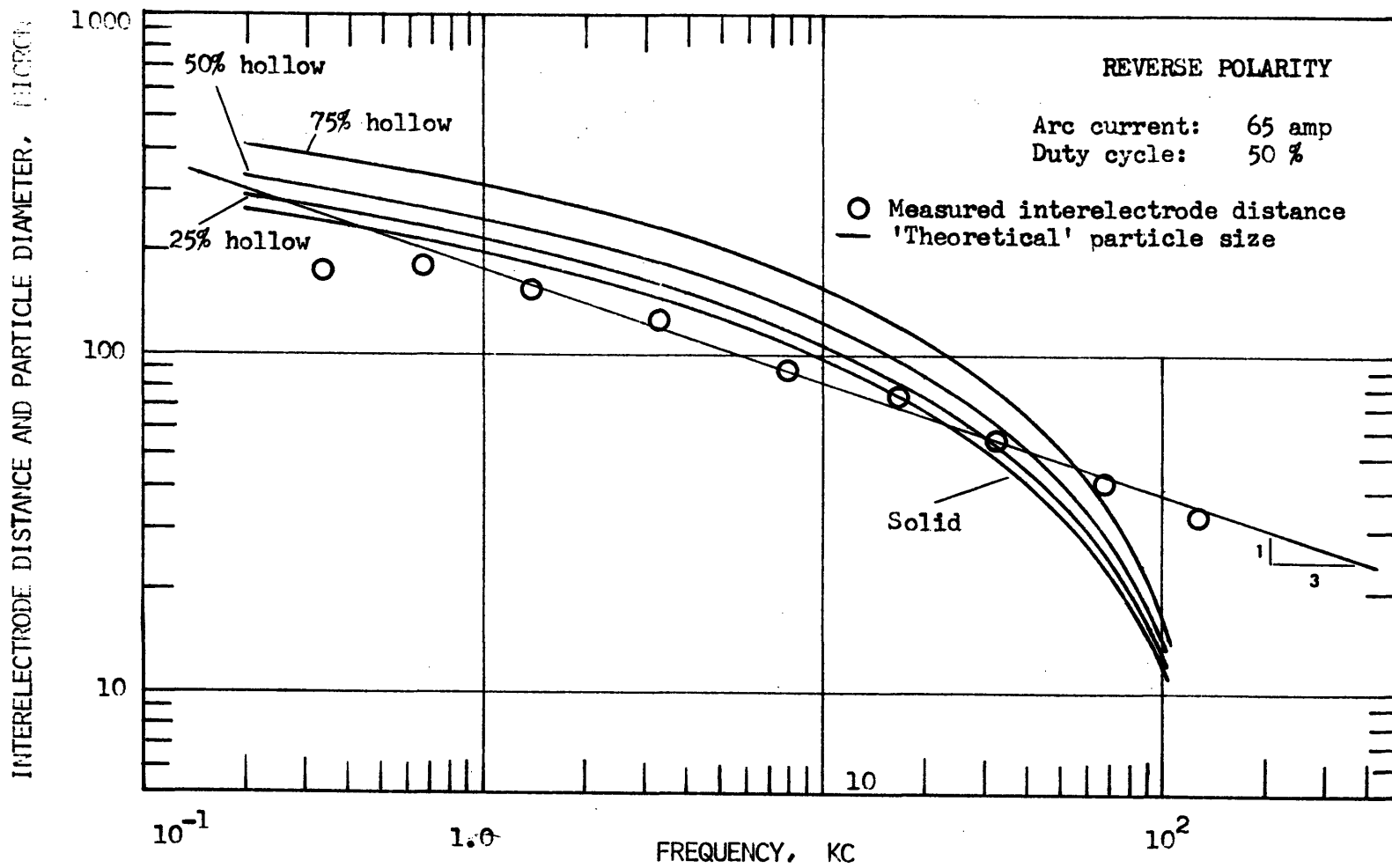
Fig. 40.   Comparison between the measured gap size and the 'theoretical' maximum particle diameter.

-100-

onto the cathode surface. Considerable tool erosion had taken place.
The initial purpose of this last test was to obtain a discharge at low
pulse energy and large electrode spacing. However, the effective
discharge occurred between the particle and the tool, and therefore
at a small gap size, thereby causing considerable tool erosion.
Clearly there was insufficient energy to melt the whole particle;
it just suffered some erosion on top. The energy required to melt
a particle is calculated in Appendix F.

To see what would happen at higher energies, the experiment was
repeated at the same gap setting and same arc power, but at a much
longer ON-time. In this case the particle certainly melted. There
was a large, shallow crater on the steel cathode (workpiece). The
anode had a small crater in the center and a large scorchmark (with
negligible damage) around the crater (Fig. 41 (b)). The shape of the
scorchmark followed the outline of the cathode crater and was roughly
circular, but of a diameter slightly smaller than the crater on the
cathode. A possible picture which emerges from this information appears
to be that of a spreading discharge from a small, rapidly moving
cathode spot to a relatively stationary, larger anode spot. The
scorchmark could have been formed by outward conduction from the
anode spot, as is usually assumed,[49] but was more likely formed by
radiation from the hot cathode spot or the plasma, or possibly from
jets of hot plasma being hurled at the anode as a result of the pinch
effect. This picture is full of interpretation, and might be all wrong,
but it does illustrate one important point: the danger involved in
calculating the current density at the electrode surface through
dividing the total current by the size of the mark left on the electrode.
And yet, this is the procedure which is usually followed,[57,58] partly

because of its simplicity, and partly because of the lack of a
better method.

<u>Tin Particles</u>.   This experiment failed to produce the desired gaps
because the tin particles apparently melted <u>before</u> getting into the
gap (Fig. 42).  Considerable erosion of the copper tool near the
point A in the diagram seems to support this picture.  Furthermore,
the gap was measured and was found to be much smaller than the
diameter of the particles injected.

These results throw some doubt onto the picture of particles
controlling the gap.  Why should particles which are formed in the
gap be able to control the gap size if injected particles cannot
do the same?  Of course, there is a difference between the two cases,
but is this difference sufficient to reconcile the results?  We may
add that in the experiments with the preset gaps, no discharges
could have occurred without the presence of the large particles,
but this need not be the case under normal machining conditions
between rough surfaces.

T   O   O   L

A                          A
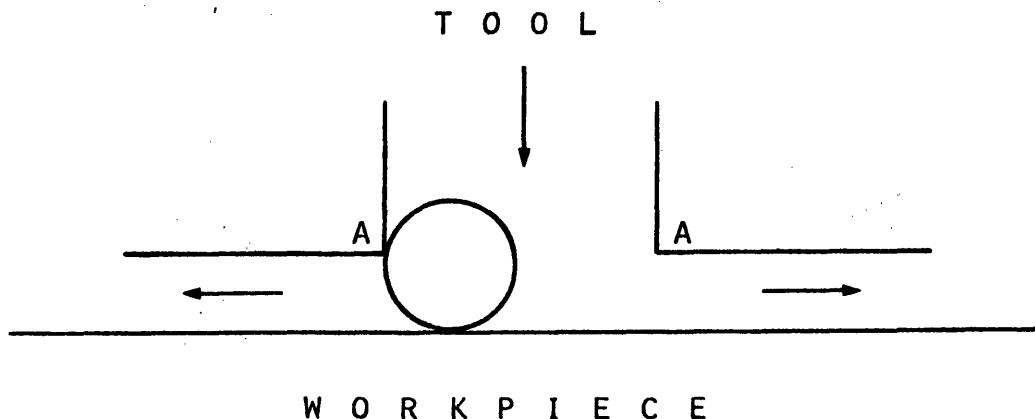
W   O   R   K   P   I   E   C   E

Fig. 42.   Interpretation of results from injecting tin particles.
-102-

4.4  Erosion Rate from Workpiece.

At constant power input and varying frequency, the erosion rate
from the workpiece (Fig. 17) falls off at high frequencies. The reason
for this is clear from Fig. 34: as the frequency goes up the ON-time goes
down, hence a larger fraction of the ON-time goes to heat the surface up
to its melting point, so less energy is left for eroding the material.
The reason for the decrease at lower frequencies is not so obvious. Less
stable machining may be part of the answer. Another solution is suggested
from results obtained by Viswanathan.[34] Using a thermal model based on
the assumption that the molten metal is removed after the pulse is over,
so that the thickness of the molten layer gradually grows, he finds that,
for materials which melt easily, the molten layer grows very rapidly, and,
since heat transfer through the layer then slows down, considerable
vaporization occurs from the outer surface. Since much more heat is
required for vaporization than for melting, the erosion efficiency falls
off. Quite likely this is what happens at lower frequencies; as the ON-time
increases the molten layer becomes thicker so more vaporization takes
place, and the result is a lower erosion rate.

The erosion rate is more or less independent of duty cycle over
the whole range tested (Fig. 18), as is to be expected from a constant
power input. In view of the above discussion regarding longer ON-times
we might expect a very slight but steady decrease in the erosion
rate with increasing duty cycle. Apparently the data are not
sufficiently accurate to detect this.

If the energy per pulse were the only factor of importance in

determining the amount of erosion, then the erosion rate should increase linearly with increasing average current. The actual increase is somewhat less than linear (Fig. 19). Here again the discrepancy is probably a result of larger molten pools and more vaporization with a resulting decrease in the erosion efficiency.

## 4.5 Wear Ratio Data

Above 1 kc the wear ratio increases with increasing frequency. According to the model, this is because the lower pulse energies give rise to shorter average arc lengths, so the power density at the tool increases, thereby causing more relative anode erosion. The slight increase in wear ratio below 1 kc suggests the possibility that the arc may now be spreading less with distance, so the change in power density is no longer sufficient to offset the longer ON-times, and consequently more tool erosion results. Also, Fig. 39 shows that the increase in interelectrode distance is not commensurate with increase in ON-time in this region, and this may further tend to increase the tool erosion rate. Part of the increase in wear ratio here is also due to the decreased workpiece erosion rate, but this is not sufficient to fully explain the results (Fig. 17).

An increase in duty cycle or average current results in a higher energy per pulse, so more material is removed per pulse, with the result that the effective interelectrode distance increases (Figs. 21 and 22) and the power density at the tool anode decreases. Hence, the wear ratio should decrease, as shown in Figs. 18 and 19.

## 4.6  Conclusions

The results of this chapter show that when the power density
at the surface is sufficiently high, the energy per pulse is the main
factor in determining the amount of erosion. Over a large range of
machining conditions the erosion at the steel cathode can be explained
through the consideration of pulse energy alone.

At very short ON-times, or at relatively low power densities,
the time required to bring the surface up to its melting point becomes
a significant fraction of the total ON-time of the pulse, so power
density must be considered in order to explain the results. For ON-
times below 20 µsec the power density is an important factor at
both electrodes. In accordance with the model, decreased power densities
and increased plating reduce the erosion of the graphite anode under
conditions when the interelectrode distance is large.

The interelectrode distance, as measured by the flow rate
method, agrees quite well with the "theoretical" particle diameter
which was calculated from the average volume of material removed per
pulse. This suggests that the volume of material removed per pulse
may be the controlling factor in determining the gap size.

# 5. DISCUSSION OF STANDARD POLARITY RESULTS

## 5.1 Interelectrode Distance

Under standard polarity conditions, just like in reverse polarity, the distance between the electrodes, as measured by the flow rate technique, increases with increasing energy per pulse. From Figs. 28 and 43 we see that:

$$(gap) \propto I_{arc}^{0.26} \, t_{on}^{1/3} \qquad (5 - 1)$$

for arc currents between 40 and 350 amps, and ON-times between 1 and 800 usec.

The volume of material eroded per pulse under standard polarity conditions may be obtained from Figs. 25 and 44.

$$\mathscr{V} \propto (I_{arc})^{0.91} \, t_{on} \qquad (5 - 2)$$

If this is what governs the interelectrode distance we should then expect the latter to be proportional to $(I_{arc})^{0.30} \, (t_{on})^{1/3}$, which is in reasonable agreement with Eq.(5-1).

## 5.2 Workpiece Erosion Rate

The erosion rate from the workpiece follows the same pattern in standard polarity as it does in reverse polarity, and the same explanations hold. When the power density is sufficiently high, the rate of power input is the determining factor, so we should, as a first approximation, expect no variation in erosion rate with frequency and duty cycle for constant average current and a simple proportionality with increasing current.
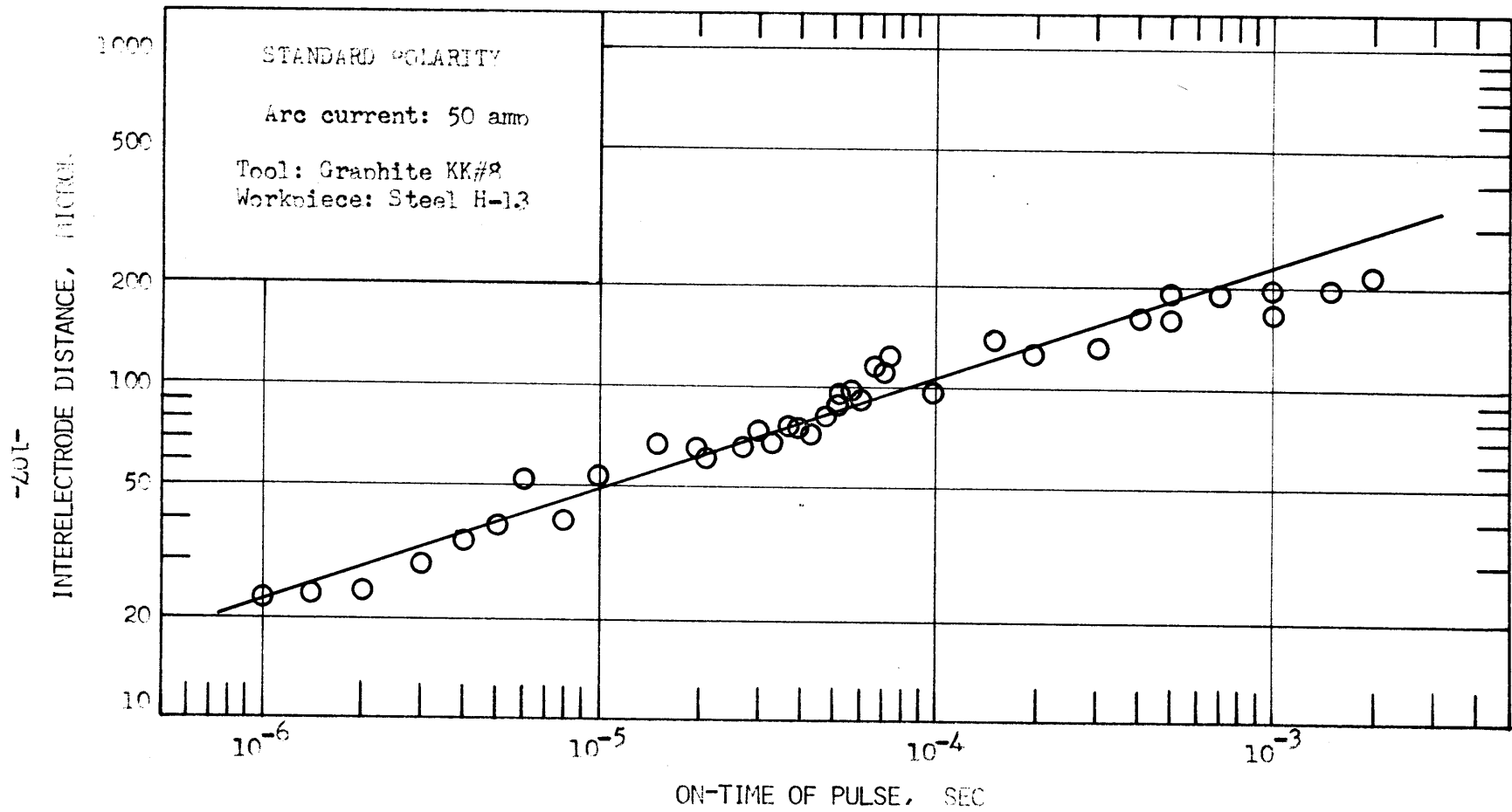
Fig. 43.   Dependence of interelectrode distance on pulse duration:   Standard polarity.
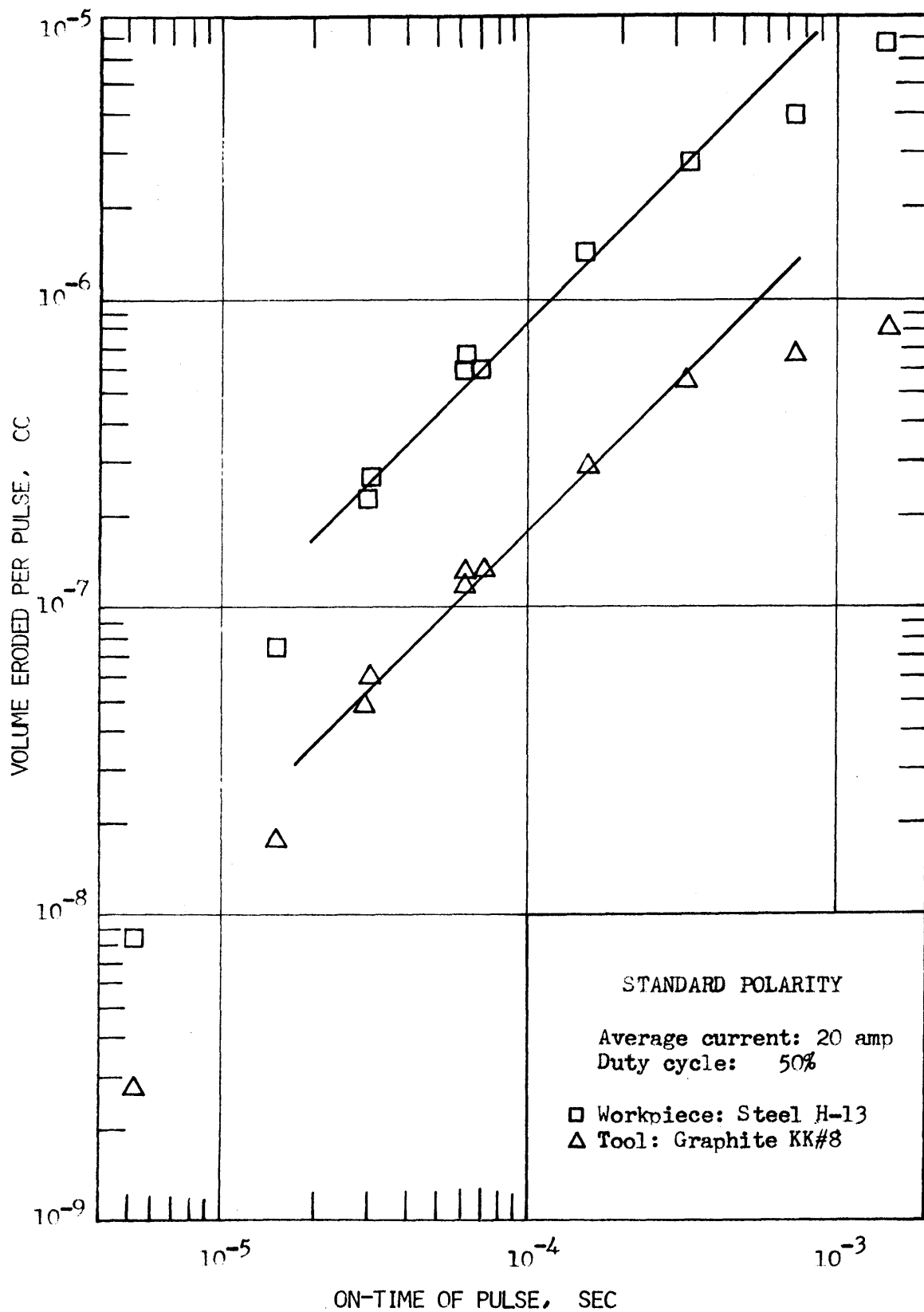
Fig. 44. Dependence of volume eroded per pulse
on pulse duration: Standard polarity.

-108-

This approximation fails at high frequencies (Fig. 23), where a substantial fraction of the ON-time goes to heat up the surface to its melting point, so the erosion rate falls off. The decrease in erosion rate at lower frequencies could again be caused by Viswanathan's theory[34] of the larger molten pool and resulting increased vaporization (section 4.4), which, in turn, results in decreased erosion efficiency. The same concept explains the slight decrease in erosion rate with increasing duty cycle (Fig. 24), and the lower than expected increase with increasing current (Fig. 25).

One important question arises here. In reverse polarity the anode erosion decreases due to a lower power density at the anode surface when the gap size increases. Why is this effect so much less pronounced at standard polarity when the gap is of the same order?

The answer seems to lie in the switch of materials, which brings about two contributing factors. First of all, for the same power density, steel is brought up to its melting point in a considerably shorter time than graphite (or copper),[15] so even if there is a lowering of power density at the steel anode as a result of the arc spreading, as there probably is, $t_m$ still remains a sufficiently small fraction of $t_{on}$ that there is no marked reduction in the erosion rate from the steel. The second contributing factor is the fact that in standard polarity there is no plating of the steel anode when a graphite tool is used. In reverse polarity, on the other hand, there is very substantial plating of the graphite anode by steel at large interelectrode distances. The effectiveness of this plating in reducing erosion of the material under the plated layer was discussed in chapter 4.

-109-

## 5.3  Wear Ratio Data

In reverse polarity the erosion rate from the cathode was
determined primarily by the rate of power input.  The same seems to
hold in standard polarity where the tool is the negative electrode.
This expectation is clearly brought out in the duty cycle (Fig. 24)
and current series (Fig. 25), and also in the frequency series at
intermediate frequencies.  It may be seen that there is negligible
change in wear ratio under these conditions.  However, at very low
frequencies the wear ratio falls, and at very high frequencies it
increases.  The reason for this is not clear.  The discrepancy at
higher frequencies could be due to a higher power density at the
tool cathode very early in the pulse.  But this need not be so.
More likely it is due to mechanical erosion caused by physical
contact with the opposite electrode at these extremely short gap
spacings.  This is suggested by the fact that both positive and
negative graphite electrodes have surprisingly high relative wear
at short gaps (high frequencies).  Further evidence is obtained
from observation of the tool motion under these conditions.
Machining is unstable and the tool vibrates with an amplitude of
the order of the gap size, making physical contact quite possible.
Another explanation of graphite erosion in general is that the
material is rather porous and may "explode" due to vaporization of
oil in the pores.  Here again we might expect flaky, rather than
spherical, erosion products.  We may further add that for current
densities above $10^6$ amp/$cm^2$ Joule heating of graphite is very
substantial.[57]

## 5.4 Conclusions

When a steel workpiece is machined with a graphite tool under standard polarity conditions, the erosion rate from both electrodes is determined primarily by the rate of power input, under most of the machining conditions investigated. The most notable exception is that of very short ON-times, where power density again plays a determining role. There is no change of importance in the wear ratio with changing duty cycle or current, at constant frequency.

The volume of material removed per pulse is approximately proportional to the pulse energy, and the interelectrode distance is roughly proportional to the one third power of the pulse energy, suggesting that the volume of material eroded per pulse may be the factor which determines the gap size.

# 6. SUMMARY

When a graphite tool is used to machine a steel workpiece
under reverse polarity conditions, the quantity of erosion at the
workpiece is determined by the pulse energy, for pulse durations
between 20 and 500 microseconds. In order to understand the erosion
caused by shorter pulses it is necessary to consider the power
density at the surface, since the time required for heating the
surface up to its melting point is now a substantial fraction of
the pulse duration. We find that the wear ratio increases with
increasing frequency, and decreases with increasing duty cycle
or increasing average current. In general, the wear ratio in
reverse polarity decreases with increasing pulse energy.

A model based on the assumptions that (1) the power density
at the anode surface decreases with increasing interelectrode
distance, and (2) there is increased material transfer from cathode
to anode at larger gaps, is suggested from the reverse polarity
erosion data. A number of experiments were carried out to test the
extent of the validity of the model.

It is found that the electrical gap remains small and more
or less constant over a range of machining conditions, as is to
be expected from the breakdown conditions, and the maximum available
voltage put out by the power supply.

The arc gap, or flow rate gap, is found to decrease with
increasing frequency, and to increase with increasing duty cycle

or increasing average current, so that, as expected, the same
conditions which give rise to a low wear ratio also yield a
large gap, in accordance with the model. For most of the conditions
tested, the flow rate gap is approximately proportional to the
one third power of the pulse energy.

The erosion products in EDM appear partly in the form of
hollow spheres, and the size distribution of the spheres is governed
primarily by the pulse energy. The diameter of the largest particles
collected and the magnitude of the interelectrode distance are of
the same order. A theoretical maximum particle size, based on the
average volume of material eroded per discharge, has a diameter
which is approximately equal to the size of the flow rate gap.

Motivated by the desire to obtain lower wear ratios at higher
frequencies where erosion rates and surface finish are more
attractive, an attempt was made to force the gap to be large by
means of injecting large particles into the gap. An increase in gap
size was not obtained, so the hoped for reduced wear ratios were not
realized either. This experiment neither supports nor refutes the
model.

Measurements of surface roughness by means of surface traces,
cross sectional cuts, roughness meters, and microscope measurements
indicate that the size of the average roughness is much smaller than
the flow rate gap, but occasional protrusions are almost as large as
the gap. Both these protrusions and the particle sizes are determined
by the volume of material removed in each pulse, and both appear to

have an effect on the gap size. However, the protrusions[*] seem to be more important since it is possible to have a large flow rate gap even in the absence of particles.

In spite of some uncertainties, the assumptions involved in the model appear to be reasonable. Spreading of the arc may occur both as a result of electrode separation and longer pulse duration. Observations also support the view that plating of the anode by material from the cathode is more prevalent under conditions which yield larger gaps.

Workpiece erosion rates under standard polarity conditions follow the same trends as in reverse polarity, mostly for the same reasons. At constant frequency the wear ratio is almost independent of duty cycle and average current. An unexpected increase in the wear ratio at higher frequencies was obtained. In standard polarity the interelectrode distance is again proportional to the one third power of the pulse energy.

---

*Appendix N

# 7. RECOMMENDATIONS

1.     The volume of material eroded per pulse is determined primarily by the pulse energy, over a large range of machining conditions. However, as the data in this thesis show, the additional erosion obtained from a steel workpiece by increasing the ON-time is not exactly the same as that obtained by increasing the arc current by the same fraction, i.e., pulse energy is important, but it is not the whole story; pulse shape is also important. Erosion of a graphite anode is even more strongly dependent on the pulse shape. Why?

2.     The accuracy of machining in EDM may be specified by the size of the overcut (the difference between the radius of the whole in workpiece and the radius of the tool, in Fig. 8). This is a quantity which is not easily measured by conventional techniques,[5] because of surface roughness, but accurate values may be obtained by using the flow rate technique developed in this thesis.

3.     More information may be gained from tests with preset gaps, of the kind discussed in section 4.3. One advantage here is that the gap size is known exactly, both before and after the discharge. It is also possible to match up craters on the two electrodes and measure the relative erosion.

4.     Analysis of the particles obtained in EDM may yield more information about the EDM process. Most of the particles appear to be hollow. A study of particles from different materials, their fraction hollow, and the solubility of different gases in these materials should be interesting.

5.     Energy balance via I-F emission (p. 123) should be attempted.

# REFERENCES

1. P. E. Berghausen, H. D. Brettschneider, and M. F. Davis, Technical Documentary Report No. ASD-TDR-7-545, Cincinnati Milling Machine., Ohio, 1963.

2. N. Mironoff, Microtecnic 19, 149 (1965); 19, 171 (1965); 19, 253 (1965); 20, 78 (1966).

3. N. Mironoff, Introduction to the Study of Spark Erosion, Microtecnic-Scriptar Ltd., Switzerland, 1967.

4. N. H. Cook, Manufacturing Analysis, Addison-Wesley Publishing Co., Reading, Massachusetts, 1965, p.121.

5. H. C. Juvkam-Wold, S. M. Thesis, M.E. Dept., M.I.T., 1967.

6. J. M. Somerville, The Electric Arc, Methuen & Co., Ltd., London, 1959.

7. E. M. Williams and R. E. Smith, AIEE Transactions 74, 164 (1955).

8. E. M. Williams and R. E. Smith, AIEE Transactions 76, 93 (1957).

9. E. M. Williams, AIEE Transactions 71, 105 (1952).

10. E. M. Williams, U.S. Patent No. 2,835,785, January 3, 1955.

11. S. L. Mandel'shtam and S. M. Raiskii, Izvestiya Akademii Nauk SSSR 13, 549 (1949).

12. H. Maecker, Z. Physik 141, 198 (1955).

13. D. W. Rudorff, Proc.I.Mech.E., 171, 495 (1957).

14. B. R. Lazarenko and N. I. Lazarenko, Physics of Electrospark Metal Working (Book in Russian), Ministry of Electrical Industry, 1946.

15. E. G. De Nigris, S. M. Thesis, M.E. Dept., M.I.T., 1967.

16. B. R. Lazarenko and N. I. Lazarenko, Vestnik Akademii Nauk. SSSR, Vol. 29, No.6 (1959).

17. B. N. Zolotykh, K. Kh. Gioyev, and Ye. A. Tarasov, Probl. Elec. Obra. Mat., p.58 (1960).

18. A. S. Zingerman, NASA Reproduction from Microfiche, Accession No. N66-11452 August 24, 1965.

19. S. A. Doret, S. M. Thesis, M.E. Dept., M.I.T., 1968.

20. J. Priestley, History and Present State of Electricity, 2nd Edition, London, 1769, p.623.

21. R. E. Schofield, A Scientific Autobiography of Joseph Priestley (1733-1804), the M.I.T. Press, Mass. USA, 1966, p.34.

22. B. R. Lazarenko, Applied Electrical Phenomena, No.5, p.311 (1967).

23. B. R. Lazarenko and N. I. Lazarenko, Author's Certificate No.70010, April 13, 1943.

24. S. Hoh, U. of Tokyo, Denki Nihon, September 1949, p.8.

25. H. Kurafuji, Paper presented at 14th C.I.R.P. General Assembly., September 1964.

26. H. Kurafuji and K. Suda, J. of Faculty of Engr., U. of Tokyo 28, 1 (1965).

27. Newsweek, p.E8, Sept.1968.

28. Foreward to Reference 3.

29. S. P. Fursov, A. E. Gittlerich, Yu. V. Goloschapov, A. S. Fedorko, and V. G. Bivol, Applied Electrical Phenomena No.2(20) p.88 (1968).

30. M. M. Barash, Ph. D. Thesis, U. of Manchester, 1958.

31. H. Kurafuji and K. Suda, Paper presented at 17th C.I.R.P. General Assembly, September 1967.

32. H. Opitz, Microtecnic 13, 147 (1959).

33. M. M. Barash and C. S. Kahlon, Int. J. Mach. Tool Des. Res. 4, 1 (1964).

34. T. Viswanathan, Sc. D. Thesis, M.E. Dept., M.I.T., 1969.

35. R. Weetman, S. M. Thesis, M.E. Dept., M.I.T., 1968.

36. R. Holm, Electric Contacts, Springer Verlag, New York, 1967, p.305.

37. B. R. Lazarenko and N. I. Lazarenko, Stanki I Instrument 17, 8 (1946).

38. G. Pahlitzch, A. Visser and W. Funk, Annals of the C.I.R.P. 16, 243 (1968).

39. G. Ecker, Ergebnisse der Exakter Naturwissenscaften 33, 1 (1961) Springer Verlag.

40. I. G. Kesaev, Cathode Processes in the Mercury Arc, Consultants Bureau, New York, 1964.

41. S. S. Mackeown, Phys. Rev. 34, 611 (1929).

42. T. H. Lee, J. Appl. Phys. 30, 166 (1959).

43. R. S. Webb, U.S. Patent No. 3,158,728, November 24, 1964.

44. W. Ullman, Technische Rundschau p.1 Feb.1958.

45. G. R. Wilms and J. B. Wade, Metallurgia 54, 263 (1956).

46. K. H. Lloyd and R. H. Warren, J.Iron and Steel Institute 203, 238 (1965).

47. N. A. Fuchs, The Mechanics of Aerosols, The Macmillan Co., New York 1964, p.9.

48. A. S. Zingerman and D. A. Kaplan, J. Tech. Phys.(USSR) 28, 387 (1958).

49. A. Spiridon, S. M. Thesis, E.E. Dept., M.I.T., 1964.

50. W. Finkelnburg, Phys. Rev. 74, 1475 (1948).

51. A. von Engel and K. W. Arnold, Phys. Rev. 125, 803 (1962).

52. E. L. Murphy and R. H. Good, Phys. Rev. 102, 1464 (1956).

53. M. Motoki, K. Hashiguchi, and K. Tokoyuma, J. Inst. of E.E. of Japan 82, 167 (1962).

54. P. A. Eckman and E. M. Williams, Appl. Sci. Res. 8, 299 (1959).

55. P. A. Eckman, Ph. D. Thesis, Carnegie Inst. of Tech., 1959.

56. J. M. Somerville and C. T. Grainger, Brit. J. Appl. Phys. 7, 400 (1956).

57. J. A. Rich, J. Appl. Phys. 32, 1023 (1961).

58. R. Basharov, E. N. Gavrilovskaya, O. A. Malkin, and E. S. Trekhov, Sov. Phys.- Tech. Phys. 10, 1428 (1966).

59. K. D. Froome, Proc. Phys. Soc. 60, 424 (1948).

60. K. D. Froome, Proc. Phys. Soc. B62, 805 (1949).

61. K. D. Froome, Brit. J. Appl. Phys. 4. 91 (1953).

62. J. D. Cobine and C. J. Gallagher, Phys. Rev. 74, 1524 (1948).

63. R. H. Fowler and L. Nordheim, Proc. Roy. Soc. (London) A119, 173 (1928).

64. R. O. Jenkins and W. G. Trodden, Electron and Ion Emission from Solids, Dover Publications, Inc., New York, 1965.

65. J. D. Cobine, Gaseous Conductors, Dover Publications, Inc., New York, 1958.

66. R. Gomer, Field Emission and Field Ionization, Harvard University Press and Oxford University Press, 1961.

67. W. W. Dolan and W. P. Dyke, Phys. Rev. 95, 327 (1954).

68. G. Ecker and K. G. Muller, J. Appl. Phys. 30, 1466 (1959).

69. S. C. Brown, Introduction to Electrical Discharges in Gases, John Wiley & Sons Inc., New York, 1966.

70. C. L. Hemenway, R. W. Henry and M. Caulton, Physical Electronics, John Wiley & Sons, Inc. New York, 1965, p.68.

71. G. Rudinger, Cornell Aero. Lab., Inc., Tech. Report CAL-96-PU (1968).

APPENDIX A:   Electron Emission Mechanisms

A number of different mechanisms of current flow between a

negative electrode and the arc plasma have been proposed in the past.

These have been discussed in detail elsewhere.[39,64] The carriers of

charge in the cathode fall region are almost exclusively positive ions

and electrons. In this Appendix we shall consider various ways in which

these electrons may be extracted from the cathode surface. The electron

emission mechanism is primarily of importance for energy balance

calculations (Appendix B).

Electrons in a metal have the Fermi-Dirac distribution of energy

(Fig. A-1). At $0^{\circ}K$ all the electrons have energies at or below the Fermi
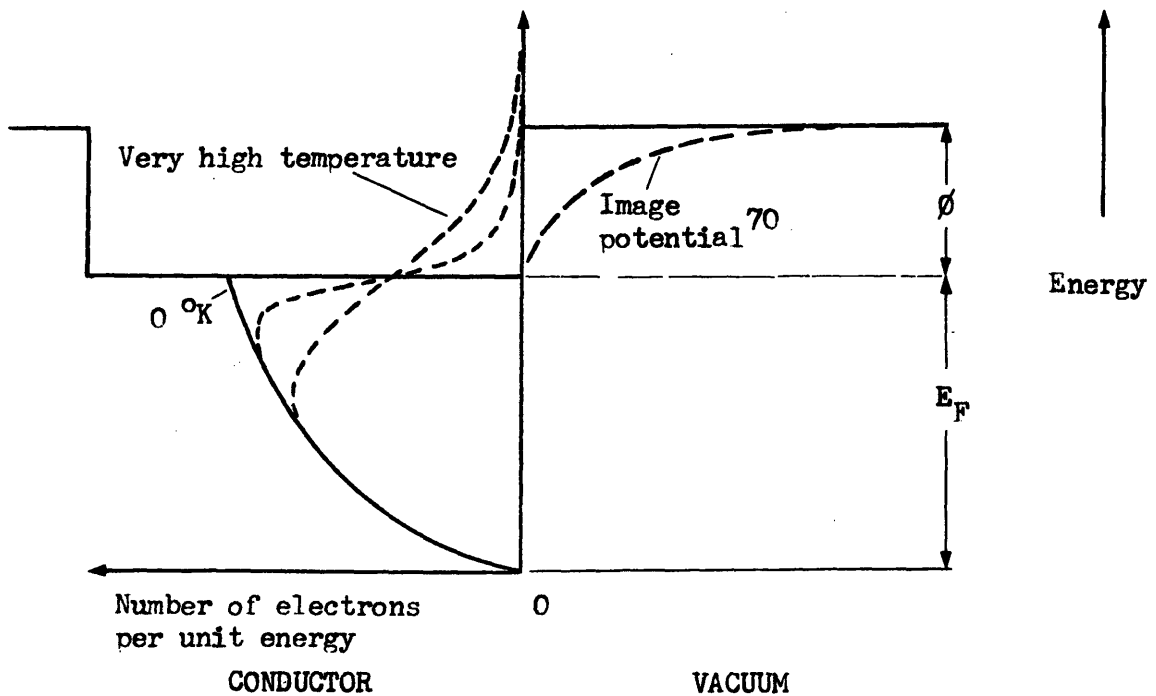


Fig. A-1.   Schematic illustration of the Fermi-Dirac distribution
            of energy for electrons in a conducting material.

level, $E_F$. At higher temperatures the distribution has a "Boltzman tail" with relatively few high energy electrons. Those electrons which have energies above $(E_F + \emptyset)$ associated with their motion perpendicular to the electrode surface have a chance of escaping over the work function barrier, $\emptyset$. This is called thermionic emission and is governed by the Richardson - Dushman equation.[65]

When a weak electric field is applied the thermionic emission is enhanced by the Shottky factor, which is in essence a lowering of the effective work function barrier (Fig. A-2 (a)). $\Delta\emptyset$ is the reduction in the effective work function. If now the electric field is increased to values of the order of $10^6$ or $10^7$ volt/cm, a completely different phenomenon occurs. Electrons now no longer have to get over the work function barrier, but may "tunnel"[66] through it (Fig. A-2 (b)). This is a quantum mechanical effect which may be explained qualitatively through the Heisenberg Uncertainty Principle. It is usually referred to as field emission. At



(a) Schottky effect          (b) Tunneling effect
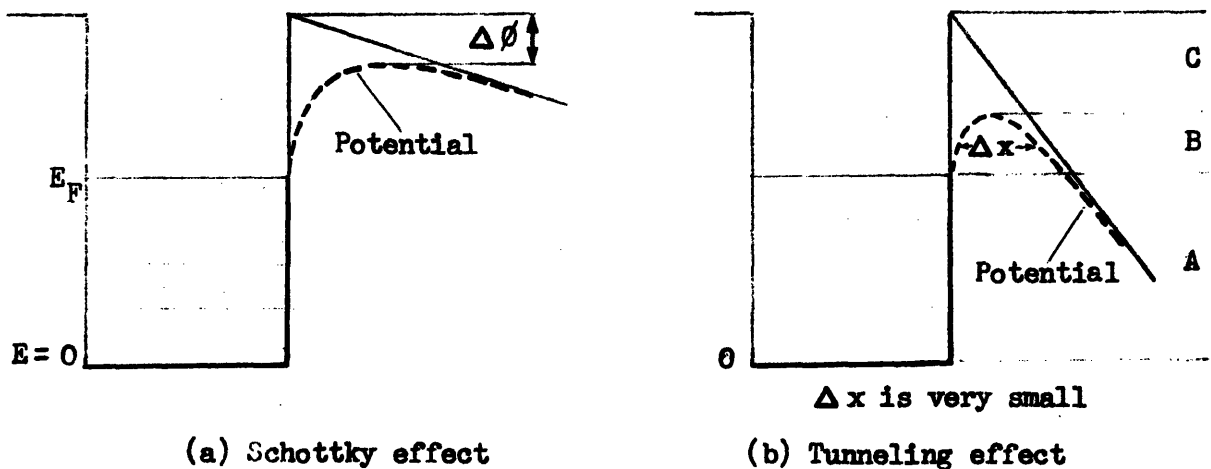
Fig. A-2. Schematic illustration of the potential near an electrode surface when an electric field is applied.

$0\ ^{\circ}K$ it is governed by the Fowler - Nordheim equation.[63]

There are two important factors resulting from field emission. First of all, electrons in the vicinity of the Fermi level may now be extracted, and since most of the electrons in a conductor have energies in this region, enormous current densities may be realized. The second point is that while in thermionic emission the "cooling" of the surface for each emitted electron is about $\emptyset$, whereas in field emission the cooling may be zero, or even negative (Appendix B). Adding the current densities predicted by the Richardson - Dushman and Fowler - Nordheim equations does not give an accurate estimate of the current emission caused by high temperatures and high fields, mainly because field emission is also influenced by changes in temperature. Dolan and Dyke[67] have suggested a mechanism they call T-F emission which takes into account both factors. According to this mechanism the current density, j, is given by:

$$j = \int_{-\infty}^{+\infty} A(T,\epsilon)\ \ D(E,\epsilon)\ \ d\epsilon \qquad\qquad (A - 1)$$

where $\epsilon$ is the difference between the electron energy and the Fermi level energy, and the energies are associated with the component of velocity normal to the surface of the conductor.

$A(T,\epsilon)$ describes the supply of electrons from the material to the surface, and

$D(F,\epsilon)$ is a transmission coefficient which gives the probability that an electron which reaches the surface will get out.

Referring back to Fig. A-2 (b), evaluation of Eq.(A-1) in the region A at low temperatures would yield the Fowler - Nordheim equation, and integration over the region C for low fields would yield the Richardson - Dushman equation. Emission from the transition region, B, indicates the

error involved in simply adding the results from thermionic and field emissions.[67]

Equation (A-1) in combination with MacKeown's equation (Eq.(C-7)) has been evaluated by Lee[42] for a large range of work functions, temperatures, and electric field strengths, using the somewhat more tractable values of $A(T, \epsilon)$ and $D(E, \epsilon)$ given by Murphy and Good.[52] Motoki and Hasaguchi[53] have applied T-F emission to energy balance calculations in EDM, and claim good agreement with experimental results.

Ecker and Muller[68] have suggested yet another mechanism, which depends primarily on an improvement on MacKeown's equation which considers the average field at the cathode. This mechanism considers the instantaneous field caused by individual ions, and is referred to as the individual field component effect, or I-F emission. It predicts much higher current densities than T-F theory does. There appears to be room for more work in this particular area.

APPENDIX B:   Energy Balance

A large number of investigators have made attempts at "energy balance" to see how much energy either, or both of the electrodes receive. A good summary of these attempts is given by Weetman,[35] who has carried out energy balance calculations for EDM arcs between a number of different materials.

In view of the amount of work already carried out in this field, we shall only present a few comments and a list of the different factors which should be taken into consideration (Fig. B-1).

Kesaev[40] suggests that in setting up an energy balance it is possible to be biased in deciding where the energy comes from and where it goes, so that this method of evaluating a theory does not deserve any particular attention. Ecker[39] states that at the cathode the phenomena are not sufficiently well known for an energy balance at this electrode to be meaningful. However, at the anode the process is sufficiently simple that a reasonable energy balance may be carried out, he says. We may add that if this is so, then it should be simple to obtain by subtraction the energy going to the cathode, since (in EDM) very little energy is dissipated in the plasma.

When an electron leaves the cathode it is usually replaced by a conduction electron, of energy, $E_F$ (Appendix A). If the emitted electron had an energy below $E_F$, then the surface is heated, rather than cooled.

At $10^6$ amp/cm$^2$ a graphite cathode receives just as much energy from Joule heating as it does from positive ion bombardment.[57]

CATHODE

← Ionization energy of ions

← Kinetic energy of ions due to cathode fall

← Thermal energy of ions

← Condensation energy of neutralized ions

← Radiation from anode

← Joule heating of electrode ——————→

← Condensation energy of atoms ——————→

← Radiation from plasma ——————→

← Conduction heating from arc ——————→

← Chemical reactions at surface ——————→

Kinetic energy of electrons due to anode fall —→

Thermal energy of electrons ——————→

'Condensation' energy of electrons ——————→

Radiation from cathode ——————→

ANODE

→ Emission of electrons

→ Electrons for neutralizing ions

→ Radiation ←——————

→ Conduction to arc ←——————

→ Conduction to electrodes ←——————

→ Melting ←——————

→ Vaporization ←——————

P L A S M A

Fig. B-2.  Schematic of energy balance at electrodes.

## APPENDIX C:    Electric Field at Cathode

In Section 1.5 it was suggested that Pahlitzsch's theory for explaining the polarity inversion appears unrealistic because the lack of positive ions early in the pulse not only prevent cathode erosion, but would also prevent reasonable electron current densities from being realized. This Appendix shows why that is so.

At the large gaps and low voltages present under normal EDM operation, the average field in the gap, obtained through dividing the applied voltage by the gap distance, is much too low for obtaining significant current densities through field emission. For example, consider a gap of $10^{-3}$ cm, and a voltage of 60 volts. Then the average field is $60/10^{-3} = 6 \times 10^{4}$ volts/cm. Based on Lee's values[42] for T-F emission, a material of 4.5 volts work function and operating at $2000°K$ would yield a current density of about $10^{-2}$ amp/$cm^{2}$, or about eight orders of magnitude less than that measured by Fromme[59,60,61] or Cobine and Gallagher.[62] Hence the field must be established by some other means.

It is now believed[6,39] that the high field in the cathode fall region is produced by the intense space charge of positive ions approaching the cathode surface. Even though most of the current in this region may be carried by electrons, the net space charge is positive because of the much heavier and slower ions. The following quantitative derivation of the field at the cathode follows for the most part MacKeown's[41] treatment.

-126-

$(V_c - V)$          E

CATHODE          X ←          POSITIVE
SURFACE               X=0          COLUMN
                        V=0
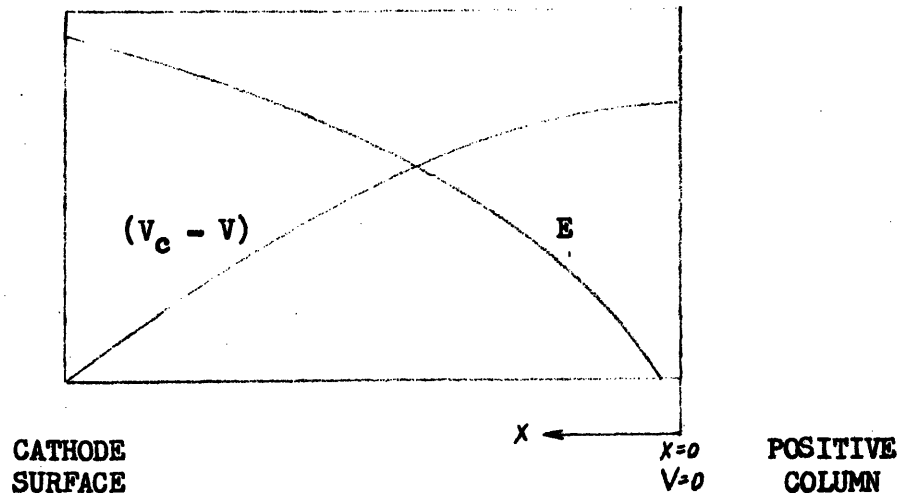
Fig. C-1.   Electric field, E, and potential, $V_c - V$, in the cathode fall region. (MacKeown[41]).

A schematic of the electric field and potential in the cathode fall region is shown in Fig. C-1.   If distance, x, and potential, V, are measured from the boundary between the cathode fall region and the positive column, Poisson's equation gives:

$$\frac{d^2V}{dx^2} = -4\pi\rho = -4\pi (j_+/v_+ - j_-/v_-)$$          (C - 1)

where $\rho$ is the space charge

   $j_+$, the ion current density

   $j_-$, the electron current density

   $v_+$, the ion velocity

   $v_-$, the electron velocity.

Let us now assume that the whole cathode fall of potential occurs within one mean free path. Conservation of energy then gives,

$$\tfrac{1}{2} M v_+^2 = eV$$          (C - 2)

-127-

for singly ionized atoms or molecules. For electrons we have:

$$\frac{1}{2} m v_-^2 = e(V_c - V) \qquad (C - 3)$$

Here  M = mass of ion

m = mass of electron

$V_c$ = cathode fall ≡-potential at cathode, in this case.

From the above three equations,

$$\frac{d^2 V}{dx^2} = -4\pi \left[ j_+ \left(\frac{M}{2eV}\right)^{1/2} - j_- \left(\frac{m}{2e(V_c-V)}\right)^{1/2} \right] \qquad (C - 4)$$

Assuming the boundary condition that    −dV/dx = E = 0  at x = 0,

MacKeown was able to integrate this equation once:

$$E^2 = \left(\frac{dV}{dx}\right)^2 = 16\pi \left\{ j_i \left(\frac{MV}{2e}\right)^{1/2} + j_e \left(\frac{m(V_c - V)}{2e}\right)^{1/2} - j_e \left(\frac{mV_c}{2e}\right)^{1/2} \right\} \qquad (C - 5)$$

i.e.  $$E^2 = 7.57 \times 10^5 \left\{ j_i (1845\, WV)^{1/2} - j_e [V_c^{1/2} - (V_c - V)^{1/2}] \right\} \qquad (C - 6)$$

where  E = electric field in volts/cm,

$j_+$  and  $j_-$  are measured in amps/cm$^2$,  and

W  is the atomic weight of the ion.

At the cathode surface the electric field, $E_c$, is given by:

$$E_c^2 = 7.57 \times 10^5 \; V_c^{1/2} \left\{ j_i (1845\, W)^{1/2} - j_e \right\} \qquad (C - 7)$$

The above equation indicates that an increase in the ion current

density will increase the field at the cathode. And Lee[42] has shown

that for T-F emission an increase in the field will cause a considerable

increase in the total current density. However, there are better ways

of illustrating this point.

ION AND ELECTRON

CURRENT DENSITY

$\left(amp/cm^2\right)$
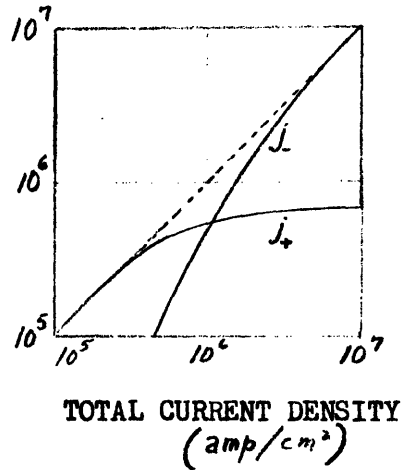
Fig. C-2.    $j_+$ and $j_-$ plotted as a function of $j = j_+ + j_-$ according to the Fowler - Nordheim and MacKeown equations (Ecker[39]).

Ecker[39] has discussed some results originally derived by Wasserab based on MacKeown's equation (C-7 above) and the Fowler - Nordheim equation.[63] Combining these for a cathode material of work function 2 eV (a rather low value) Fig. C-2 was obtained. The message from this typical curve is clear. With small values of the total current density, j, there is no adequate field for F-emission (Appendix A), and j is proportional to $j_+$ . At large current densities, $j_+$ is practically constant since, when dealing with extreme fields a small alteration of $j_+$ produces a large change in $j_-$ ; so here $j_-$ is proportional to j. When operating in tnis region of high fields and high current densities, Pahlitzsch's theory therefore seems questionable, since an increase in the positive ion current density would bring about a much larger increase in the electron current density.

$r_1 = 0.238$ cm

$r_2 = 0.952$ cm
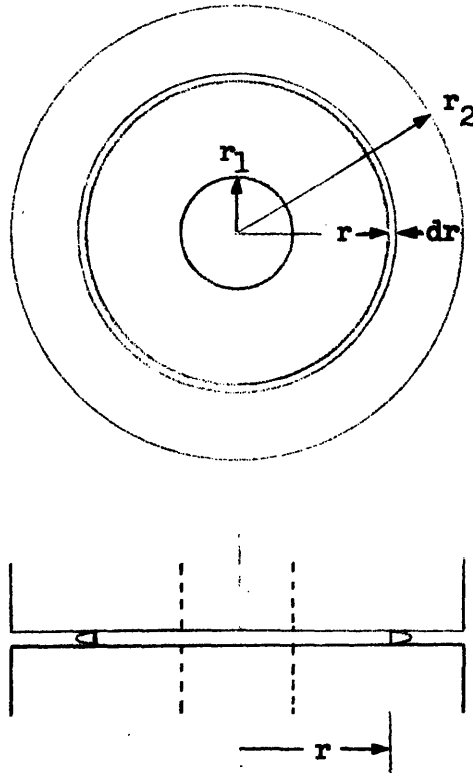
Fig. D-1.    Illustration of flow geometry. Fluid enters the gap
through the axial hole in the lower electrode.

It was suggested in the text that some breakup of particles may

occur due to discharges initiating through the particles in the gap.

This, of course, is only possible if the particles remain in the gap

sufficiently long. Let us first calculate how fast the fluid moves.

For perfectly smooth, parallel, cylindrical electrodes (Fig. D-1)

the radial flow rate of fluid, Q, at radius, r, is given by:

$$Q = 2\pi r G v(r) \qquad\qquad r_1 \leqslant r \leqslant r_2 \qquad\qquad (D - 1)$$

where   G  is the gap size,

v(r) is the average fluid velocity at radius r.

Consider  a gap of 0.01 cm   (100 μm).   From Fig.13,   $Q = 50.6$ cm$^3$/min.

At $r = r_1$,        $v(r_1) = Q/(2\pi r_1 G)$   = <u>56.3 cm/sec</u>

At $r = r_2$,        $v(r_2) = Q/(2\pi r_2 G)$   = <u>14.1 cm/sec</u>

It is clear from Eq.(D-1) that, for constant Q and G, v(r)

decreases linearly with increasing r between $r_1$ and $r_2$. The average

fluid velocity in the gap at a pressure drop of 155 mm of Hg and at

30 °C, is tabulated for different gap sizes in Table D-1, and is

plotted in Fig. D-2.

TABLE D-1.   Average velocity of fluid in gap.

| Gap size (μm) | 10 | 20 | 50 | 100 | 200 | 500 |
|---|---|---|---|---|---|---|
| $v(r_1)$  (cm/sec) | 0.563 | 2.25 | 14.1 | 56.3 | 225 | 1410 |
| $v(r_2)$  (cm/sec) | 0.141 | 0.563 | 3.52 | 14.1 | 56.3 | 352 |

How much time, t, does a fluid particle spend in the gap?

By definition,    $v(r) = dr/dt$

therefore,              $t = \int dr/v(r)$

Substituting for v(r) from Eq.(D-1),    $t = \int_{r_1}^{r_2} (2\pi r\ G/Q)\ dr$

Integrating,          $t = (\pi G/Q)\ (r_2^2 - r_1^2)$                    (D - 2)

-131-
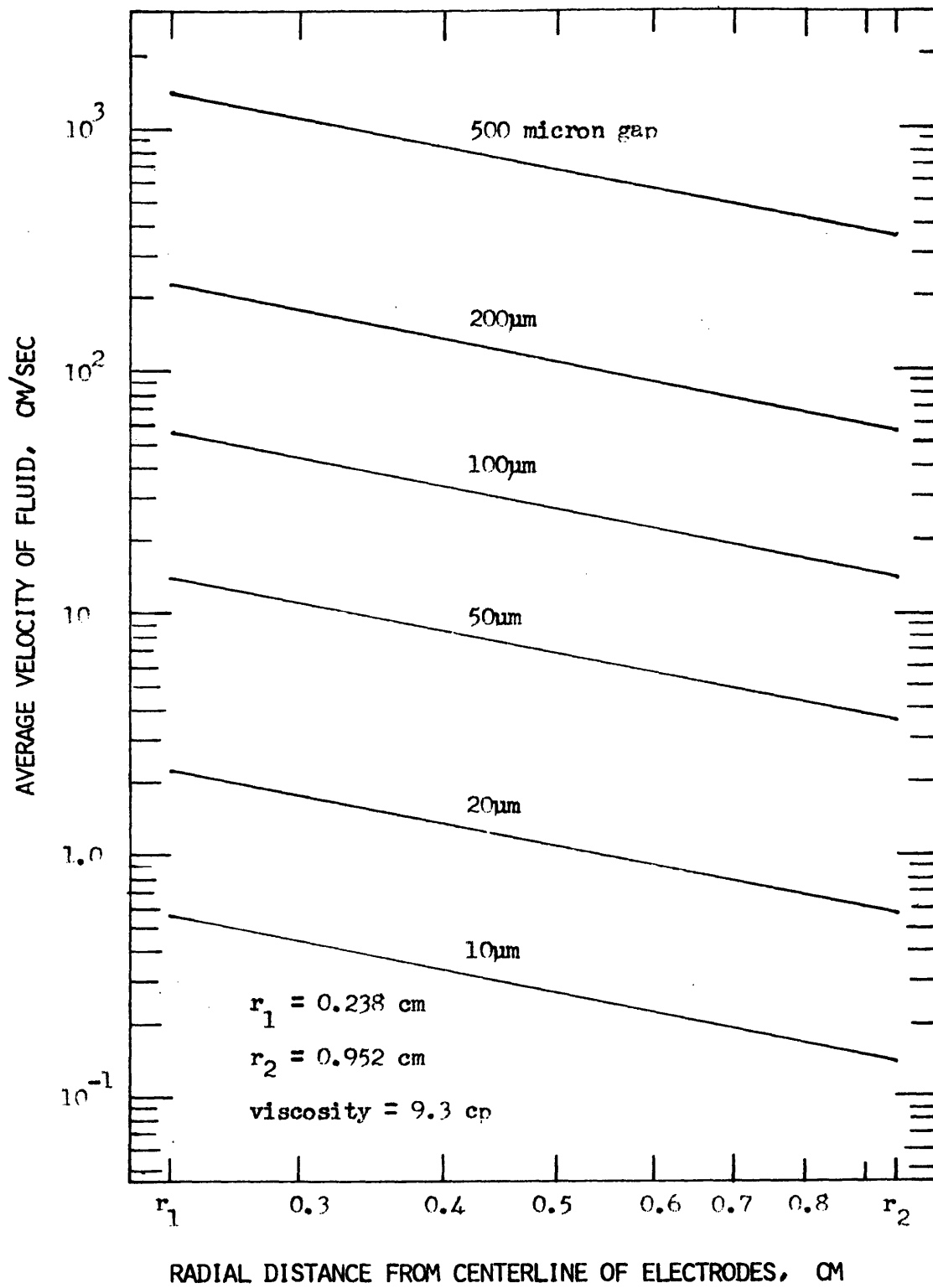
Fig. D-2. Dependence of average fluid velocity on radial distance from centerline of electrodes, and on gap.

According to Eq.(D-2), for a gap of 100 $\mu$m, a fluid particle spends 3.16 x $10^{-2}$ seconds in the gap.

Let us make the assumption that an eroded particle moves radially in the gap at a velocity equal to the average fluid velocity. (For a 50$\mu$m particle moving in a 100$\mu$m gap the relaxation time is about 0.2 % of the time which it takes the fluid to move through the gap (if the fluid is gaseous). For smaller particles and smaller gaps the assumption is very good. For larger particles and larger gaps it gradually gets worse.)[71]

The time which such a particle spends in the gap depends on where it is formed. If it were formed at radius, r, it would, according to the above calculations, spend the following time, $t_p$, in the gap:

$$t_p = (\pi G/Q)(r_2^2 - r^2) \qquad\qquad (D-3)$$

This equation has been evaluated for a large number of values of r and G, and the results are plotted in Fig. D-3. According to the above equation a particle formed at r = $r_1$ in a 10$\mu$m gap would remain in the gap for 3.16 seconds. At 30 kc 9.48 x $10^4$ discharges would occur in this time, so it seems highly unlikely that this particle would escape intact. If the gap instead were 500$\mu$m the particle would spend 1.26 x $10^{-3}$ seconds in the gap. At 0.37 kc and 50% duty cycle the next discharge would occur at about the same time that the particle leaves the gap. It seems quite likely that this effect may have influenced the particle size distribution, accounting for more small particles when the gap was small and the frequency high.

-133-

1000

INTERELECTRODE DISTANCE, MICRON

100

10

0.238

Radius at which particle is formed (cm) ⟶ 0.8    0.6    0.3

0.5

0.7    0.4

$10^{-3}$            $10^{-2}$            $10^{-1}$            1.0

TIME PARTICLE SPENDS IN GAP,  SEC
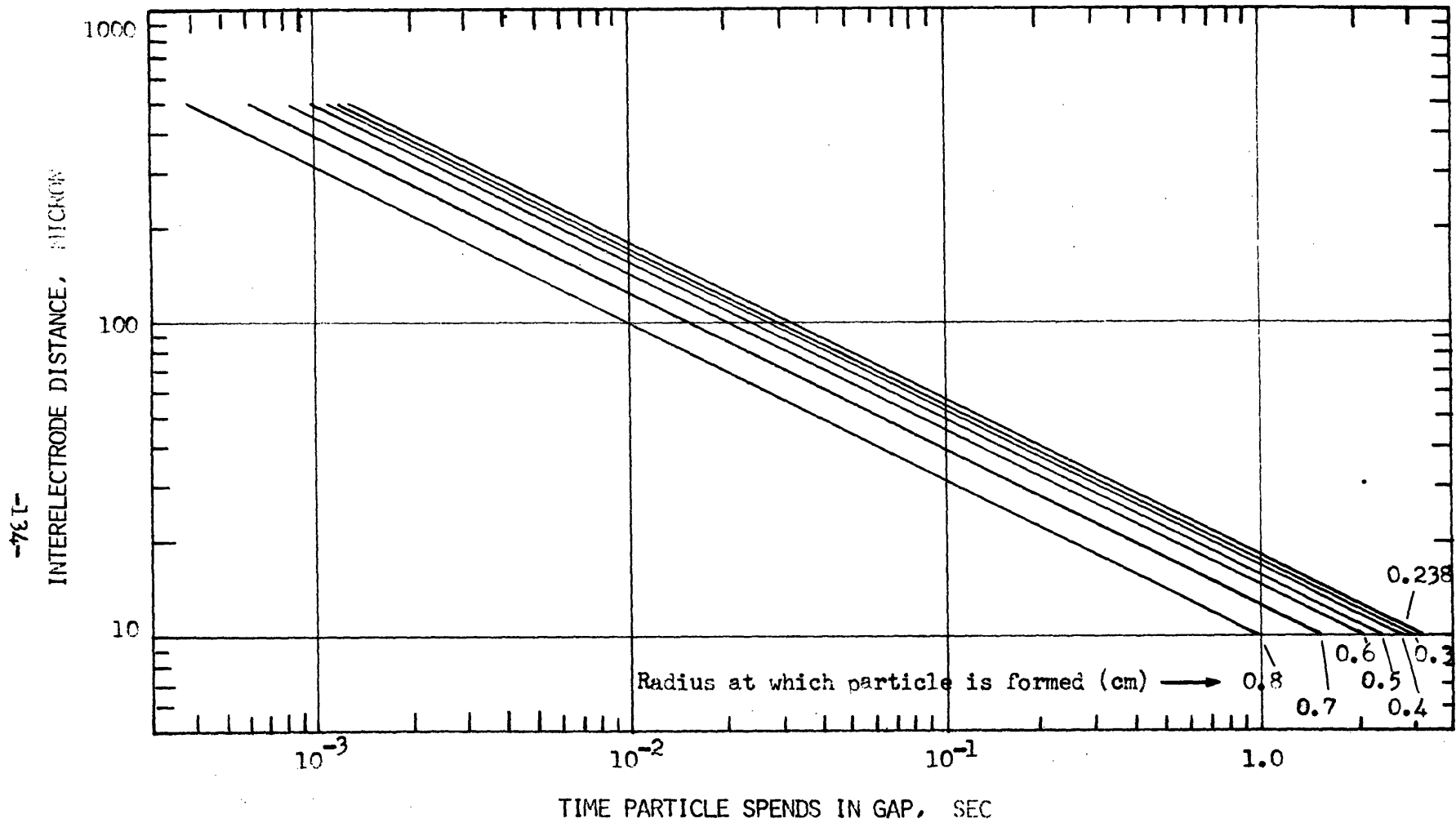
Fig. D-3.  Time which particle spends in gap as a function of
gap size and radius at which particle is formed.

APPENDIX E: <u>Number of Particles in Gap at Any Given Time</u>

Let us first calculate the average time, $t_{avg}$, spent in the gap by any one particle. For simplicity let us <u>assume</u> that each discharge results in the formation of only one particle.

During any relatively long time interval an equal number of discharges occur on each unit area of the surface, so the fraction of the total number of discharges occurring on a given surface is equal to the fractional size of that area. Hence the fraction of all the particles that is formed between r and r + dr in a given time interval is $(2\pi r\, dr)/\pi(r_2^2 - r_1^2)$ (see Fig. D-1). From Eq. (D-3), each of these particles spends a time $t_D(r) = (\pi G/Q)\,(r_2^2 - r^2)$ in the gap.

The average time, $t_{avg}$, which a particle spends in the gap is then $t_D(r) \cdot 2\pi r\, dr/\pi(r_2^2 - r_1^2)$, integrated over all possible values of r.

i.e., $$t_{avg} = \int_{r_1}^{r_2} (\pi G/Q)\,(r_2^2 - r^2)\,(2r/(r_2^2 - r_1^2))\ dr$$

Integrating,  $t_{avg} = \underline{1.34\ (G/Q)}$        (E - 1)

where $t_{avg}$ is measured in seconds, G in cm and Q in $cm^3/sec$.

Let us consider machining at 1 kc and 65 amp arc current. The gap is then $1.65 \times 10^{-2}$ cm, and the flow rate is $1.44 \times 10^4$ $cm^3/sec$. Equation (E-1) then gives a value for $t_{avg}$ of $\underline{5.53 \times 10^{-3}}$ sec. The values for the gap and the flow rate were obtained from Figs. 20 and 13. Values for different frequencies are tabulated below.

TABLE E-1. Number of particles in gap when machining steel at 65
amps arc current, using a positive graphite tool.

| Frequency (kc) | 0.34 | 1.0 | 5.0 | 30 | 130 |
|---|---|---|---|---|---|
| Gap (cm) | $1.8 \times 10^{-2}$ | $1.6 \times 10^{-2}$ | $1.1 \times 10^{-2}$ | $5.7 \times 10^{-3}$ | $2.7 \times 10^{-3}$ |
| Flow rate ($cm^3$/min) | 330 | 240 | 66 | 9.2 | 0.98 |
| $t_{avg}$ (sec) | $4.4 \times 10^{-3}$ | $5.5 \times 10^{-3}$ | $1.3 \times 10^{-2}$ | $5.0 \times 10^{-2}$ | $2.2 \times 10^{-1}$ |
| Avg. no. of particles in gap at any one time | 1.5 | 5.5 | 66 | 150 | $2.9 \times 10^4$ |

Note that at 0.34 kc there are, on average, only one or two
particles in the gap when the next discharge occurs, whereas at
130 kc there may be as many as 29 000 particles in the gap at any
time. We know from the text that machining is usually unstable at
very high and at very low frequencies. Perhaps too many, or too few,
particles in the gap at any given time is conducive to unstable
machining...

APPENDIX F:   Time Required to Melt Workpiece Protrusion

There are different ways in which this problem may be approached.
If energy balance could tell us exactly how much power is reaching the
surface, and at what power density, we could allow for heat transfer
losses and resistance heating, and from this get a good approximation
of the rate of melting of the workpiece protrusion. However, due to
lack of accurate information along these lines we shall adopt a
completely different approach.

Consider the case illustrated in Fig. F-1 where the flow rate

T O O L

A R C

Electrical gap = $2.5 \times 10^{-3}$

$3.35 \times 10^{-3}$

Flow rate gap = $10^{-2}$

$7.5 \times 10^{-3}$

$2.0 \times 10^{-2}$

$2.5 \times 10^{-3}$

Bottom of crater

$3.0 \times 10^{-3}$

Resolidified layer
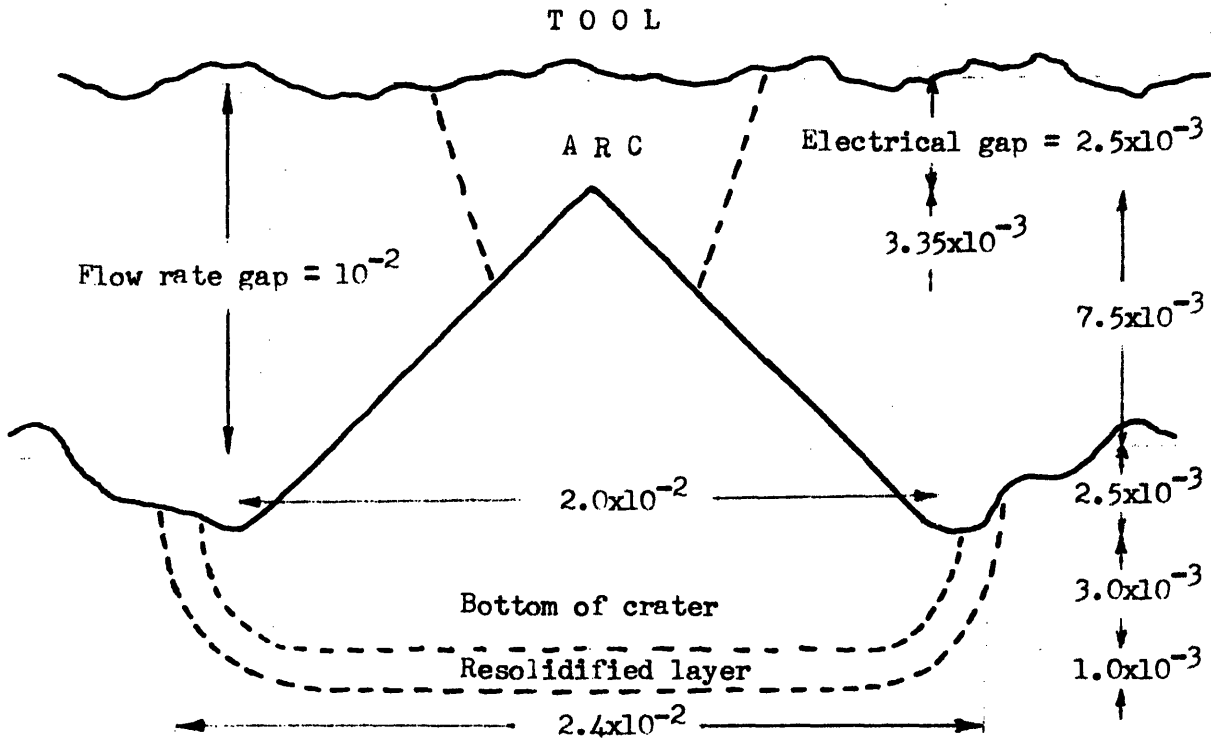
$1.0 \times 10^{-3}$

$2.4 \times 10^{-2}$

Fig. F-1.   Illustration of geometry of workpiece protrusion before
discharge, and of crater and resolidified layer after
the discharge has occurred. (dimensions in cm).

gap is $10^{-2}$ cm, the electrical gap is $2.5 \times 10^{-3}$ cm, arc current is 50 amp and the current density is $10^{6}$ amp/cm$^2$. Clearly, different shape protrusions may exist. Let us first consider a right circular cone. We are interested in finding out the actual arc length as a function of time, from the moment that melting starts, and shall assume that during this time the rate of melting is constant. First of all, we know that a crater will be left after the discharge is terminated, and also that there will be a resolidified layer below the bottom of the crater. Reasonable dimensions[34] are indicated on the diagram (Fig. F-1).

The total volume of material melted during the discharge is approximately:

$$\text{Volume of cone} + \text{volume of cylinder} = 2.85 \times 10^{-6} \text{ cm}^3.$$

The cumulative quantity of material as a function of distance from the tool is easily calculated, and from this we may obtain the arc length as a function of time (Fig. F-2). Note that only about 15 % of the material to be melted lies above the bottom of the flow rate gap, so after a very short time the length of the arc is equal to the flow rate gap. By this time a shallow molten pool has formed, and the liquid-solid boundary gradually progresses, but the surface of the molten pool never gets very far below the bottom of the flow rate gap, if our assumed geometry is anywhere near right, and if the molten material is removed primarily after the power is turned off, as Zolotykh et al.[17] claim. If, instead of being like a cone, the protrusion is in the form of a hemisphere or a sphere, but of the same height as the cone considered, then the fraction of material to be melted that lies above the bottom of the flow rate gap is respectively 34 % and 22 %.
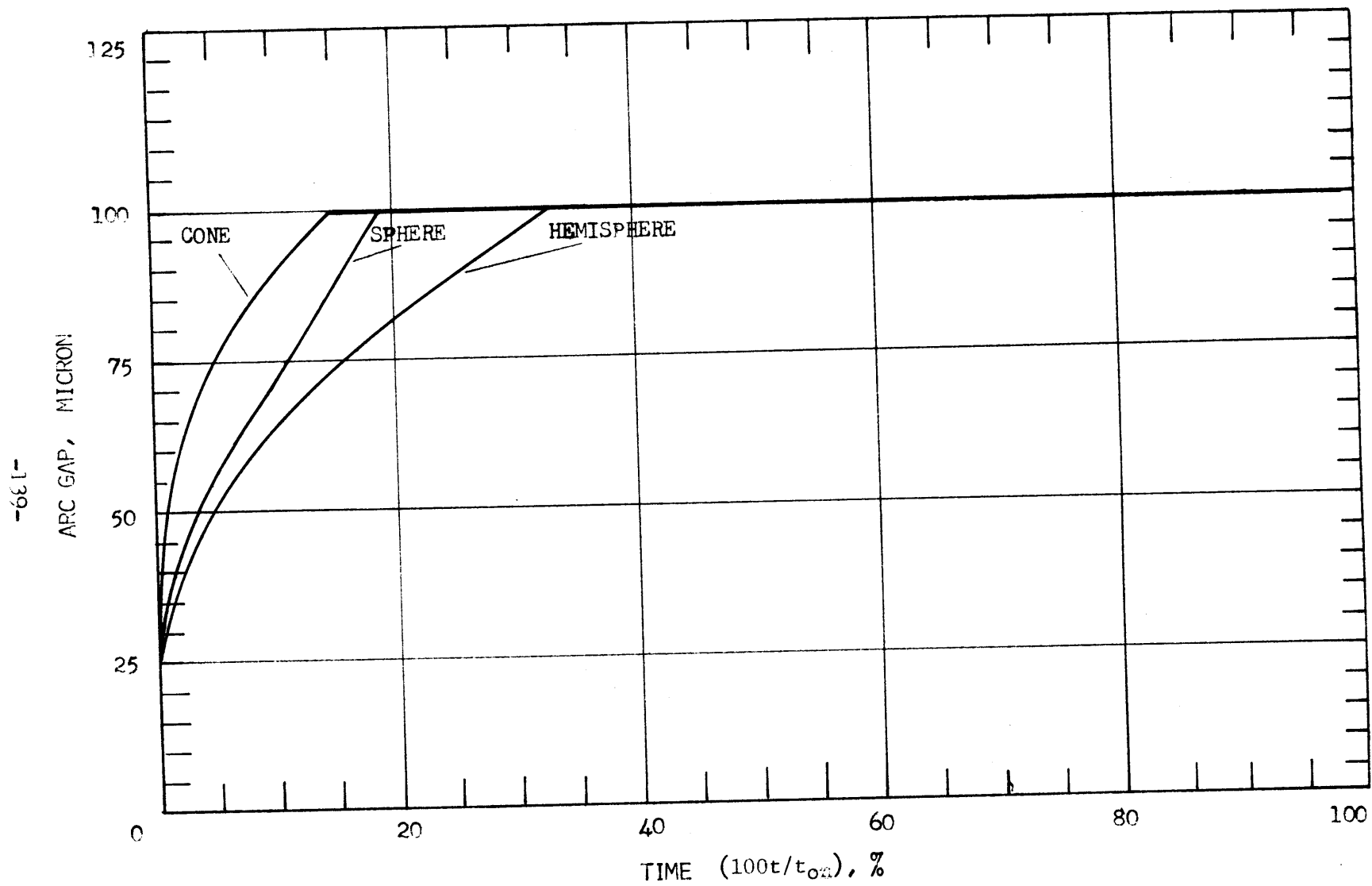
Fig. F-2. Variation of arc gap with time during pulse under conditions specified for Fig. F-1.

-139-

This Appendix is not meant to prove that the flow rate gap and the arc gap are identical. They are not, but in general they are of the same order, and may in fact be very close in size. Furthermore, it is quite clear that, for some chosen geometry, a change in the flow rate gap brings about an almost identical change in the arc gap. The above assumption that the arc gap keeps growing until it reaches the size of the flow rate gap seems justified on the basis of the definition of the flow rate gap (section 2.3).

It was noted above that if the surface protrusion were a sphere stuck to the surface 22 % of the energy going into melting would be used up in melting the protrusion. If now the frequency were raised by a factor of 20 there would be sufficient energy to melt less than one quarter of the above sphere in one pulse. This is what happened in the experiments with injection of steel particles. The particles were produced at 0.34 kc, and were used in experiments at 9 kc. For this reason the particles were too large to be melted (section 4.3).

APPENDIX  G:    'Theoretical' Particle Size

In this Appendix we shall calculate the 'theoretical' diameter of
of the largest particle. To do this we consider the total volume of
material eroded in a given time, and divide this by the total number of
pulses put out by the power supply in the same time. We shall also allow
for the fact that most of the particles are hollow.

Assumptions:

(1)  Each pulse put out by the power supply results in an
     effective discharge.

(2)  The particles are 50 % hollow by volume.

Under the machining conditions listed in Fig. 20, the erosion
rate at 1 kc is 0.177 cc/min (Table G-1). At this frequency there are
$10^3$ x 60 pulses per minute. The volume of material eroded per pulse is
therefore  2.95 x $10^{-6}$ cc/ discharge. But the particles are 50 % hollow,
so the volume occupied by the largest particle is 5.90 x $10^{-6}$ cc. For a
spherical particle this yields a diameter of 224 $\mu$m which compares
favorably with the measured gap of 165 $\mu$m, according to Fig. 20. If,
instead, we assume the particle to be solid, the 'theoretical' particle
size comes out to be 178 $\mu$m.

To get some idea of the validity of the second assumption made above,
ten particles were measured and weighed. The fraction hollow varied from
41 % to 79 %, and the average fraction hollow was 48 %. In view of the
wide scatter and small sample size let us see how sensitive the results
are to changes in the assumption, at different frequencies. Let us

first tabulate the results for particles which are 50 % hollow, and next consider in turn solid particles, particles which are 25 % hollow, and particles which are 75 % hollow.

TABLE G-1:    Theoretical diameter for 50 % hollow particles.

| Frequency (kc) | Erosion rate (cc/min) | Number of discharges per minute | Volume per discharge (cc) | Volume of particle (cc) | Particle diameter (micron) |
|---|---|---|---|---|---|
| 0.2 | 0.120 | $1.2 \times 10^4$ | $1.0 \times 10^{-5}$ | $2.0 \times 10^{-5}$ | 336 |
| 1.0 | 0.177 | $6.0 \times 10^4$ | $2.95 \times 10^{-6}$ | $5.90 \times 10^{-6}$ | 224 |
| 3.0 | 0.213 | $1.8 \times 10^5$ | $1.18 \times 10^{-6}$ | $2.36 \times 10^{-6}$ | 165 |
| 7.0 | 0.236 | $4.2 \times 10^5$ | $5.62 \times 10^{-7}$ | $1.24 \times 10^{-6}$ | 133 |
| 10 | 0.232 | $6.0 \times 10^5$ | $3.87 \times 10^{-7}$ | $7.74 \times 10^{-7}$ | 114 |
| 20 | 0.194 | $1.2 \times 10^6$ | $1.62 \times 10^{-7}$ | $1.34 \times 10^{-7}$ | 85 |
| 40 | 0.069 | $2.4 \times 10^6$ | $2.83 \times 10^{-8}$ | $5.66 \times 10^{-8}$ | 52.6 |
| 60 | 0.030 | $3.6 \times 10^6$ | $8.33 \times 10^{-9}$ | $1.66 \times 10^{-8}$ | 31.6 |
| 100 | 0.004 | $6.0 \times 10^6$ | $6.67 \times 10^{-10}$ | $1.33 \times 10^{-9}$ | 13.6 |

Solid particles:    In the case of solid particles the particle volume would be 1/2 as large as that obtained for 50 % hollow particles. The diameter would therefore be $(1/2)^{1/3}$ or 0.795 times as large.

25 % hollow particles:    The particle volume in this case would be 4/3 that of the solid particle. The diameter would therefore be $(4/3)^{1/3}$ or 1.10 times as large as that of the solid particle, i.e., 0.875 times

-142-

as large as the diameter of the 50 % hollow particle. Similarly, the diameter of a 75 % hollow particle would be 1.26 times as large as that of a 50 % hollow particle.

The results are plotted in Fig. 40. In view of the assumptions the agreement is surprisingly good., especially between solid particles and gap size. The fact that the 'theoretical' particle diameter is of the same order as the gap, and that the largest particles collected are of the same order, strongly suggests that there is a finite probability that only one or two particles may be formed in a given discharge. However, from the particle size distributions it is clear that the probability of obtaining several particles from each discharge is much higher. This is also suggested by Fig. 40, since the theoretical particle size is usually slightly higher than the size of the gap.

APPENDIX  H:   <u>Fluid Mechanics of Gap Measurements</u>

The problem of the radial flow between two plane, parallel, cylindrical electrodes has been carried out in great detail by Eckman,[55] who obtained the following result:

$$Q = (\pi G^3 \Delta p)/6\mu \ln(D/d) \qquad (H - 1)$$

where   $Q$  is the total flow rate of fluid

$G$  is the distance between the electrodes

$p = (p_o - p_a)$  is the pressure drop in the gap

$\mu$  is the viscosity of the fluid

$d, D$  are the internal and external diameters of the electrodes (referring to Fig. D-1, $d=2r_1$, $D=2r_2$)

Equation (H-1) may also be derived by a simpler approach, based on Poiseuille flow. This approach, of course, assumes fully developed flow, so it is, strictly speaking, not applicable right at the entrance to the gap, but is a good assumption a few values of $G$ downstream.

Poiseuille flow:    $-dp/dr = 12\,\mu\,Q(r)/G^3$ $\qquad (H - 2)$

where   $Q(r)$ is the flow rate per unit "depth" at radius, $r$, and the "depth" is, of course, $2\pi r$.

From continuity, the total flow, $Q$, is independent of $r$.

Hence   $Q(r) = Q/2\pi r$ $\qquad (H - 3)$

Substituting in Eq.(D-2):    $-dp/dr = 12\,\mu\,Q/2\pi r G^3$

Integrating once, and inserting the boundary condition that at $r = d/2$,
$p = p_o$,     $p_o - p = 6 \mu Q \ln(r/\tfrac{1}{2}d) / \pi G^3$

But at $r = D/2$, $p = p_a$, and $p_o - p_a = \Delta p$

Hence, $\Delta p = 6 \mu Q \ln(D/d) / \pi G^3$

i.e.,     $Q = (\pi G^3 \Delta p)/6 \mu \ln(D/d)$                    (H - 1)

_____

Poiseuille flow was assumed so Eq. (H-1) is valid only for
laminar flow. Let us therefore calculate the Reynolds number for the
flow at the point where the velocity is the highest.

$Re = \rho v(r_1) G/\mu = \rho Q G/2\pi r_1 G \mu$,        since $Q = 2\pi r_1 v(r_1) G$

Using values of 9.3cp for $\mu$, 0.83gm/cc for $\rho$, and 0.238cm for $r_1$ we get:

When $Q = 1$ cc/min,   $Re \simeq 0.1$

When $Q = 10^3$ cc/min, $Re \simeq 100$

so the flow is, at all times, well within the laminar regime.

When the flow rate is very high there may be significant head
losses at the entrance and exit of the gap. The pressure loss at the
exit is simply that corresponding to the loss of the total velocity
head, $p_v = \rho v^2/2g$.

At $Q = 10^3$ cc/min, $v(r_2) = Q/2\pi r_2 G \simeq 10^2$ cm/sec.

This corresponds to a pressure loss of approximately 3.2 mm of Hg
which is about 2 % of the pressure drop in the gap. The loss at the
entrance is of the same order.    These losses are neglected in our
measurements since the above values represent upper limits.

Effect of Surface Roughness. In section 2.3, in the flow rate vs. gap measurements, different flow rate vs. gap curves were obtained for different surface roughnesses. For smooth surfaces the position of the curve was adjusted until a straight line of slope 1/3 was obtained. This procedure may be justified for very smooth surfaces by making comparisons with the theoretical flow rate, and comparing with absolute measurements, using a microscope. However, it is not possible to justify the curves obtained for the rougher surfaces in the same way.

In an attempt to understand the influence of surface roughness, two completely different geometries are considered below. In Fig.H-1(a) the protrusions from the workpiece consist of circular rings over which the flow has to pass. These protrusions may be considered as
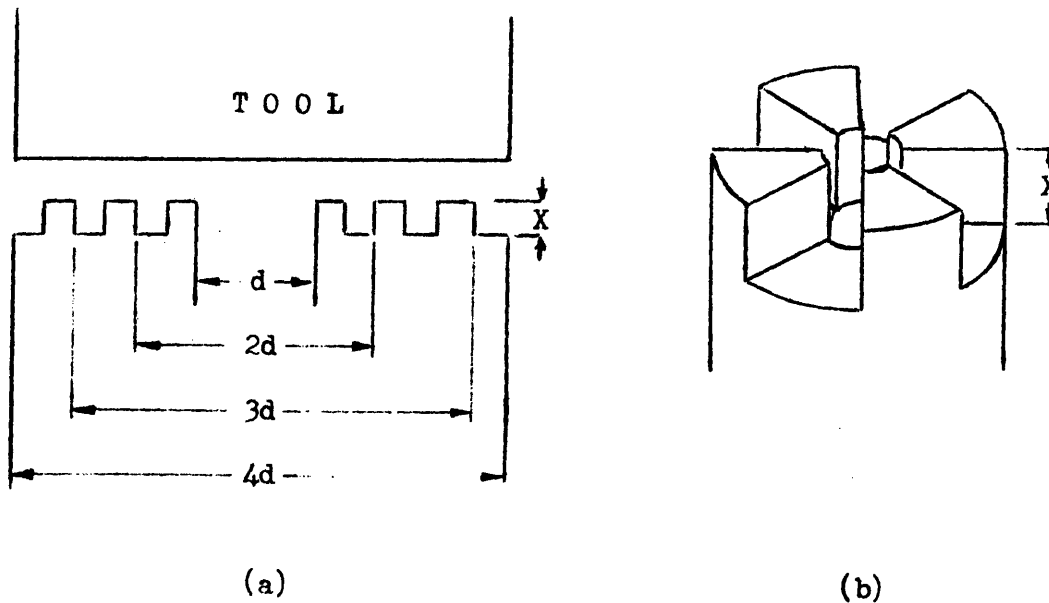


(a)                                                        (b)

Fig. H-1.   Illustration or restrictions to flow:
            (a) in 'series', (b) in 'parallel'.

restrictions in 'series' since all the flow has to pass over all the restrictions. The corresponding 'parallel' arrangement is shown in Fig. H-1 (b). The top electrode (the tool) is assumed to be perfectly smooth in both cases. The distance which the protrusion sticks out is in each case 'X'. The effect of varying the gap with these geometries, calculated on the basis of Poiseuille flow, is shown in Fig. H-2 for different values of X. The interelectrode distance is, in this case, taken to be the minimum distance between the electrodes plus $\frac{1}{2}$X. This corresponds approximately to the geometrical average gap. The curves above the straight line correspond to the geometry of Fig. H-1 (a), and those below the line to that of Fig. H-1 (b). The circle shown on some of the lines corresponds to the point at which the minimum distance between the electrodes is X. The points where the lower curves end correspond to physical contact between the electrodes.

It may be seen that the curves corresponding to Fig. H-1 (b) closely resemble the experimental curves obtained for our own surfaces (Fig. 13). Note that in all cases in Fig. H-2 the curves approach the straight line of slope 1/3 as the flow rate increases. This straight line corresponds to the theoretical flow rate that would be obtained if the protrusions were plastically levelled out, i.e., the case where X = 0.

The assumption of Poiseuille flow is rather poor in the case of Fig. H-1 (a), but is quite good for the case of Fig. H-1 (b) which is the case of interest to us. From the above results it seems that our way of defining the gap is entirely justified.
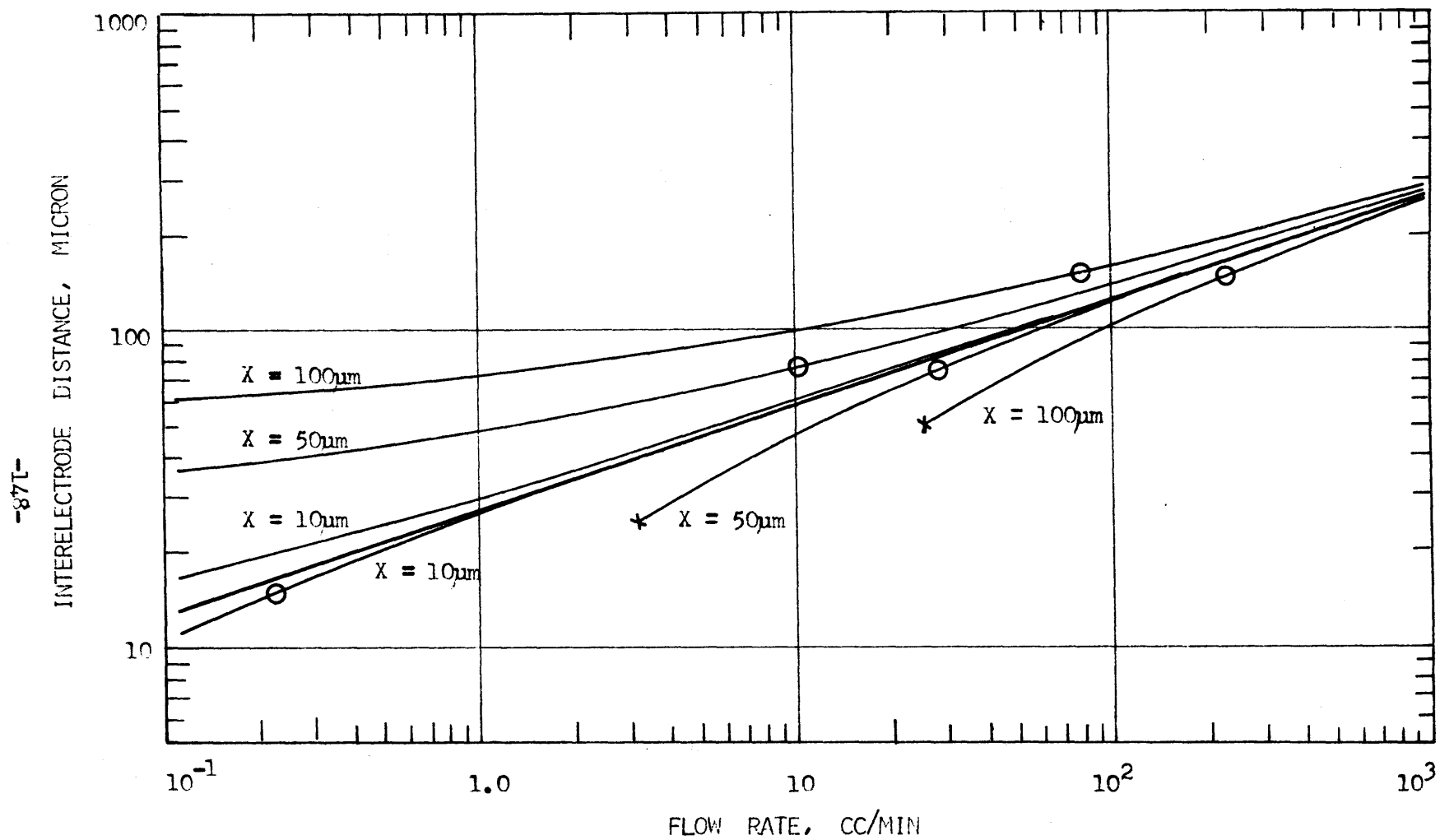
Fig. H-2. Dependence of fluid flow rate on magnitude of surface roughness of type illustrated in Fig. H-1, and on interelectrode distance.

APPENDIX I:   Measurements of Electrical Gap

Procedure:

1. Machine until conditions are as stable as possible.

2. Turn off the power supply; this causes the tool automatically to be withdrawn upwards; pumping ceases.

3. Turn pump on again.

4. Gradually feed tool downwards until electrical contact between the electrodes is established. Note this position relative to the point where machining ceased.

Results:  The results from measurements made in standard and reverse polarities are shown in Fig. I-1. The data points represent average values of at least ten measurements for each point, and the 'error brackets' indicate the scatter.  In general, electrical gaps are small under all conditions, compared with flow rate gaps under similar conditions (Figs. 20 and 26). In reverse polarity electrical gaps are, on average, smaller than in standard polarity. The negative values probably indicate either large surface protrusions or particles stuck to the surfaces. Negative values are much more frequent in reverse than in standard polarity. Note that there is little change in electrical gap with frequency, particularly in reverse polarity.
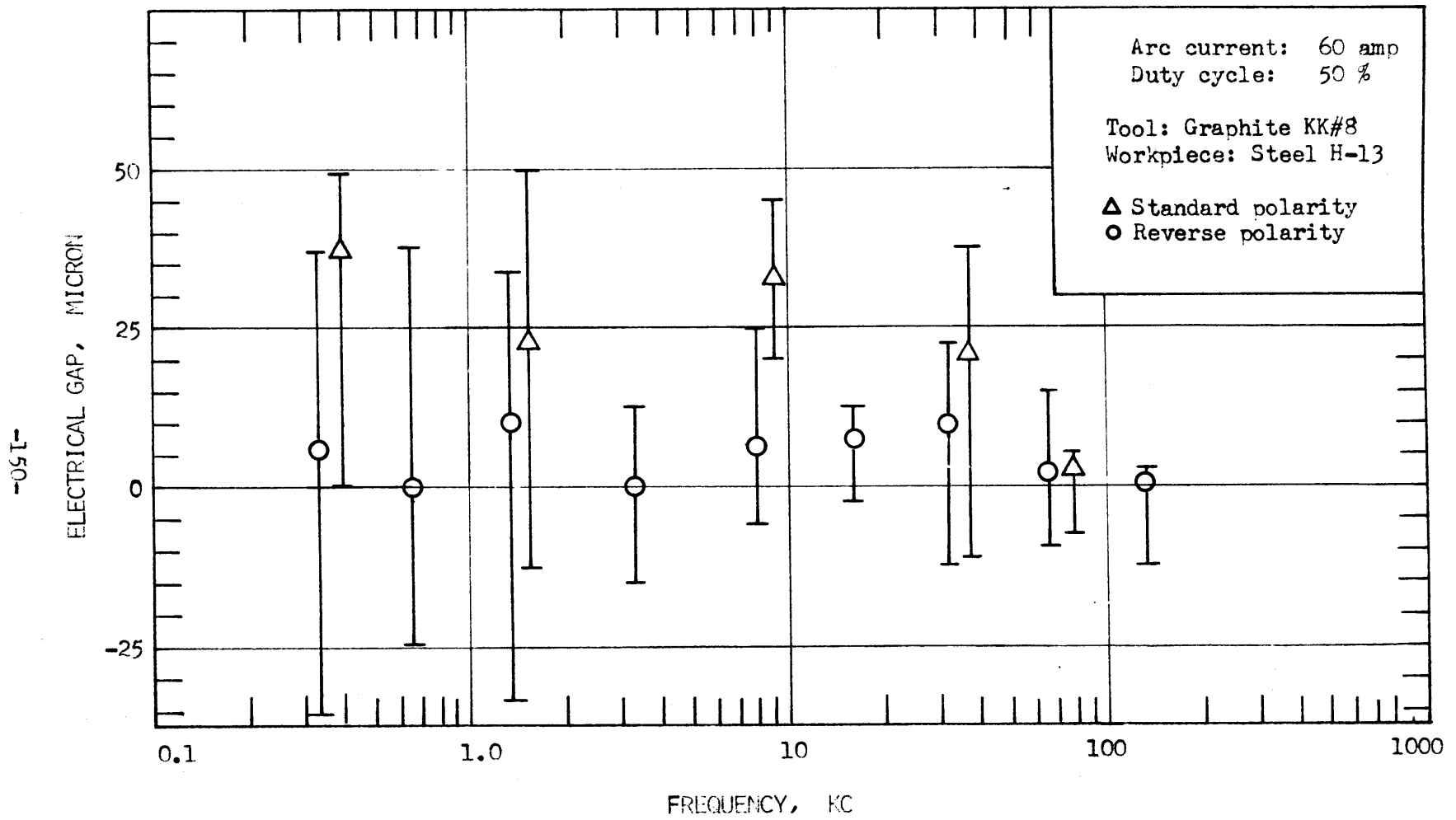
Fig. I-1: Dependence of electrical gap on frequency.

APPENDIX J:   Results Obtained With Refractory Electrodes

TABLE J.1:   Interelectrode distance* when machining
with refractory electrodes.

| Cathode (-) | Anode (+) | Freq. (kc) | Duty cycle (%) | Arc current (amp) | Gap size (μm) |
|---|---|---|---|---|---|
| Graphite KK#8 | Graphite KK#8 | 0.38 | 50 | 75 | 70 |
| " | " | 1.4 | 30 | 75 | 48 |
| " | " | 9.0 | 15 | 75 | 31 |
| Tantalum | " | 0.68 | 26 | 75 | 53 |
| " | " | 1.4 | 30 | 100 | 55 |
| " | " | 9.0 | 25 | 75 | 39 |
| " | " | 9.0 | 30 | 75 | 42 |
| " | " | 33 | 32 | 100 | 28 |

The most noteworthy aspect of these results is that the gap
size is considerably smaller than that obtained under similar pulse
energies when steel is one of the electrodes (by a factor of 2-4).

The erosion products from machining with graphite - graphite
electrodes contain no spheres, only irregular particles and flakes.
When machining with tantalum and graphite the erosion products contain
a considerable amount of spheres, —undoubtedly from the tantalum.
At 9 kc, 30% duty cycle, and 75 amps arc current the great majority
of the spheres have diameters below 44μm.

*These values are, as usual, flow rate gaps.          -151-

APPENDIX K:  Surface Roughness

Measurements of surface roughness show that higher pulse energies yield rougher surfaces,[3] as one might expect, since the volume of material eroded per pulse increases with increasing pulse energy (chapter 4).

Figure K-1 shows some typical surface traces of EDM machined surfaces.  These traces were obtained using a stylus of radius 2.5 micron and a linear variable differential transformer.  From the traces one may obtain the maximum difference between the peaks and the troughes.  Approximately half this difference would yield the size of the largest surface protrusions.  This latter value is compared with the measured magnitude of the interelectrode distance in Fig. K-2.

One disadvantage of the surface trace technique is that there is no guarantee that the stylus will go through the top of the protrusions or the bottom of the craters; it may cross partly to one side.  A different method which overcomes this disadvantage is to use a microscope to focus on the highest and on the lowest points in view.  At high magnification this method yields good values for a small surface area, but since the field of view is very limited this technique also tends to underestimate the maximum size of the surface protrusions over a relatively large surface.  Measurements using this technique are included in Fig. K-2.  It may be seen that measurements by both techniques yield a value for the largest surface protrusions of about half the interelectrode distance.  However, Fig. K-1 shows that most of the protrusions are considerably smaller, and
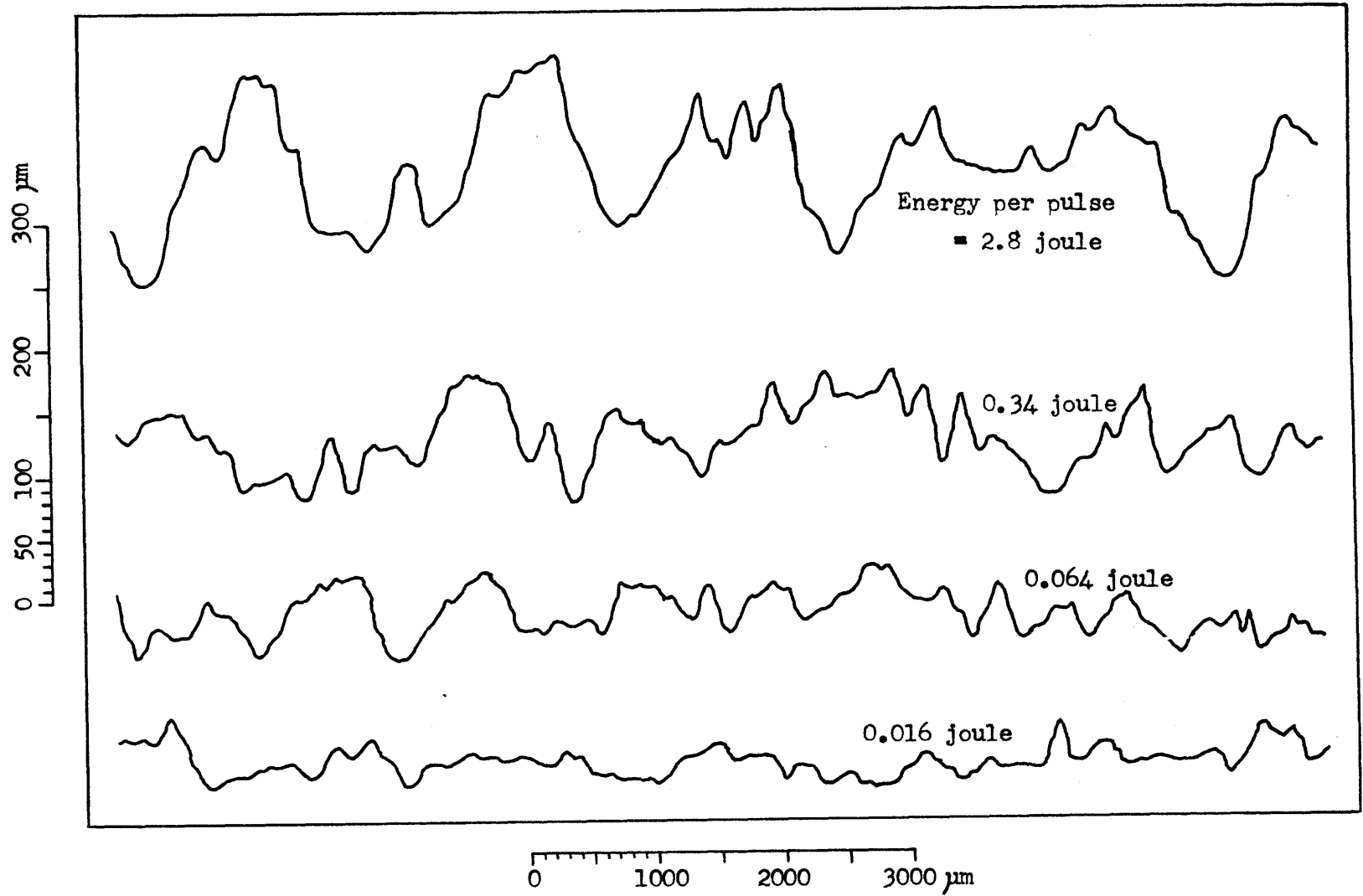
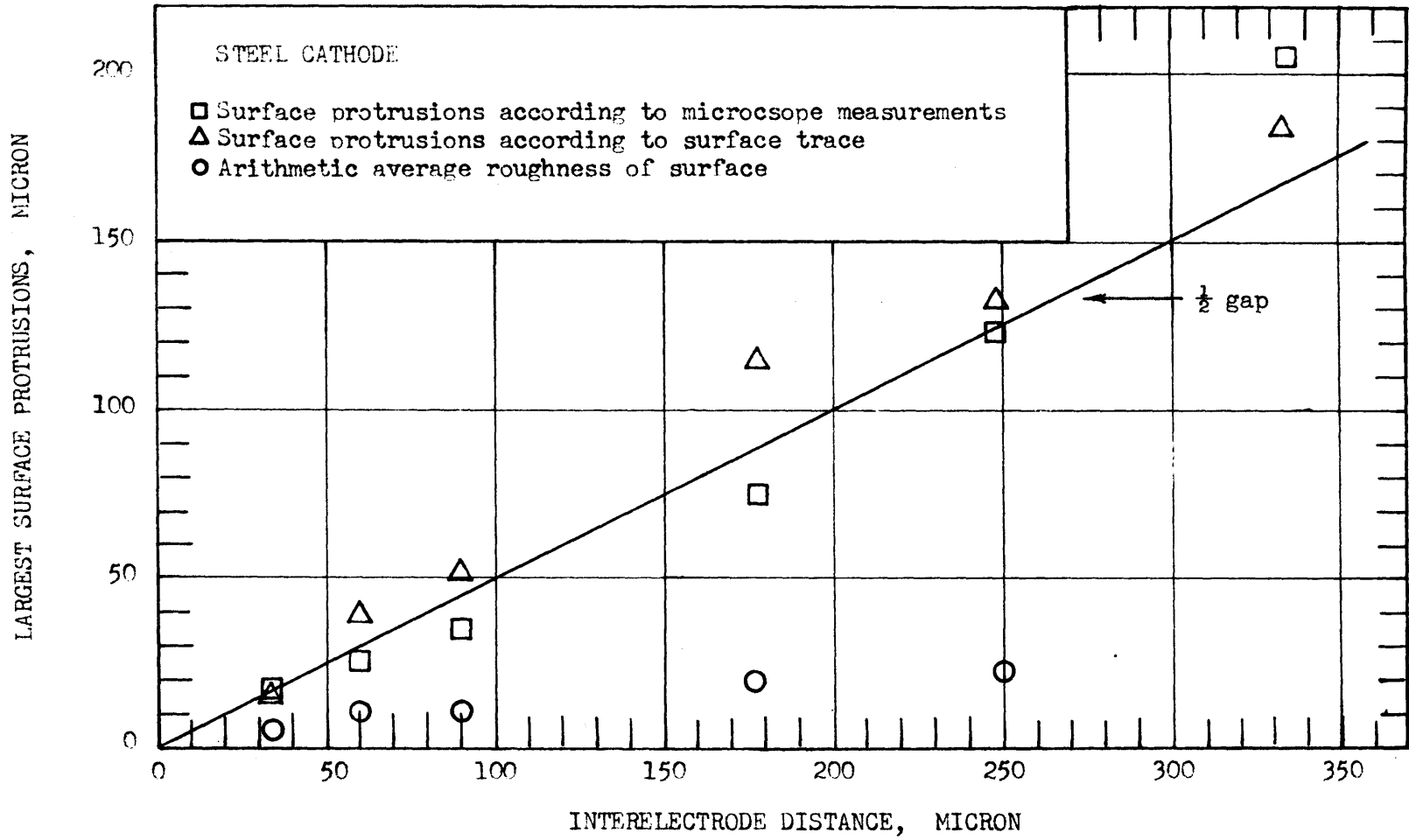Fig. K-1. Traces from EDM surfaces machined at different pulse energies.

Fig. K-2. Comparison between the size of the largest surface protrusions and the measured magnitude of the interelectrode distance.

values for the arithmetic average roughness of the surface is about one order of magnitude smaller than the size of the largest protusions (Fig. K-2).

APPENDIX L:  Temperature Dependence of Viscosity of EDM Fluid

The viscosity of the fluid is highly temperature dependent.
For simplicity, all flow rates were converted to the corresponding
flow rates at 30 $^{\circ}$C, using the values reported in Table L.1.
The information in the table was obtained by measuring the flow
rate of the fluid at temperatures between 28 and 48 $^{\circ}$C through
a plastic tube immersed in a temperature bath.  The flow in the
tube and in the gap took place at all times at Reynolds numbers
well within the laminar range.  In the gap Re varies from about
0.05 to about 200 (Appendix H).

TABLE L.1:    Ratio of viscosity of EDM fluid at temperature
              $T^{\circ}C$ to the viscosity at 30 $^{\circ}C$.

| $^{\circ}C$ | .0 | .1 | .2 | .3 | .4 | .5 | .6 | .7 | .8 | .9 |
|---|---|---|---|---|---|---|---|---|---|---|
| 28 | 1.073 | 1.069 | 1.065 | 1.061 | 1.058 | 1.054 | 1.050 | 1.046 | 1.043 | 1.039 |
| 29 | 1.035 | 1.031 | 1.028 | 1.024 | 1.020 | 1.016 | 1.013 | 1.009 | 1.006 | 1.003 |
| 30 | 1.000 | .996 | .992 | .988 | .985 | .982 | .978 | .975 | .972 | .968 |
| 31 | .965 | .961 | .958 | .955 | .951 | .948 | .945 | .941 | .938 | .935 |
| 32 | .932 | .929 | .926 | .923 | .920 | .917 | .914 | .911 | .908 | .905 |
| 33 | .902 | .899 | .896 | .894 | .891 | .888 | .886 | .883 | .880 | .878 |
| 34 | .875 | .872 | .870 | .867 | .864 | .862 | .859 | .856 | .853 | .850 |
| 35 | .848 | .845 | .843 | .840 | .838 | .835 | .833 | .830 | .828 | .825 |
| 36 | .823 | .820 | .818 | .815 | .813 | .810 | .808 | .806 | .803 | .801 |
| 37 | .799 | .797 | .794 | .792 | .790 | .788 | .785 | .783 | .781 | .779 |
| 38 | .777 | .775 | .773 | .770 | .768 | .766 | .764 | .761 | .759 | .757 |
| 39 | .755 | .753 | .751 | .749 | .746 | .744 | .742 | .740 | .738 | .736 |
| 40 | .734 | .732 | .730 | .728 | .726 | .724 | .722 | .720 | .718 | .716 |
| 41 | .714 | .712 | .710 | .708 | .707 | .705 | .703 | .701 | .699 | .697 |
| 42 | .695 | .693 | .691 | .690 | .688 | .686 | .685 | .683 | .681 | .679 |
| 43 | .677 | .676 | .674 | .673 | .671 | .670 | .668 | .667 | .665 | .663 |
| 44 | .661 | .660 | .658 | .657 | .655 | .654 | .652 | .651 | .649 | .648 |
| 45 | .646 | .645 | .643 | .642 | .640 | .639 | .637 | .636 | .635 | .633 |
| 46 | .632 | .631 | .629 | .628 | .626 | .625 | .623 | .622 | .620 | .619 |
| 47 | .618 | .616 | .615 | .614 | .612 | .611 | .610 | .609 | .608 | .607 |
| 48 | .606 | .605 | .604 | .603 | .601 | .600 | .599 | .598 | .596 | .595 |

APPENDIX M:  Comparison of Different Gap Measuring Techniques

When the electrode surfaces are perfectly smooth, the electrical gap, the arc gap, and the flow rate gap are all the same. Furthermore, if the outer edges of the electrodes are sharp, a microscope gap may be defined and measured, and this measurement should agree with the above gaps. After machining with very low energies per pulse ($4 \times 10^{-3}$ joules), a comparison was made between the flow rate gap and the microscope gap. The gap was changed stepwise using a dial gauge, and the results are shown in Fig. M-1. The flow rate gap agrees very well with the dial gauge settings, and the microscope gap is within $2 \times 10^{-3}$ cm of these two. At intermediate and high pulse energies the surface becomes so rough that microscope readings become meaningless. For this reason we have no independent way of fixing the zero point of the flow rate gap when the surfaces are rough. However, by defining the flow rate gap as we do, this limitation is not important.

The electrical gap, or shortest physical distance between the electrodes, is often located far from the outer surface of the electrodes, so its value cannot easily be checked microscopically.

The relative accuracy of the flow rate technique is apparent in Fig. M-1.

REVERSE POLARITY

Tool: Graphite KK#8
Workpiece: Steel H-13

Frequency:    130 kc
Duty cycle:    25 %
Arc current: 350 amp

☐ Microscope gap
O Flow rate gap

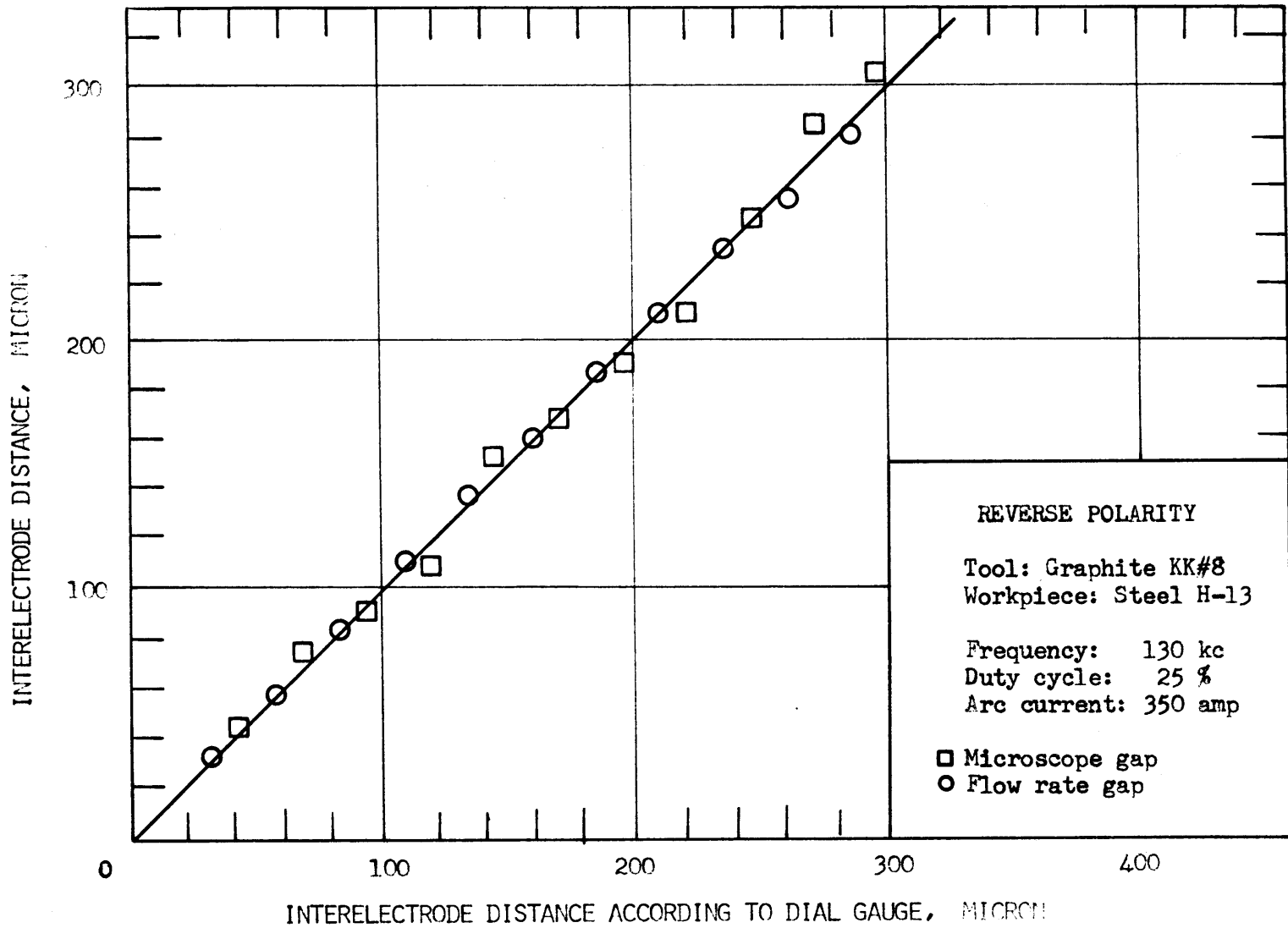INTERELECTRODE DISTANCE ACCORDING TO DIAL GAUGE,  MICRON

Fig. M-1.  Comparison between different gap measuring techniques.

APPENDIX N:    Particles vs. Surface Protrusions

What controls the size of the gap?

When two smooth electrodes are slowly brought together (60 volt pulses), machining does not commence until the distance between the electrodes is of the order of 10 μm. When machining commences, the tool retracts with the first few pulses, sometimes as much as 100 μm, or even more. We believe this is either because of particles in the gap, or because of large protrusions, caused by molten material being resolidified on the edges of the craters. Let us next retract the tool even further, and allow all the particles in the gap to get washed out. Next, lower the tool again. Note that if the particles were keeping the gap large, then machining should commence close to the initial 10 μm gap. If the protrusions control the gap size, then machining should resume close to the point where it was stopped, i.e., at the 100 μm gap.

What actually happens in most of the cases is that machining resumes at a gap which is slightly smaller than the gap size at which machining was stopped, e.g., at a 90 μm gap in the 100 μm case.

We conclude:

1.  In the absence of both particles and protrusions the gap will be small.

2.  In the absence of particles, but with protrusions present, the gap will be large.

3.  With both protrusions and particles present, the gap may be yet a bit larger.

# BIOGRAPHY OF AUTHOR

The author was born on December 1, 1936 in Trondheim, Norway. He received his elementary education in Norway, and attended highschool in Barbados, West Indies, where he graduated from Harrison College in 1956. After six years of working in the oil fields of Eastern Venezuela, he entered the University of Oklahoma. Eight months later, in September 1963, the author transferred to the Massachusetts Institute of Technology. While at M I.T. he was a member of the Honors Course and was elected to the following honors societies: Pi Tau Sigma, Tau Beta Pi, and Sigma Xi. He received his Bachelor's Degree from the Department of Mechanical Engineering in 1966 and his Master's Degree in 1967. Thesis topics were: Neutralization of Space Charge in Thermionic Energy Converters, and, An Experimental Investigation of Electrical Discharge Machining Using Reverse Polarity, for the Bachelor's and Master's degrees, respectively.

During his years in college the author has held fellowships from a number of sources.

The author was married to Constance V. Allen in June, 1965.